



**Cape Peninsula
University of Technology**

Faculty of Engineering

Department of Mechanical Engineering

Smart Alignment Systems Research Group

**The development of an 'active' surface
using Shape Memory Alloys**

By

S C Saal NDipME, BTechME

**Thesis submitted towards partial fulfilment of the Masters Degree in
Technology: Mechanical Engineering (MTechME)**

Under the supervision of

Dr. Oscar Philander (DTech, CPUT Bellville Campus)

CAPE TOWN, 2006

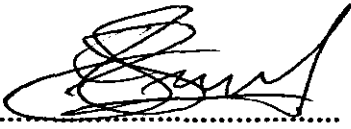
Declaration of Originality

This thesis work was conducted in the *Department of Mechanical Engineering* at the *Cape Peninsula University of Technology (CPUT)* and was submitted towards the partial fulfilment of the *Masters Degree in Technology: Mechanical Engineering*. During the research period the work contained in this thesis was carried out under the supervision and guidance of *Dr. O. Philander* at the university's *Bellville Campus*.

The specific research focus and the awareness of the technology presented in the thesis emanated from experience gained in the field of *Smart Materials*. Keen interest started in graduate level with research into *shape memory alloys* and its applications.

The experimental work detailed in *Chapter 2* was conducted in tandem with a fellow researcher in the *Smart Alignment Systems Research Group (SASRG)*, *Doctor Mukhawana*. His involvement with experimental data collection and related discussions is acknowledged.

The work presented for this degree is my own and has not been presented for a degree at this or any other institution. To my knowledge all other work of authors contained in this thesis, has been fully acknowledged.

A handwritten signature in black ink, appearing to read 'Sheldon Saal', is positioned above a horizontal dotted line.

Sheldon Saal (BtechME, PENTECH)
Smart Alignment Research Group
Cape Town, South Africa
June 2006

Acknowledgements

The author makes use of the opportunity to thank those whose efforts helped and supported him throughout this thesis work. I would like to thank the Father Almighty for blessing one with talents. This thesis is evidence of your continuous blessings of dedication, patience and persistence.

A special word of thanks to my supervisor, Dr Oscar Philander (Principal of SASRG) for his superb guidance and support through all my endeavours. Your constant work ethic, patience and motivation are second to none, and are thoroughly appreciated. Thanks to Mr. Keith Jacobs (HOD of Mechanical Engineering) and his colleagues for creating an atmosphere for constant learning and growth. Special mentions to Mornay Riddles (Rapid Prototyping Centre), Rozetta Ziegler and Andrew Cousins (post-graduate MechEng -UCT) for their active contribution. Their ideas and constructive criticism are acknowledged. The invaluable contribution of Prof G. Oliver, through his research guidance and extensive knowledge in a variety of subject matter, is noted and duly acknowledged.

The work has been supported by grants from the National Research Foundation (NRF) of South Africa. Their strong presence through funding for equipment and other necessities were of immense value. Sincere gratitude to

both the NRF and Cape Peninsula University of Technology for my scholarship during my years of study.

Many thanks to fellow graduates, Doctor Mukhawana, Zhe Xing, Selbourne Makhomo and Simphiwe Nqabisa for their involvement in an exciting project. Your support and sanity through extremely difficult times are appreciated.

A special word of thanks to my parents, Kobus and Margie Saal, for their undying support and faith in me. Your love and guidance brought me a long way and would continue to do so. To my younger brother, Wayne, thank you for your part in all of this. Finally I would like to thank the rest of my family and friends for their encouragement, love, and understanding during my studies.

Abstract

Recent years have witnessed a tremendous growth and significant advances in “smart” composites and “smart” composite structures. These smart composites integrate active elements such as sensors and actuators into a host structure to create improved or new functionalities through a clever choice of the active elements and/or a proper design of the structure. Such composites are able to sense a change in the environment and make a useful response by using an external feedback control system. Depending on their applications, smart composites usually make use of either the joint properties of the structure or the properties of the individual elements within the composites. The accumulation in the understanding of materials science and the rapid developments in computational capabilities have provided an even wider framework for the implementation of multi-functionality in composites and make “smart” composites “intelligent”.

This thesis is a contribution towards the global endeavour to innovate using smart structures to enhance our everyday lives. One of the phenomena of shape memory alloys, the shape memory effect was put to use in the development of an active surface. Here the pre-stressed shape memory alloy (in its de-twinned martensitic state) is surrounded or embedded in a non-SMA matrix material. This active surface can be used in a variety of applications that requires active shape control to change the shape of a flexible structure

member such as a submarine stern, aerospace control surfaces and aircraft wings.

An experimental protocol was developed to treat or stabilize shape memory alloys that are used as actuators within composite structures. Shape memory alloys exhibit complex behaviour during their quasi-plastic material response. The complex behaviour includes variability in yield values and the transformation region/range. Two treatment methods were employed to obtain similar behaviour (uniform mechanical properties) between neat SMA wires.

The remarkable behaviour, shape memory alloys exhibit, is categorized into two unique material responses, ascribed to thermo-elastic martensitic forward and reverse phase transformations, being the shape memory effect and the pseudo-elastic effect. The shape memory alloy actuator used in this study harnesses the shape memory effect, hence the investigation into an important aspect of the shape memory effect, the quasi-plastic material response. Although shape memory alloys exhibit this behaviour under different loading conditions when in its low temperature martensitic state, the behaviour was analysed under tensile loading conditions. These tests gave a good indication of the material's mechanical properties and provided the opportunity to create comparative plots of individual shape memory alloy wires.

All the tensile experiments on different rod geometries were conducted at the Strength of Materials Laboratory, Dept. Mechanical Engineering at the Cape Peninsula University's Bellville Campus.

A shape memory alloy hybrid composite (SMAHC) was manufactured using a novel approach. Nickel-Titanium (NiTi) wires were embedded into a very flexible polyurethane matrix through a vacuum casting process. Unlike the methodology used by Tsoi et al. [45] who built fixture jigs to constrain the shape memory alloy wires to the required amount of pre-strain, an easy lay-up technique was used which allowed the part to cure at room temperature. This manufacturing technique negated the danger of inducing the forward transformation of martensite to austenite, which is often caused by high

temperature curing (evident in most work, [27], [28], [37], [38], [43-46], [52], [54]).

To categorize the composite as smart or active, numerous tests were conducted to analyse the macroscopic behaviour of the SMA-polymer hybrid composite plates. Another experimental protocol was developed from these tests and was used to investigate:

- Active and Passive Deflection of the SMA-polymer hybrid composite;
- The change in flexural rigidity of the SMA-polymer hybrid composite as a function of ambient temperature conditions; and
- The time taken for the deformed SMA-polymer hybrid composite plate to return to an un-deformed configuration.

The deflection tests provided encouraging results that served as good foundation work for ongoing research. These tests quantified how shape memory alloys altered the structural properties of a smart composite plate.

Contents

CONTENTS PAGE

| | |
|---|---|
| Declaration of Originality | i |
| Acknowledgements | i |
| ii | |
| Abstract | |
| v | |
| Table of contents | |
| viii | |
| List of Figures | |
| xi | |
| List of Tables | |
| xvi | |

CHAPTER 1 INTRODUCTION

1.1 Problem Statement

1

1.1.1. Statement of the first sub-problem

2

1.1.2. Statement of the second sub-problem

2

1.2 Objectives

.....
2

1.3 Background

.....
4

1.4 Review of the related literature

.....
9

1.4.1 Characterization of the material

.....
9

1.4.2 Applications using the shape memory effect (SME)

.....
10

1.4.3 Super Elastic Applications

.....
11

1.4.4 A review on Smart Composites or Active Surfaces

.....
12

1.4.5 A review on Shape Memory Actuated Devices

.....
17

1.4.6 Review of experimental validation for SMA behaviour

.....
20

1.5 Scope of the thesis

.....
25

CHAPTER 2 PREPARATION OF SMA WIRES

2.1. Introduction

.....
26

2.2. Materials tested

.....
27

2.3. Experimental procedure

.....
28

2.4. Quasi-plastic material response exhibited by NiTi SMA

.....
29

2.5. Results and discussion

.....
30

2.6. Concluding Remarks

.....
35

2.6.1. Procedure for stabilizing SMA wire

.....
38

CHAPTER 3 MANUFACTURING OF A SMAHC

3.1 Introduction

.....
39

3.2 Manufacturing procedures

.....
41

3.2.1 Passive Applications

.....
41

| | |
|--|----|
| 3.2.2 Active Applications | 44 |
| 3.3 The manufacture of a polymeric composite with embedded SMAs | 47 |
| 3.3.1 Designing a RP master and mould making | 48 |
| 3.3.2 Embedding SMA and casting of part | 52 |
| 3.3.3 Part removal and finishing | 56 |
| CHAPTER 4 EXPERIMENTAL ANALYSIS ON SMAHC PLATE | |
| 4.1 Introduction | 58 |
| 4.2 Active and Passive Deflection Testing | 58 |
| 4.2.1 Conceptualising the theoretical model for passive testing | 59 |
| 4.2.2 The governing equation for deflection of plate | 61 |
| 4.2.3 Testing the deflection of passive SMAHC plates | 62 |
| 4.2.4 Testing of an active SMAHC | 68 |
| 4.3 The change in flexural rigidity as a function of ambient temperature | 70 |
| 4.4 Analysing the composite's recovery after deformation | 74 |
| 4.4.1 Objective | 74 |
| 4.4.2 Methodology | 74 |
| 4.4.3 Results and Discussions | 79 |
| CHAPTER 5 CONCLUSIONS | |
| 5.1 Conclusions | 83 |
| 5.1.1 Experimental Investigation | 84 |
| 5.1.2 The manufacturing of the composite | 85 |
| 5.1.3 The implementation of a testing technique | 86 |
| 5.2 Recommendations | 87 |
| REFERENCES | 89 |

APPENDICES

| | |
|--|----|
| Appendix A: Force Displacement Graphs of Experimental Results... .. | A1 |
| Appendix B: Plate thickness measurements..... | B1 |
| Appendix C: Load –deflection behaviour for SMAHC plates | C1 |
| Appendix D: Selected Load-deflection graphs for SMAHC plates | D1 |
| Appendix E: Deflection-of-beams calculations applied to SMAHC plates | E1 |

List of figures

Chapter 1

Figure 1.1: The Shape Memory effect and psuedo-elastic effect of Shape Memory Alloys [18]

Figure 1.2: Shape memory alloy adjustable camber (SMAAC) control surface internal actuator concept [2]

Figure 1.3: Schematic of Shape memory Effect in Stretching

Chapter 2

Figure 2.1: Graphical representation of three regions displayed by quasi-plasticity

Figure 2.2: Load – Extension behaviour for a 2mm diameter NiTi wire

Figure 2.3: Load – Displacement behaviour for a 3mm NiTi wire in tension

Figure 2.4: Load – Displacement behaviour for a 3mm NiTi wire after cycling

Figure 2.5: Comparative plot for an aged and untreated NiTi specimen

Figure 2.6: Load – Displacement behaviour for a 3mm NiTi wire subjected to thermo-mechanical cycles

Figure 2.7: Quasi-plastic behaviour of 3mm diameter NiTi shape memory alloy wires when (a) untreated / no heat treatment [47] and (b) aged at temperatures in excess of 200°C

Chapter 3

Figure 3.1: Fabrication procedure for SMA wire wound prepreg [53]

Figure 3.2: A typical SMA Composite frame, designed by EPFL [45]

Figure 3.3: The SMA-composite specimens after curing [45]

Figure 3.4: Schematic drawing of SMA/CFRP laminates.

Figure 3.5: Clamping device and mould [55]

Figure 3.6: Schematic of the plate detailing wire placement

Figure 3.7: Dummy plate with inserts simulating SMA wires

Figure 3.8: Parting plane and Suspenders on boundary of part

Figure 3.9: Completed box with suspended part

Figure 3.10: Mixing bucket for silicone

Figure 3.11: Liquid silicone in box

Figure 3.12: Vacuum chamber with silicone mould

Figure 3.13: Mould halved along cutting weave

Figure 3.14: Lacing/Embedding SMA wires into mould-base

Figure 3.15: Cavity with longitudinally laced SMA wire

Figure 3.16: Closing mould with staples along split-line

Figure 3.17: Measuring Cups for two-part resin

Figure 3.18: Part B resin added to the mixing bowl (part A)

Figure 3.19: Resin poured slowly from the tipper into the funnel

Figure 3.20: Polymer Composite plate with embedded SMA

Figure 3.21: Transparent Urethane from Smooth-On

Figure 3.22: Similar Urethane from Axson

Chapter 4

Figure 4.1: Top view of simply supported plate

Figure 4.2: Plate with loading condition

Figure 4.3: Top view of the plate with boundary conditions

Figure 4.4: Trends for a 4mm plate deflected by 8mm

Figure 4.5: Trends for the second 4mm plate deflected by 8mm

Figure 4.6: Load –displacement behaviour for 8mm plate

Figure 4.7: Experimental setup for deflection tests

Figure 4.8: Comparison of 8mm plate under different temperature conditions

Figure 4.9: Schematics of the deflection tests conducted with (a) no heating, (b) induced load and temperature, (c) induced temperature

Figure 4.10: 3D and cross-sectional view of the plates

Figure 4.11: Curved 4mm SMAHC plate

Figure 4.12: Curved 4mm SMAHC plate

Figure 4.13: Curved 6.7mm SMAHC plate

Figure 4.14: Curved 7.7mm SMAHC plate

Figure 4.15: A 4mm plate at the start of the experiment, $t = 0$ sec

Figure 4.16: The recovery of the plate after 90 seconds

Figure 4.17: Experimental set-up for imaging SMA plate deflections

Figure 4.18: SMAHC plate in the horizontal position

Figure 4.19: The SMAHC plate bulging (negative curvature)

Figure 4.20: End of experiment showing very slight positive curvature

List of tables

Chapter 2

Table 2.1: Properties and other data of SMA material

Chapter 3

Table 3.1: Properties of three Urethane plastics

Chapter 4

Table 4.1: Constants for uniformly loaded rectangular plates with simply supported edges [56]

Table 4.2: Experimental data imposed on deflection equation

Table 4.3: Temperature fluctuation during loading experiment

Table 4.4: Deflection of SMAHC plate at an elevated temperature

Table 4.5: Stiffness results for the various plates

Table 4.6: Data for the time elapsed (in seconds) during the tests of flattening the plates

Chapter 5

Table 5.1: The percentage increase in flexural rigidity of a SMAHC beam subjected to elevated temperatures

CHAPTER 1

Introduction

1.1 Problem Statement

As with so many other innovations, the natural evolution of structural materials started moving from searches for particular properties, through the need to reduce manufacturing and production costs, towards a greater flexibility and functionality of the part. Few if not all conventional structural composite materials can fulfil the last requirement, hence the recent interest in adaptive or smart composite materials. Shape Memory Alloys (SMAs) are such materials with abilities to change their material properties such as Young's Modulus and Damping capacity [38]. The generation of large internal forces [54], when it is integrated with composite material structures, allow active control of their static and dynamic behaviour.

The intention is to develop a smart composite to be used as an active surface with controllable shape. By embedding SMA elements into composite material structures one creates new materials and technologies that would enable more original and more advanced applications for composite materials.

1.1.1 Statement of the first sub-problem

By embedding shape memory elements into a host material novel material characteristics can be generated through the fusion of the two uniquely different materials. It is widely reported how complex the shape memory alloy behaviour is, which makes it difficult to predict the behaviour of the “new” material. Some of the complexities regarding shape memory alloys that were reported included the variability of elastic yield values, non-homogeneous transformation regions and inconsistent measures of strain. This proves that even before you can embed this smart material one should have a good account of its material behaviour.

This can be acquired through experimental techniques, in which some of these complexities are alleviated, that would provide consistent behaviour. The consistent behaviour of the shape memory alloys would make them predictable and attention can shift to the interface and the effect of the constraint placed by the surrounding matrix.

1.1.2 Statement of the second sub-problem

One of the major problems encountered during previous attempts at manufacturing composites with embedded SMA, is the SMA material behaviour at elevated curing temperatures (130-180°C). It is well documented that shape memory alloys transform to their initial state at elevated temperatures. When SMA's undergo this transformation during the curing process the behaviour of the embedded constituent is compromised and the composite loses its shape control ability. The design concept for the fabrication of the composite should include a low temperature curing process to prevent any transformation of the embedded shape memory alloy.

1.2 Objectives

This work is aimed at developing a shape memory alloy hybrid composite with active shape control (ASC). The conformability is controlled by an embedded shape memory alloy constituent thus becoming an “active surface”.

In order to succeed in the development of this structure a few key objectives should be met.

- Develop a protocol for preparation of SMA wires that need to be embedded into any host structure.
 - Characterize the quasi-plastic material response through repeated thermo mechanical cycling
 - Effect an aging treatment to reduce or erase the hardening like behaviour that was apparent in SMA rods.
- Manufacture an active surface
 - Determine a suitable composite fabrication technique that utilises low temperature curing.
 - Select the type, form and size of the shape memory element
 - Obtain a host material with suitable properties for the required application
- Establish the change in stiffness of the composite
 - Determine the flexural stiffness of the overall composite through beam or plate theory
 - Quantify what happens to the stiffness when the composite is heated at an elevated temperature
 - Compare the stiffness in room temperature to the stiffness of the composite material during elevated temperatures
- Establish the transformation time of the composite to return to its original configuration
 - Deform the material to a pre-determined shape
 - Heat the material (composite) at a temperature that is sufficient to actuate the shape memory alloys.
 - Record the time elapsed from the deformed to the original configuration

1.3 Background

There are a number of remarkable materials, such as shape memory alloys (SMAs), piezoelectric materials, magnetostrictive materials, etc., which exhibit strong coupling between their mechanical behaviour and other fields, such as thermal, electric or magnetic fields, respectively. These materials are often referred to as “interactive”, or “smart” materials, in that they sense a change in their environment and respond in a mechanical way. The unique properties of these materials are not new; having been discovered 30 to 60 years ago [18], yet their use for application in active structures is relatively new and recently seems to be gaining momentum.

One such application that is currently researched and investigated is the use of Shape Memory Alloy Hybrid Composites (SMAHC). Shape Memory Alloy Hybrid Composites are conventional composite structures with an embedded SMA constituent. Active applications use the SMA behaviour to control the shape of the composite structure [39]. In this study shape memory alloy wires are used to actuate a fairly thin composite structure thus bringing about a change in its shape. The surface of this composite/structure from here on in is termed the “active surface”.

To use the Shape Memory Alloy wire as actuator a complete understanding of the behaviour of this alloy have to be established before it is used in a desired application. Shape Memory Alloys compose of two Metallurgical phases, i.e. Martensite and Austenite [49]. This alloy has the amazing property of forward and reverse thermo-elastic martensitic transformation. When cooled to the critical temperature the SMA will mainly compose of martensite and can easily be manipulated to give very large strain ranges [49]. When heated above a critical temperature the alloy will change back to its Austenitic phase. The previous elastic strain recovers and the alloy resumes the shape it normally has at high temperatures, i.e. the shape memory effect [49]. At high temperature the applied stress may cause martensitic transformation and the SMA may deform apparently plastically, both of which may be recovered as applied stress is removed. This alloy exhibits two unique characteristics: the shape memory effect and psuedo-elasticity as seen in figure 1.1.

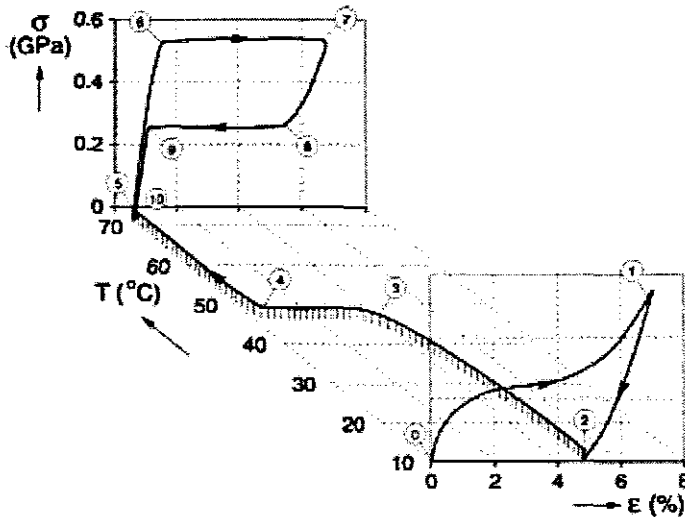


Figure 1.1: The Shape Memory effect and psuedo-elastic effect of Shape Memory Alloys [18]

The shape memory effect (given by the indications 0-4 on the graph above) is the alloy's ability to be mechanically deformed (seemingly permanent) at a temperature below a certain transition temperature. The material will then return to its original shape when heated above transition temperature [7]. This remarkable phenomenon is used in the development of the "active surface". (See figure 3 for a schematic of this characteristic). Psuedo-elasticity (5 – 10) refers to the materials ability to be strained significantly and return to its unstrained state when load is removed. Both this phase and the shape memory effect can be obtained from temperature-induced or stress-induced transformation [49].

In an attempt to clarify the concept used within this thesis focus is drawn on adaptive materials and hybrid composites. Jan Van Humbeeck [2] makes a valid and seemingly very accurate observation when he concurs that Smart, adaptive, functional, intelligent are terms that seem to confuse many authors since they are often used for the same material or structure. He is of the opinion that it has more to do with some opportunism in drawing attention, than with a correct description of the reality. For the sake of clarity the author emphasized that SMA by themselves are not smart materials. Depending on the goal of their use, they can be classified as adaptive or functional.

Smart materials involve, per definition, three functions: sensor, actuator, and control [51]. Those three functions are generally combined by using different materials in combination with a control unit. Combination of several materials leads to structural elements that can be called hybrid composites. Hybrid composites connected with a control unit can then be used eventually as a smart structure.

The sensing functions of SMA are limited. Temperature changes, if in the appropriate range, will be directly converted in a shape change or a recovery stress. Both effects allow the component, of which the SMA element can be part, to adapt its shape or its performance to the environmental temperature. In case the SMA element is purposely heated, it does not act as a sensor but as an actuator. We should also distinguish between adaptive or smart control by SMAs and the performance of SMAs embedded in a matrix (hybrid composite).

Adaptive control is generally a topic in smart material conferences and publications, but regarding the SMAs it is an effective use of an SMA element as an actuator. The use of a torsion tube for trailing the edge trim tab control on helicopter rotors is a typical example of the smart blade technology [2]. The main goal of this technology is to reduce noise and vibrations, leading to a higher efficiency and significant noise reduction in the environment. Another envisaged application is the smart wing for aeroplanes. For similar reasons as in the helicopter rotor blades, the shape of the wing should be adaptive, depending for example on the actual speed of the plane, at the same time improving efficiency and noise reduction. An example of such a wing has been described in work by Beauchamps et al. entitled: Shape memory alloy adjustable camber (SMAAC) control surfaces. A drawing of this smart wing is shown in Fig. 1.2. The SMAAC control surface concept is an adjustable camber foil, which is actuated by SMA wires to control the flight of hydrodynamic or aerodynamic vehicles.

The SMAAC concept employs a flexible spring backbone, which is actuated by contracting SMA wires and is covered by a pliable elastomer skin to produce an adjustable foil shape. The advantage of such a system is a much higher lift force than rigid foils in particular cases and a much smaller wake behind the SMAAC foil than the rigid foil at an equivalent lift.

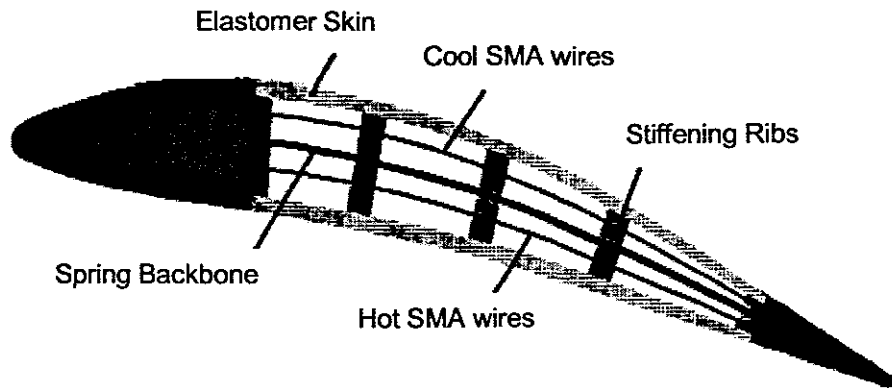


Figure 1.2: Shape memory alloy adjustable camber (SMAAC) control surface internal actuator concept [2].

More important for future new technologies are hybrid composites in which SMAs can perform their specific role. The most envisaged applications for SMAHC were summarised by Van Humbeeck as follows:

- **Active strain energy tuning (ASET)**

Restrained wires are embedded in the matrix. If such a composite plate vibrates at resonance, the wires can be heated which will develop a recovery stress at the composite matrix wire interface. This produces a change in energy balance.

- **Active modal modification (AMM)**

Unstrained wires are embedded. To change the modal response, the wires are heated resulting in a large increase of the elastic modulus of wires during the martensitic transformation.

- **Active shape control (ASC)**

The shape memory effect is used to change the shape of the composite matrix.

- **(Active) Fatigue life and impact resistance improvement (self-repairing or self-healing)**

Super-elastic embedded deformed wires create compressive stresses inhibiting crack growth and even promoting crack closure. Embedded strained martensitic wires can also be activated by heating.

- **(Active) Stress-relaxation**

Stress- or strain-induced martensite can relax imposed stresses due to specific loading, differences in thermal expansion coefficients or thermal shocks. Depending on the type of application, the SMAs can be embedded as thin wires, fibres, particles, thin films, while the matrix can be metallic material, ceramics, polymers or composites.

A very detailed overview on SMAs and hybrid composites for smart systems has been prepared recently by Wei et al. [53], while another interesting review can be found in the work from Paine and Rogers. [52].

One of the main problems however is the production of hybrid composites. Temperature limitations during processing (i.e. curing), the problems of interfacial bonding and related void formation, influence of edge-effects, the influence of the constraining effects of the surrounding matrix on the transformation characteristics of the embedded SMA create limiting constraints and are the subject of important research projects.

1.4 The review of the related literature

An extensive literature review into SMAs concentrated on research conducted on SMAs, the concept of Smart Composites or Active surfaces, Smart Devices and Experimental Analysis on the material.

1.4.1 Characterization of the material

Shape Memory Alloys (SMAs) is a group of metallic materials that demonstrate the ability to return to some previously defined shape or size when subjected to the appropriate thermal procedure. Generally, these materials can be plastically deformed at some relatively low temperature, and upon exposure to some higher temperature will return to their shape prior to the deformation [25].

In 1932 Chang and Read recorded the first observation of the shape memory transformation [25]. They noted the reversibility of the transformation in AuCd by metallographic observations and resistivity changes, and in 1951 the shape memory effect (SME) was observed in a bent bar of AuCd. In 1938, the transformation was seen in brass (CuZn). However, it was not until 1962, when Buehler discovered the effect in equiatomic nickel-titanium (NiTi), that research into both the metallurgy and potential practical uses began in earnest. Within 10 years, a number of commercial products were on the market, and understanding of the effect was much advanced. As the shape memory effect became better understood, a number of other alloy systems that exhibited shape memory were investigated. Of all these systems, the NiTi alloys and a few of the copper-base alloys have received the most development effort and commercial exploitation.

In some applications, the shape memory component is designed to exert force over a considerable range of motion, often for many cycles. Such an application is the circuit-board edge connector made by Beta Phase Inc. [12]. In this electrical connector system, the SMA component is used to force open a spring when the connector is heated.

This allows force-free insertion or withdrawal of a circuit board in the connector. Upon cooling, the NiTi (Nickel Titanium) actuator becomes weaker and the spring easily deforms the actuator while it closes tightly on the circuit board and forms the connections.

Based on the same principle, CuZnAl shape memory alloys have found several applications in this area. One such example is a fire safety valve, which incorporates a CuZnAl actuator designed to shut off toxic or flammable gas flow when fire occurs.

1.4.2 Applications using the shape memory effect (SME)

There are a wide variety of uses for the shape memory alloys. The following will illustrate one or two products in several categories of application.

1.4.2.1 Free recovery

This is illustrated when an SMA component is deformed while martensitic, and the only function required of the shape memory is that the component return to its previous shape (while doing minimal work) upon heating. A prime application of this is the blood-clot filter developed by M. Simon [14]. The NiTi wire is shaped to anchor itself in a vein and catch passing clots. The part is chilled so it can be collapsed and inserted into the vein, then body heat is sufficient to turn the part to its functional shape.

1.4.2.2 Constrained Recovery

The most successful example of this type of product is undoubtedly the Cryofit hydraulic couplings made by Raychem Corporation [15]. These fittings are manufactured as cylindrical sleeves slightly smaller than the metal tubing they are to join. Their diameters are then expanded while martensitic, and, upon warming to austenite, they shrink in diameter and strongly hold the tube ends.

The tubes prevent the coupling from fully recovering its manufactured shape, and the stresses created, as the coupling attempts to do so are great enough to create a joint that, in many ways, is superior to a weld.

Similar to the Cryofit coupling, the Betalloy coupling [16] is a CuZnAl coupling also designed and marketed by Raychem Corporation for copper and aluminium tubing. In this application, the CuZnAl shape memory cylinder shrinks on heating and acts as a driver to squeeze a tubular liner onto the tubes being joined. A sealant coating on the liner enhances the joint strength.

1.4.2.3 Proportional Control

It is possible to use only a part of the shape recovery to accurately position a mechanism by using only a selected portion of the recovery because the transformation occurs over a range of temperatures rather than at a single temperature. A device has been developed by Beta Phase Inc. [17] in which a valve controls the rate of fluid flow by carefully heating a shape-memory alloy component just enough to close the valve the desired amount. Repeatable positioning within 0.25 millimetres is possible with this technique.

1.4.3 Super-elastic Applications

A number of products have been brought to market that use the pseudo-elastic (or superelastic) property of these alloys. Eyeglass frames that use superelastic NiTi to absorb large deformations without damaging the frames are now marketed, and guide wires for steering catheters into vessels in the body have been developed using NiTi wire, which resists permanent deformation if bent severely. Arch wires for orthodontic correction using NiTi have been used for many years to give large rapid movement of teeth.

The properties of the NiTi alloys, particularly, indicate their probable greater use in biomedical applications. The material is extremely corrosion resistant, demonstrates excellent biocompatibility, can be fabricated into the very small

sizes often required, and has properties of elasticity and force delivery that allow uses not possible in any other way.

1.4.4 A review on 'Smart' Composites or Active Surfaces

One of the phenomena of shape memory alloys, the shape memory effect was put to use in the development of active or smart composites [34], [35], [36]. Here the pre-stressed shape memory alloy (in its de-twinned martensitic state) is surrounded or embedded in a non-SMA matrix material.

The idea of embedding shape memory alloys in a matrix material started in 1988 when Rogers and Robertshaw [26] introduced SMA actuators in a composite laminate for structural control.

Liang, Jia and Rogers [27] built on this work and subsequently became of the first researches to embed NiTi wires into a polymer. Their attempt proved unsuccessful due to poor interfacial bonding between the SMA wires and the polymer. This led to Chaudry and Rogers [28] incorporating their shape memory alloy wires into a polymer using mechanical fasteners. Later Baz and Ro [29] embedded the wires through coupling sleeves in the host material.

In 1993 Bidaux, Bataillard et al. [11] measured significant differences in the dynamic behaviour between plain SMA wires and SMAs polymer composites. This change in response indicated that only the ends of the embedded wires transformed. The studies into the behaviour started to increase as Paine and Rogers [30] reported that process induced residual stresses alter the martensite and austenite start temperatures of SMA wires embedded in an elastomeric composite.

Furuya and Taya et al. [31] found that embedding SMA fibres in an elastoplastic metal matrix will enhance overall yield and hardening characteristics of the composite at an elevated temperature if the shape memory alloys are properly prestrained at low temperature.

Shape memory alloy composites can be used as actuating surfaces in structures, to reduce vibration, enhance impact damage resistance and crash worthiness of structures, or shape control. Liang and Rogers reported on the use of these active metal matrix composites in helicopter rotor blades [27]. Chaudry and Rogers and Hughes and Wen [32] used SMAs in active shape control applications to be used in mechanisms such as the adaptive aerodynamic lifting surface or variable camber wing.

The shape memory alloy component within the composite can be used actively or passively. Boyd and Lagoudas [34] and Lagoudas et al. [35], [36] made use of both forms when they used the SMA in active and passive applications.

There are different ways in which embedded SMAs can be used actively. Active applications use the SMA behaviour to control the shape of the composite structure [39]. Birman and Lee [40] used another such way, as they used the SMA behaviour to alter the buckling response of the composite structure.

Passive applications use the shape memory alloy components to change the composite's stiffness [34], to strengthen the composite, and to close or repair cracks [39].

The matrix or host materials that have been used included polymers [27], [28], [29], metals, and even plaster. Gupta Sawhney et al. used a fiber-glass epoxy and the work by Lee and Lee [40] featured a carbon-epoxy composite.

By this time the research increased steadily, ultimately leading up to a contribution by Paine and Rogers in which the pair reviewed SMA hybrid composites and their applications. Hebda and White [37] examined issues in the manufacturing of composites such as void content and the SMA wire training effects. With the abovementioned authors focussing on the manufacturing process more findings came to the fore in work by Hebda,

White et al. [38]. They discussed the issue of local residual stresses in regard to manufacturing high quality SMA composites.

Kline, Jonnalagadda and Sottos utilised photoelasticity to investigate the interaction between embedded SMA wires and a polymer matrix. The same method was used to quantify the internal stresses induced by the actuation of thin SMA ribbon in a polymer matrix by Jonnalagadda, Sottos et al [1].

In 2001 Travis Turner developed a thermomechanical model to study the static and dynamic response of shape memory alloy hybrid composite (SMAHC) structures. He followed this study up with results from an experimental validation of his thermoelastic model for SMAHC structures. The model captures the material nonlinearity of the material system with temperature and is capable of modelling constrained, restrained, or free recovery behaviour. The author provided static and dynamic experimental configurations for the SMAHC specimens and presented the results for thermal post-buckling and random response. Excellent agreement was achieved between his measured and predicted results, fully validating the theoretical model for constrained recovery behaviour of SMAHC structures.

Turner, Lach & Cano [43] discussed the fabrication and characterisation of a SMAs hybrid composite. They fabricated beam specimens from their conventional SMAHC and discussed the practical fabrication issues others before them encountered. In a typical application, such as adaptive stiffening of aerospace structures the SMA elements would be activated through an inherently elevated temperature of the service environment. This effect can be simulated in experiments by various means, of which the most practical is resistive heating [43]. Resistive heating has the advantages of simple heating, relatively uniform heating, and excellent controllability.

The abovementioned investigators selected a glass-epoxy for the matrix material system to avoid any potential electrical conduction problems. Their material system also afforded them the added advantage of visual flaw detection due to its translucency.

For the actuator component they used NiTi ribbons, in lieu of NiTi wires, to *simplify the fabrication procedure, allow for more flexibility in fabrication, and desensitise the actuators to interface voids and stress concentrations*. Turner, Lach and Cano adopted this approach because they felt that recent SMAHC fabrication efforts involving wire-type actuators have suffered from various disadvantages.

These disadvantages include complicated fabrication procedures because of the relatively large number of actuators usually needed, sensitivity to actuator/matrix interface flaws because voids can be of significant relative size, *and relatively high rate of actuator breakage during cure because of sensitivity to stress concentrations at the mechanical restraints* [43]. Finally, they reason that it is difficult to achieve a desirable overall volume fraction of SMA in wire form when trying to optimise the integration of the actuators by placing them in only selected layers. Conversely, ribbon-type SMA elements can be placed in strips cut out of particular matrix laminae to result in a rather simple lay-up operation, while keeping the volume fraction high in the desired locations.

The key aspect of this adaptation of shape memory alloys is whether the unique capabilities of the material are being suppressed by embedding/constraining the wires. To this extend Tsoi, Stalmans and Schrooten [45] investigated and discussed the transformational behaviour of SMA wires embedded into a fibre reinforced epoxy composite. The effects on the transformational temperature, heats of embedded SMA wires and generation of recovery stresses within the composites shown to be related to reversible martensitic transformation of SMA wires. Their contribution detailed the effects of the constraining matrix on the transformations of self-accommodating and preferentially oriented martensite. It was found that there was little change in the transformation temperatures of the constrained SMA wires with increasing pre-strain, but that the measurable transformation heat decrease significantly with increasing pre-strain.

They concluded that the transformation of self-accommodating martensite is *nearly not affected by the constrained matrix*, whereas the transformation of the preferentially oriented martensite is suppressed.

Thanks to the amount of research now spent on SMAHC the many drawbacks, that were so evident in early attempts, are becoming fewer. The fabrication methods and processes evolved to the extend where Masuda, Sone et al. [46] conducted a feasibility study to investigate the future potential of textile composites with shape memory alloys. In a recently published journal paper they presented two different ideas of SMA-based textile composites. *The first of which was using SMA wire in the form of woven fabric.* They expected that by using woven SMAs the resulting composite plate would become quasi-isotropic, and that the fabrication process would become handier because a piece of woven SMA can be handled as a preformed independent layer. Their second idea involved combining SMA wires with the textile performs by stitching techniques. The stitched SMA wires were expected to give the composites multi-functions such as tunable stiffness and damping capacity, active actuation and sensing capability.

The dynamic behaviour of the fabricated specimens, in particular focussing on the stiffness tuning capability, was investigated by simple impact vibration tests. Although the stiffening effect observed was much less than they anticipated, it could be improved by increasing the volume fraction of SMA, and by controlling the pre-strain more accurately during the lamination process.

The response of SMAs composites has been simulated using a variety of methods, including micro-mechanical methods and finite element analysis. In the finite element approach, one method is to develop special composite elements. Lagoudas, Moorthy et al. [33] simulated the response of SMAs composites through the finite element approach using multi-layered composite plates in the analysis. The same accounted for Marfia, Sacco et al who used a layered beam in 2003. A more general way of using finite element analysis for composites models the matrix and the reinforcing members separately.

Several researches pursued this strategy for a composite beam actuated by *SMA wires or ribbons bonded to the matrix* [41], [42].

One recent study performed a finite element analysis of the buckling of a laminated composite shell with one-dimensional elements for wires; however the SMA model did not consider twinned martensite [40].

1.4.5 A review on Shape Memory Actuated devices

Shape memory alloys have been the subject of active research for over three decades due to their many unique attributes and the resulting potential for a variety of applications. Early work focused on alloy characterization and discovery of the micro-mechanics causing the unique properties. A variety of applications ranging from self-erecting structures and energy-conversion devices to thermally actuated fasteners and biomedical devices were also identified in this early effort [21].

Metallurgical work in recent years has seen significant growth, partly due to a substantial increase in applications research that has been stimulated by interest from the biomedical and smart materials communities. Recent (the last two decades) smart materials and structures work have shown that SMAs have significant potential for vibration, structural acoustic, and structural shape control applications.

Van Humbeeck [2] reviewed all the non-medical applications involving SMAs quite extensively and Birman [3] published a comprehensive review of the work performed in the areas of SMA constitutive modelling and applications.

These smart materials possess two quite unique phenomena, which is used with success in commercial products [2]. It is important however to attain detailed knowledge of the materials behaviour before attempting to use it in any application. To this extend the shape memory effect and pseudo-elastic behaviour is investigated.

(a) The Shape Memory Effect

The shape memory effect (indicated in Fig.1.3) is caused by a temperature dependent crystal structure. When an SMA is below its phase transformation temperature, it possesses a low yield strength crystallography referred to as Martensite [4]. While in this state, the material can be deformed into other shapes with relatively little force. The new shape is retained provided the material is kept below its transformation temperature. When heated above this temperature, the material reverts to its parent structure known as Austenite causing it to return to its original shape.

The following figure explain the shape memory effect schematically

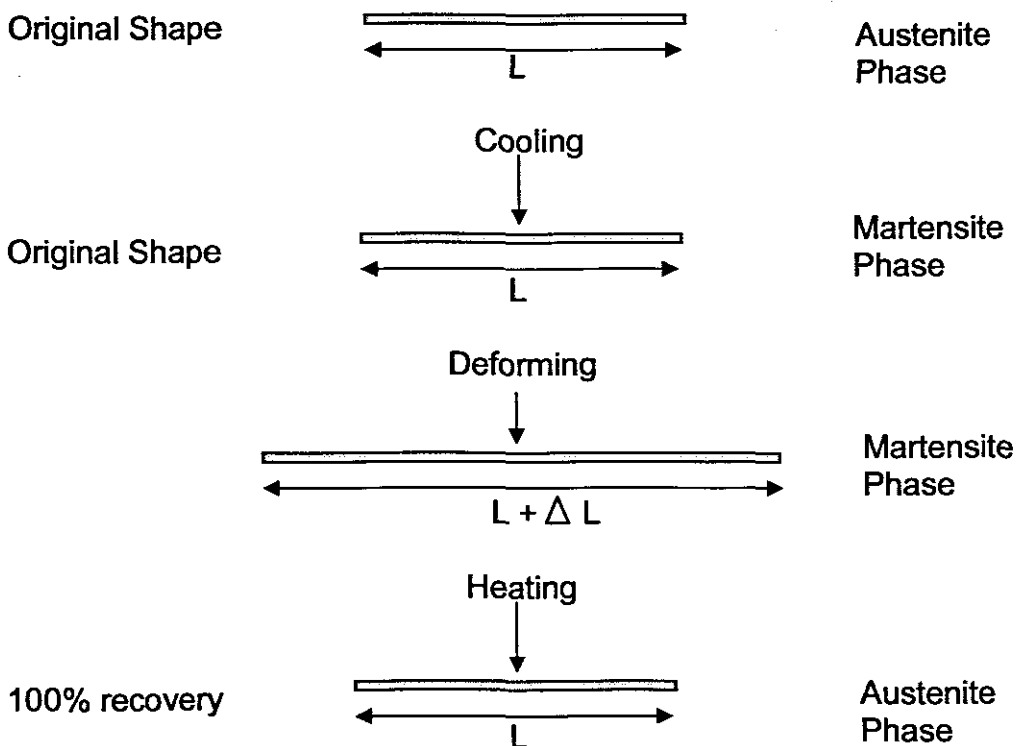


Figure 1.3: Schematic of Shape memory Effect in Stretching

(b) Pseudo-elasticity

At conditions above the transformation temperature the material can be deformed to obtain relatively large strains by mechanical loading.

The difference here however is that because of the elevated temperature, the material “springs” back to its original dimensions. This phenomenon that occurs at a single temperature is known as the pseudo-elastic effect. It is pseudo-elastic in the sense that the strain is completely recovered, but the loading cycle is path dependant, known to be hysteretic (lag in effect) path.

In order to understand what causes the Shape Memory effect one needs to study the crystallography and numerical modelling of the martensitic microstructure and its phase transformations. The work provided by Bhattacharya gives a good account of this. In the low temperature state, SMAs exist as different variants of martensite commonly known as the martensitic twinned variants or the product phase.

The material will remain in this state until intervention in the form of an external stimulus takes place. The external intervention will either transform the material’s crystallographic structure to austenite through a temperature induced transformation that cause no change in the materials macroscopic appearance, or a de-twinned martensite through a stress-induced transformation at low temperature. Stress-induced transformation causes only those twinned martensite variants that are sensitive to the applied stress to reorientate and induce a change in the macroscopic dimensions of the material. The apparent plastic deformation (described above as the change in macroscopic dimensions) that occurs due to the stress-induced transformation will remain until an increase in temperature transforms this de-twinned martensite back to austenite.

Upon cooling from the austenite region the material will once again transform to the twinned variants of martensite with no residual stresses. This back and forth transformation is what is termed the shape memory effect. The transformation from de-twinned martensite to austenite produces an actuation force that can be used in various engineering systems. The magnitude of this force is dependant on a number of factors that may include the dimensions of the material, the degree to which the twinned martensite was transformed, the

type of loading applied (tension, compression torsion etc.) and the type of heating (electrical or ambient).

At high temperatures when the material is in its austenite state [47], and subjected to mechanical loading, it will first perform elastically as what is expected of most crystalline solids. The elasticity of the material will remain until a yielding or transformation stress is reached. The austenite will now transform to de-twinned martensite and induce a macroscopic change in the material's dimensions. Macroscopically this change is similar to the hardening phenomenon of classical engineering steels [47]. Upon subsequent unloading from this region however, the material follows a hysteretic unloading path. During this process all the de-twinned martensite transforms back to austenite and the material regains its original dimensions. The hysteretic loading and unloading process that takes effect is what is known as pseudo-elasticity or the pseudo-elastic effect with inherent energy dissipation.

The impact of this smart actuator gained momentum as researchers used micro-miniature shape memory alloy actuators in robotic systems where strain measurements from the actuator were used for position feedback. Davidson et al. [57] and Jardine et al. [58] investigated the usage of shape memory alloys for torque tube actuators in aircraft wings. Rediniotis et al. reported on how he used shape memory alloys as actuation devices for hyper silent naval submersibles [59].

The pseudo-elastic effect and its inherent energy dissipation could be used in innovative applications as reported by Deurig et al. [60]. Sachdeva and Miyazaki [61] found applications for pseudo-elasticity in orthodontic wires and the energy dissipation of shape memory alloys were used for damping applications by Graesser and Cozzarelli [68] and Boyd and Lagoudas [36].

1.4.6 Review of experimental validation for SMAs behaviour

It is conclusive that the unique material responses that shape memory alloys exhibit lies within its austenite (A) \leftrightarrow twinned martensite (M^T) transformation

upon heating or cooling, the austenite (A) \leftrightarrow de-twinned martensite (M^{DT}) transformation at elevated temperatures due to an induced stress and the twinned martensite (M^T) \Rightarrow de-twinned martensite (M^{DT}) transformation at low temperature due to an induced stress (either tension, compression, tension, etc.) These phase transformations have been the focus and basis of many experimental studies since the discovery of shape memory alloys 40 years ago [9], [22].

The early pioneers reported that the remarkable behaviour of shape memory alloys is caused by interplay of a high temperature austenite phase and low temperature martensite phase [18], [19], [20]. Furthermore, Wasilewski et al. [62], and Miyazaki et al. [63] demonstrated that the transformation temperature and other properties of shape memory alloys could be altered by small changes in the compositions of the alloy and by various thermo-mechanical heat treatments. Shaw [6] reported that most researchers used a differential scanning calorimeter to study the phase transformations exhibited by shape memory alloys.

For most practical engineering applications, shape memory alloys are usually used in NiTi alloy wire forms [21]. After the shape memory effect was first observed in NiTi alloys a great amount of metallurgical research has gone into it and Wasilewski and Miyazaki were among the first researchers to experimentally study NiTi [6]. These experiments looked at the effects of strain range, temperature and mechanical cycling on NiTi alloys.

Due to the complexities of the energy dissipation associated with the hysteretic nature of pseudo-elastic behaviour, most researchers appeared to study this phenomenon experimentally more than the shape memory effect. Wayman et al. [64] were among these researchers while Muller and Xu, and Fu, Muller and Xu were among the first to experimentally study the interior of the hysteresis loop [65], [22].

Shaw and Kyriakides [7] found that the pseudo-elastic material response of shape memory alloys is associated with significant temperature variations.

Furthermore, the stress-induced austenite (A) \leftrightarrow de-twinned martensite (M^{DT}) transformation at elevated temperatures occurs in well defined stress-temperature regions, it is dependant on the kind of mechanical - loading – unloading and thermal – heating-cooling cycles, and the combined effects of the mechanical and thermal cycles.

The stress-induced austenite (A) \leftrightarrow de-twinned martensite (M^{DT}) transformation at elevated temperatures is an unstable transformation and thus produces inhomogeneous macroscopic deformations [19], [7], [23]. From a crystallographic point of view, the de-twinned martensite (M^{DT}) nucleates and grows as interfaces within the austenite phase until all the austenite has transformed to de-twinned (M^{DT}). Ingo Muller [22] indicated that pioneers like Larche and Cahn, Robin, Heidug and Lemer, and Johnson and Alexander were among the first researchers to study the equilibrium conditions of these interfaces and motion of the interfaces between regions of two phases. Salzbrenner and Cohen [66] performed investigations to study the motion of these interfaces by controlling the temperature.

The most detailed and beneficial experimental investigations into the unstable transformation and inhomogeneous macroscopic deformation of shape memory alloys, was provided by the work of Shaw and Kyriakides [7], [23], [24]. A brief summary of their findings follows below:

- Experimental observations show that stress-induced martensitic transformation in certain polycrystalline NiTi shape memory alloy can lead to strain localization and propagation phenomena when uniaxially loaded in tension;
- The Number of nucleation events and kinetics of transformation fronts were found to be sensitive to the nature of ambient media and imposed loading rate due to release / absorption of latent heat and the material's inherent temperature sensitivity of transformation stress;
- Nucleation stress is higher than the transformation stress;
- During unstable transformation, deformation is distinctly inhomogeneous;

- Each nucleation spawns 2 transition fronts and active deformation of the transition fronts is limited to the neighbourhood of these fronts;
- As a result, latent heat is released in discrete local regions rather than distributed over the entire length of the specimen (suggest strong thermo-mechanical coupling);
- Higher nucleation stress and displacement rates results in multiple fronts;
- Coexisting fronts travel at the same speed;
- The front speed is proportional to the rate of the applied end displacement;
- The front speed is inversely proportional to the number of active fronts;
- More proportions of fronts implies lower front speed and reduced local rate of heating;
- Distinct instability and Luders-like deformations occurs under isothermal conditions;
- Within an insulating media and higher loading rates the material cause self-heating, which leads to higher force-displacement response and multiple transformation fronts; and
- As the number of fronts increase the deformation appears to become homogeneous.

The type of loading cycle (tension, compression, torsion, etc.) to induce the austenite (A) \leftrightarrow de-twinned martensite (M^{DT}) transformation at elevated temperatures, and the twinned martensite (M^T) \Rightarrow de-twinned martensite (M^{DT}) transformation at low temperature also has important implications to the shape memory alloy material response [47]. Adler et al. [67] showed experimentally that shape memory alloys subjected to compressive loading showed lower recoverable strains, steeper hardening behaviour, and higher transformation stress levels compared to tensile behaviour. Leo et al. [69], Shaw and Kyriakides [24], Sittners et al. [70], Gall et al. [71], and Zang et al. [72] studied the effects of tension – compression asymmetry on shape memory material response.

Gall and Sehitoglu [71] performed experiments on one-dimensional shape memory alloy bars loaded in tension and compression. Their results showed that the shape memory alloys phase transformations is influenced by the texture of the specimen.

Experimental work by Sittner et al. [70] studied the three-dimensional constitutive behaviour of shape memory alloys. They investigated the stabilization of transformation behaviour in stress-induced martensitic transformation in NiTi alloy hollow bar. The loading cycles were for combined Tension and Torsion. The specimen was then loaded either in tension or torsion. The results revealed strain anisotropy, which implies the existence of other strain components.

Lim and McDowell [73] conducted experiments on shape memory alloy torque tubes using proportional and non-proportional loading conditions. They investigated the stress-temperature coupling in tension, torsion and compression. Their results showed that more latent heat was available in compression, notable in the larger temperature increases in compression than in tension for the completion of a phase transformation. They also found that the thermo – mechanical behaviour in positive and negative torsion was found to be symmetrical.

This review revealed that all these experimental efforts attempted to bridge the gap between the microscopic and macroscopic material responses of shape memory alloys. The experimental findings detailed above shows the strong coupling between thermal and mechanical properties of shape memory alloys. The mechanical material response is dependent on many factors including temperature, strain range, thermo-mechanical history loading rate, specimen geometry, nature of ambient medium, and the interactions of some of these [23-24]. Phase transformations associated with the shape memory effect and the pseudo-elastic effect produces unstable material behaviour and inhomogeneous deformations due to the propagating phase transformation phenomena, which is also temperature and load dependant. Added to this is the sensitivity of the phase transformations on magnitude and type of the applied loading and unloading conditions [47].

All of these material complexities make the full commercialisation of shape memory alloy based products (especially those related to smart composites) an enormous task.

1.5 Scope of the thesis

Chapter 2 describes the procedure followed during an experimental investigation that was conducted on Nickel-Titanium (NiTi) shape memory alloy wires. Based on the experimental findings from two employed techniques a protocol was proposed to stabilize SMA wires before they are embedded into a host matrix

Chapter 3 provides a comprehensive description of the manufacturing technique used to produce a shape memory alloy hybrid composite (SMAHC).

Chapter 4 introduces an experimental testing technique to be used in analysing shape control and proposes a method to verify the experimental data

CHAPTER 2

Preparation of SMA wires through heat treatment and cycling procedures

2.1 Introduction

The shape memory effect (SME) in NiTi is linked to the recovery of an apparent deformation when a load is applied to this material. Substantial recovery stresses (up to 800 MPa [53]) are generated when this shape recovery is restrained during heating. These stresses are released during cooling or during the complete strain recovery. The ability to generate relatively high recovery stresses, even during a partial strain recovery, arises in many devices such as bias-type two-way shape memory components, SMA pipe couplings, robot applications, and SMA composites [52].

SMA composites are outcomes of a relatively new research field that combines properties of a matrix with the functional properties of SMA elements, such as wires [43, 3], ribbons, and particles, embedded in the matrix. The selection of the proper type, shape and size is crucial for obtaining the optimum functional behaviour of SMA composites. The functional properties of SMA composites are a direct outcome of the peculiar thermo-mechanical behaviour of the embedded SMA wires. In this respect, the ability of the SMA wires to generate high recovery stresses is the most relevant shape memory property. The generation of recovery stresses is also affected by the stiffness and thermal expansion of the matrix. In this work shape

memory alloy wires are used as actuators to impart strain to a surrounding matrix hence bringing about a change of shape in the structure. It becomes imperative that the shape memory elements all behave uniformly and that same amount of recovery strain is imparted by all the wires to bring forth significant levels of shape change.

As reported earlier the exhibition of the shape memory effect is directly related to the amount of subsequent recovery strain. To this extend all the shape memory alloys need to have similar thermo-mechanical properties and this can be ensured through the application of 'training' techniques. This chapter describes the experimental procedure that was followed, discuss the resulting findings from the experiments and concludes by proposing a method to "stabilize" shape memory alloys. The experiments were all conducted in the Strength of Materials Laboratory, Dept. Mechanical Engineering at the Cape Peninsula University of Technology, Bellville Campus.

2.2 Materials Tested

The experiments were performed on commercially available NiTi shape memory alloy wires of different diameters. The material (1, 2 and 3mm in diameter) was obtained from an American supplier, Johnson Matthey, with properties displayed in Table 2.1. The supplier provided these properties for the as-packaged material, but the transformation temperatures could not be verified through the absence of a differential scanning calorimeter.

| Diameter (mm) | Chemical Composition | | | | | Temper | Surface | Active Af (°C) |
|---|----------------------|-------|--------|--------|------------------|-------------------|---------|----------------|
| | Ni | Ti | C | O | Total All Others | | | |
| 1 | 55.32 | 44.67 | ≤ 0.05 | ≤ 0.05 | 0.2 | Straight Annealed | Oxide | 60.7 |
| 2 | 55.38 | 44.62 | ≤ 0.05 | ≤ 0.05 | ≤ 0.20 | Straight Annealed | Oxide | 60.5 |
| 3 | 55.32 | 44.67 | ≤ 0.05 | ≤ 0.05 | ≤ 0.30 | Straight Annealed | Oxide | 73 |
| All Others are components: Al, Co, Cr, Cu, Fe, Mn, Mo, Nb, Si, W | | | | | | | | |
| These materials were obtained from Johnson Matthey, San Jose, CA, USA | | | | | | | | |

Table 2.1: Properties and other data of SMA material

2.3 Experimental procedure

A composite plate of 6 or 5mm diameter was initially considered, hence the decision to test NiTi shape memory alloy wires of both 3mm and 2mm diameters. The dimensions of the final composite was based on a rectangular “dummy plate” made of PERSPEX with the following dimensions: 308 × 294 × 6mm. The width of the plate was subdivided into 9 equal parts, resulting in 8 wires equally spaced and 32mm apart. Subsequently, 32 specimens were cut from a wire reel into 340mm long each, using an industrial bolt cutter. These specimens were then divided into four sets equating to eight specimens per set. Each set were placed in a KILN, which is a scaled down furnace, at 200, 250, 300 and 350 degree Celsius respectively. The specimens were placed in the furnace for ten hours to ensure that all the specimens transformed to their parent structure, i.e. austenite ($A_f = 70^\circ\text{C}$). After the ten hours, the specimens were removed from the furnace and allowed to cool to room temperature in still air, which initiated the transformation back to the martensitic state. Note that a heat treatment time of 10 minutes would generally be long enough to induce the parent phase, but the intention was to “age” the wire during a longer heating cycle. It was expected that, as with most other classical steels, the crystallography and metallurgical structures could be altered to a desired configuration. The results of the “aging” treatment are discussed later.

A Hounsfield Tensile Tester was used for tensile experiments. The specimens were clamped at an effective gauge length of 300mm. The remaining 40mm length was used by the grips (20mm top grip and 20mm bottom grip) to ensure that no slippage occurs during testing. A 5kN load cell was used to measure the load and the displacement was measured by a built-in digital encoder. All specimens were subjected to a displacement rate of 5 mm/min and the machine was limited to a maximum load of 500N, which would stop the machine from exerting any tensile force. This was done in an attempt to ensure that the material does not reach its plastic region or fracture during the tests. The abovementioned end conditions, such as displacement rate and maximum load for the respective wires were obtained from tests conducted by Philander et al. [47]. A Pre-load of 2N was programmed into the tensile testing

machine prior to loading. This was done to relieve the wires of any slack after it has been located and tightened in the gripper devices. More importantly, this precautionary measure accounted for more accurate extension readings as any slack whatsoever would cause exaggerated displacements.

After unloading, the specimens were placed back in the furnace at 100°C for more than 10 minutes to restore the wires to their original geometric properties. This procedure was further examined by another researcher in the Smart Alignment Systems Research Group where he specifically investigated the effect of repeated cycles (later termed thermo-mechanical cycling) on the quasi-plastic material response of the same NiTi wire. The most significant findings from these experiments are recommended later for shape memory alloy wires used in smart composites. Most of the following discussion assumes a qualitative mode at material behaviour during the tensile tests.

2.4 Quasi-Plastic Material Response exhibited by NiTi Shape Memory Alloys

The quasi-plastic material response is a term that was created to describe the unique material response of shape memory alloys when it exhibits the shape memory effect. When the shape memory material is in its low temperature phase, and a load is applied to it, it will deform causing an apparent plastic deformation, more commonly known as quasi-plasticity. This deformation is maintained until the material is exposed to an increase of temperature, which in turn causes the deformation to disappear completely. A general discussion of this material response is presented here, but key considerations and observations are reported with specific emphasis on the significance of the material behaviour for an embedded constituent.

2.5 Results and Discussion

The quasi-plastic material response displays three distinct regions when it is plotted graphically. Due to an absence of clearly defined terminology for these regions in literature, the three regions would be labelled in the accompanying illustration (Fig. 2.1) to facilitate discussion.

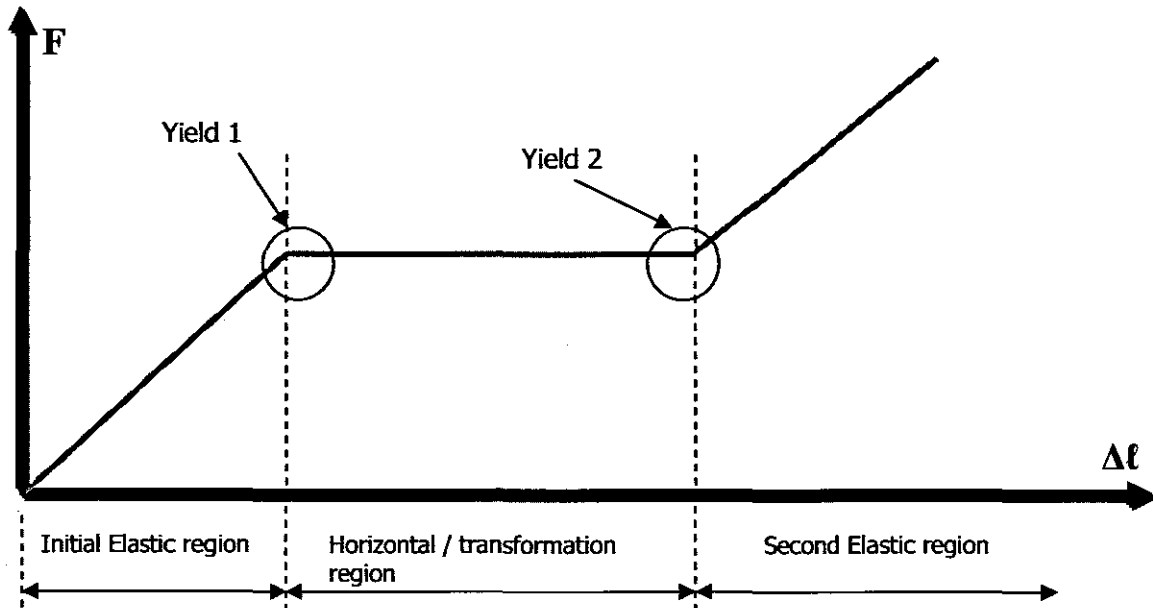


Figure 2.1: Graphical representation of three regions displayed by quasi-plasticity

The graph as displayed above includes an initial elastic region (IE), a nearly horizontal region (NH), and finally another elastic region (FE). A closer look at the graphs from the experiments (see figure 2.2) show that all of these regions contain a certain amount of yielding. The regions 1 and 3 show elastic behaviour, which implies full strain recovery upon removal of the load. These two 'elastic' regions also suggest that a macroscopic change occurs in which the specimen changes from its initial state to some final state. Another key observation is that the slopes of both regions look similar, which could imply that they share the same elastic constant.

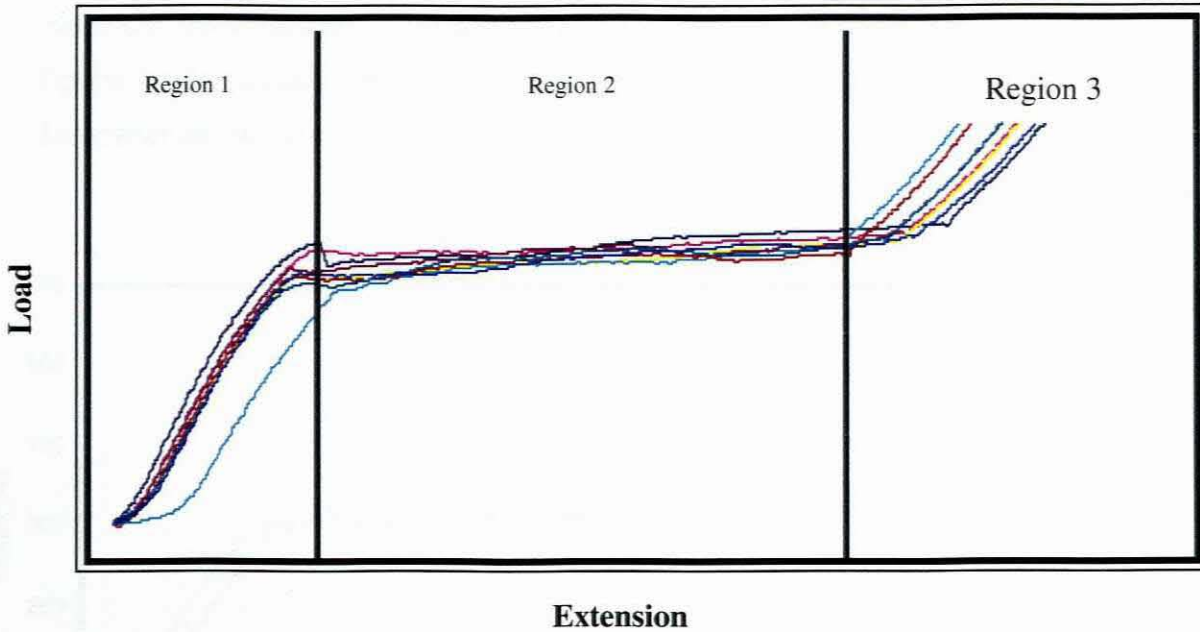


Figure 2.2: Load – Extension behaviour for a 2mm diameter NiTi wire

The biggest ratio of displacement takes place during the middle region (NH). As indicated in the previous illustration this region also resembles transformation from one phase to another, and it is clearly notable that the end of the transformation coincides with a distinct point. Various approaches and explanations [6],[7],[49] exist for why shape memory alloys behave this way and what the determining factors are, both micro – and macroscopically. Recent work by Philander [47] took a critical look at some of these descriptions in view of some contrasting observations in his experimental work.

The significance of the quasi-plastic behaviour, depicted in the previous illustration, is that the material response for each individual wire are shown and by plotting them on one axis creates a comparative view of all the shape memory elements. A first prerequisite to the 'design' of this smart structure (SMAHC) is that the materials' behaviour of the composing elements is known and predictable. The key to this requirement lies with uniform wires with the same properties i.e. yield stresses, transformation and elastic strains.

The variability in these regions is evidenced in the results from 3 wires that were cut from the reel to be pre-strained for the lay-up of the composite. The figure below shows the material response after heating (to transformation temperature, A_f) and uniaxial loading.

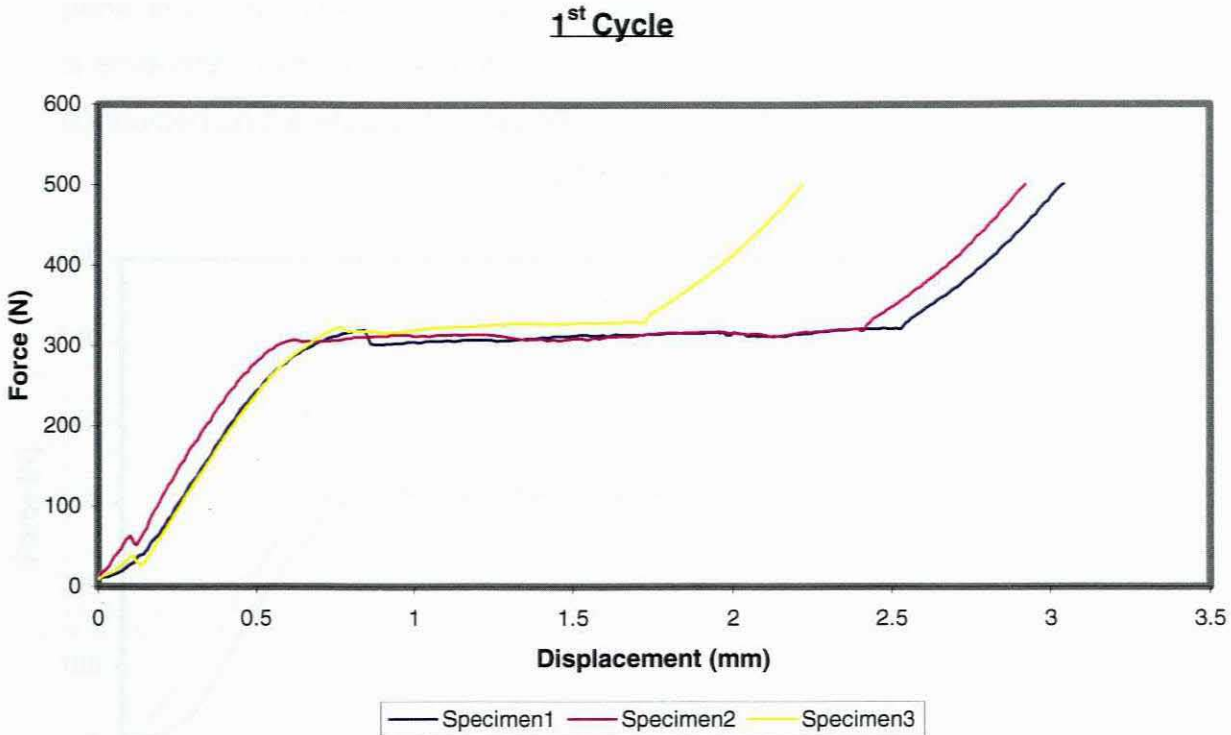


Figure 2.3: Load – Displacement behaviour for a 3mm NiTi wire in tension

A closer look at the graphs, displayed above, reveals the very essence and motivation behind this analysis. Just from this one set of graphs there are a few mentionable occurrences. Two of the graphs, specimen 1 and 3 in particular, started to display similar behaviour but only for the first part of the curves. The yield loads are consistent and the subsequent apparent plasticity, given by the horizontal region appears uniform as well, however that is where the similarities end. Specimen 3 shows that it takes less displacement for it to transform to its final elastic region, which would mean that considerably less recovery displacement (strain) is obtainable. The quasi-plastic material response of the second specimen is probably more favourable with respect to the first. The only negative aspect could be that the same yield values occur at less displacement. The spikes that occurred right at the start of the tensile

tests of both specimens 2 and 3 can be attributed to possible slack in the wires. It was for this very same reason that a pre-load was introduced.

These findings are once again testimony of how difficult it is to path the behaviour of the shape memory alloy let alone predict its performance when it is embedded into a host material. The findings from further experimental tests conducted on the shape memory alloy wires, are now presented.

3rd Cycle

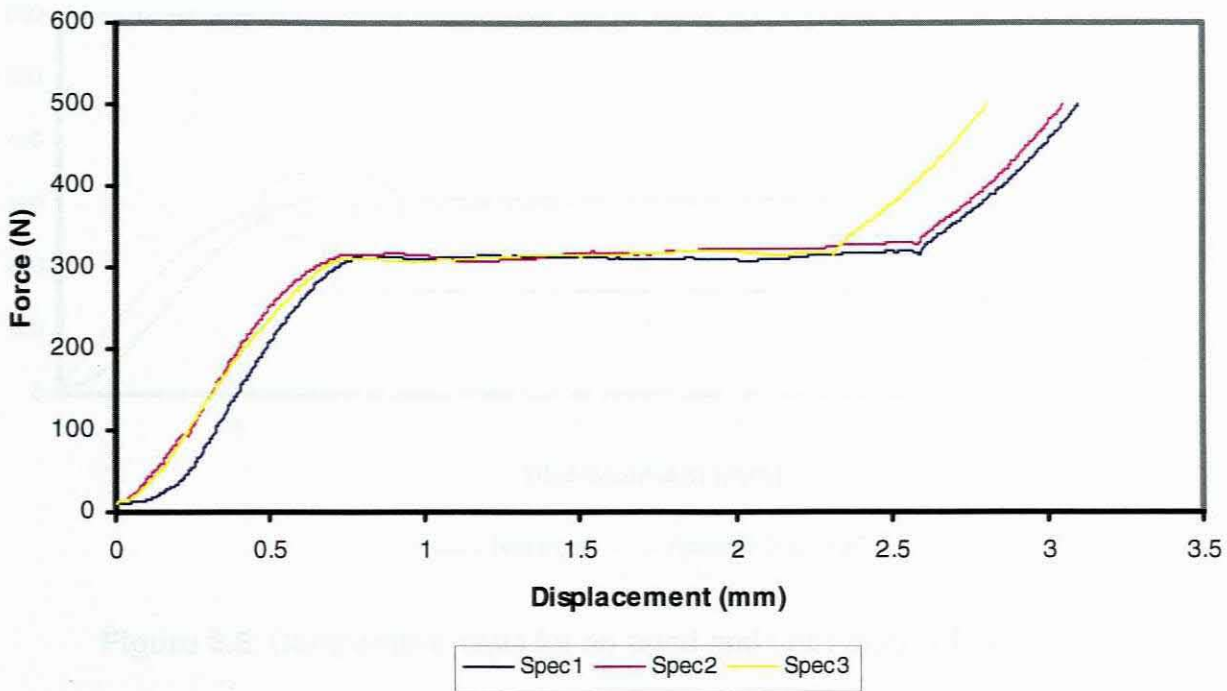


Figure 2.4: Load – Displacement behaviour for a 3mm NiTi wire after cycling

A distinct alteration was notable after the specimens used in figure 2.3 were subjected to more cycles of the testing regime followed before. These are the graphs displayed after only three cycles and the effect is easy to see. The material still displayed the ideal characteristic (given in the schematic, Fig 2.1), but more importantly all curves appear identical to the first set of curves with the same yield and displacement values. The third specimen, which was a concern in the first set of tests, now experienced a change in its properties that brought about the “lengthening” of its transformation region. This specific result was assuring in that the ‘second elastic region’ would inevitably nestle between the other curves upon further cycling.

It was expected that by aging the material through a heat treatment procedure the material properties would change leading to differences in microstructure and martensitic transformations. Even without microscopic examination it was evident that the aging treatment altered the specimens' properties, as seen in the characteristic curves in the figure below.

Effect of Aging treatment on NiTi wire

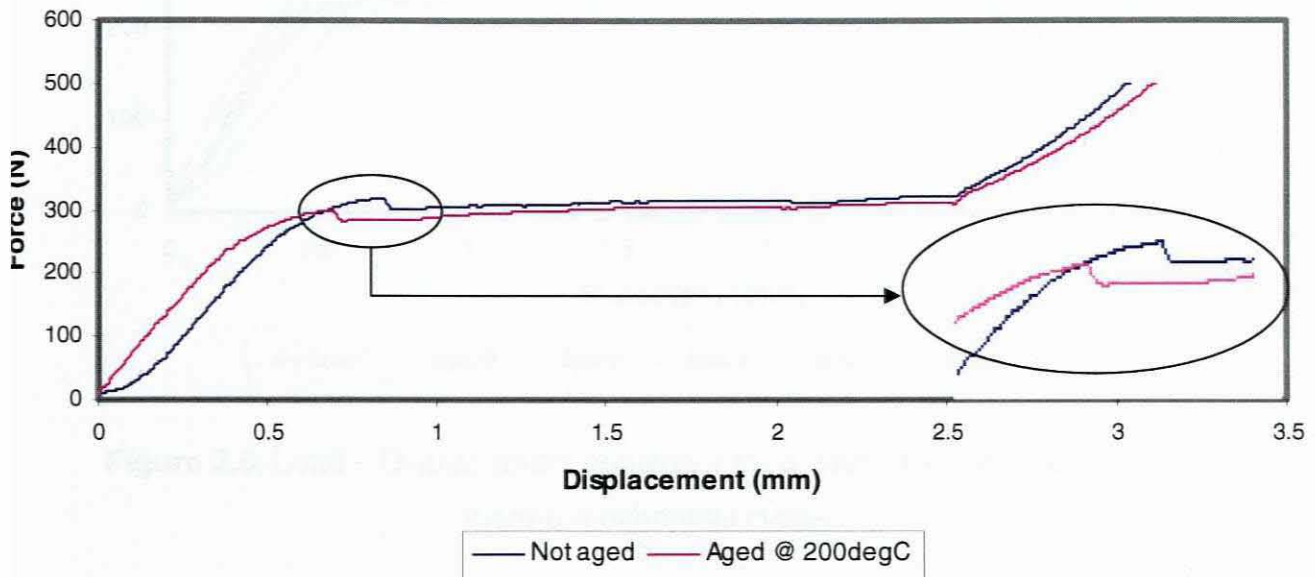


Figure 2.5: Comparative plots for an aged and untreated NiTi specimen

The effect of the aging treatment can be seen around the first yield point. The second specimen was heat-treated at a temperature of 200°C and as a result the value of the yield load decreased. For the sake of quantification, the yield values for the two wires were 320N and 270N.

Further experimental investigations were conducted into the material and therefore a more homogeneous behaviour from the 8 specimens was greatly anticipated, however the results showed that these two "treatments", aging and cycling, do not stabilize the material when used in tandem.

08 Cycle @ 200 degC

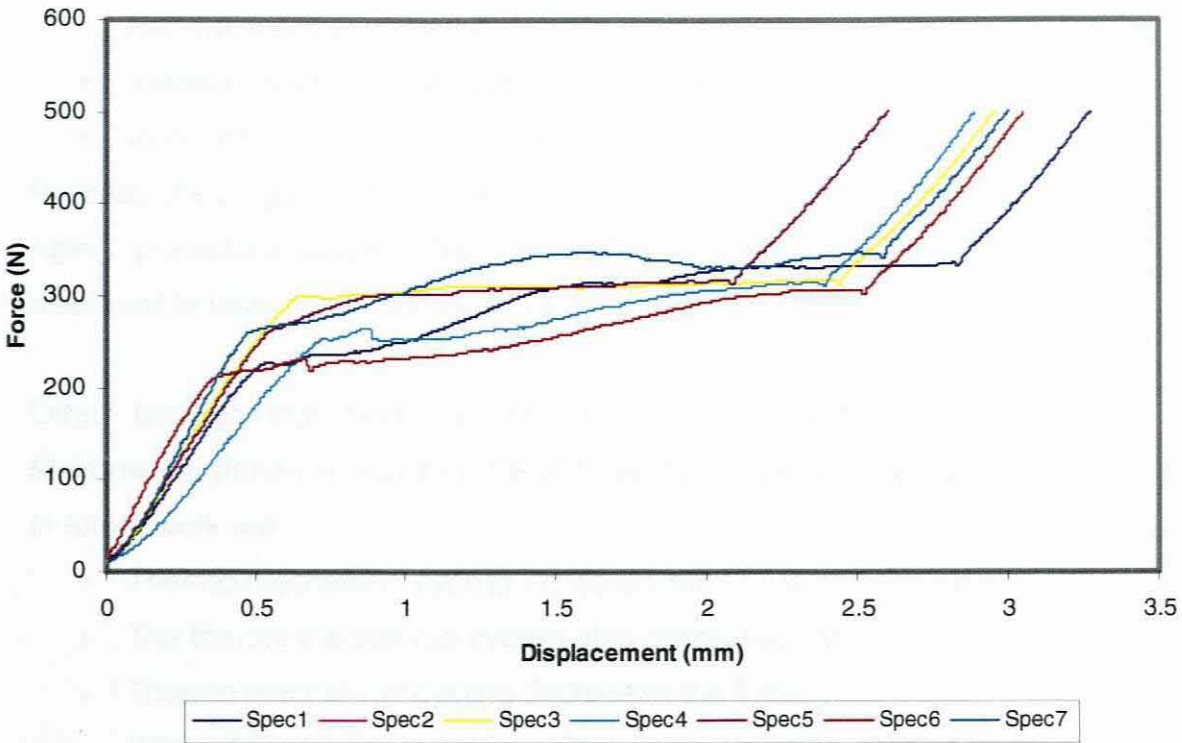


Figure 2.6: Load – Displacement behaviour for a 3mm NiTi wire subjected to thermo-mechanical cycles

The curves displayed quite erratic behaviour with no two curves following the same trend. Quantitatively the curves make pinpointing of critical parameters such as yield load and related displacement values increasingly difficult. These curves also display some sort of hardening behaviour, which is common with classical steels, within its transformation region. This phenomenon was discussed in previous experimental work by Philander [47].

2.6 Concluding remarks

The key aspects of the experiments conducted on the 2mm and 3mm NiTi shape memory alloy wires are summarized by the following remarks. The results confirmed and supported the views that often appear in literature i.e.

that the nature of the behaviour exhibited by shape memory alloys is quite complex. Some of these complexities include:

- Non-homogeneous transformation regions
- Variable elastic yield values
- Inconsistent measures of strain

Probably the single biggest outcome was how aging affected the material. The Aging procedure erased the hardening-like behaviour that the material displayed in tests conducted by Philander in 2004. (See Fig. 2.7)

Other findings that were reported in the unpublished work by Doctor Mukhuwana (fellow researcher, CPUT) that might become critical parameters in future work are:

- Thermo mechanical cycling increases the transformation strain
- The thermo mechanical cycling also decreased the initial elastic strain
- Thermo mechanical cycling decreased the initial yield loads
- When NiTi Shape memory alloy wires undergo thermo mechanical cycling it removes the variability in both initial elastic strains and yield loads.

The experimental representations from where these conclusions were deduced are all displayed in Appendix A

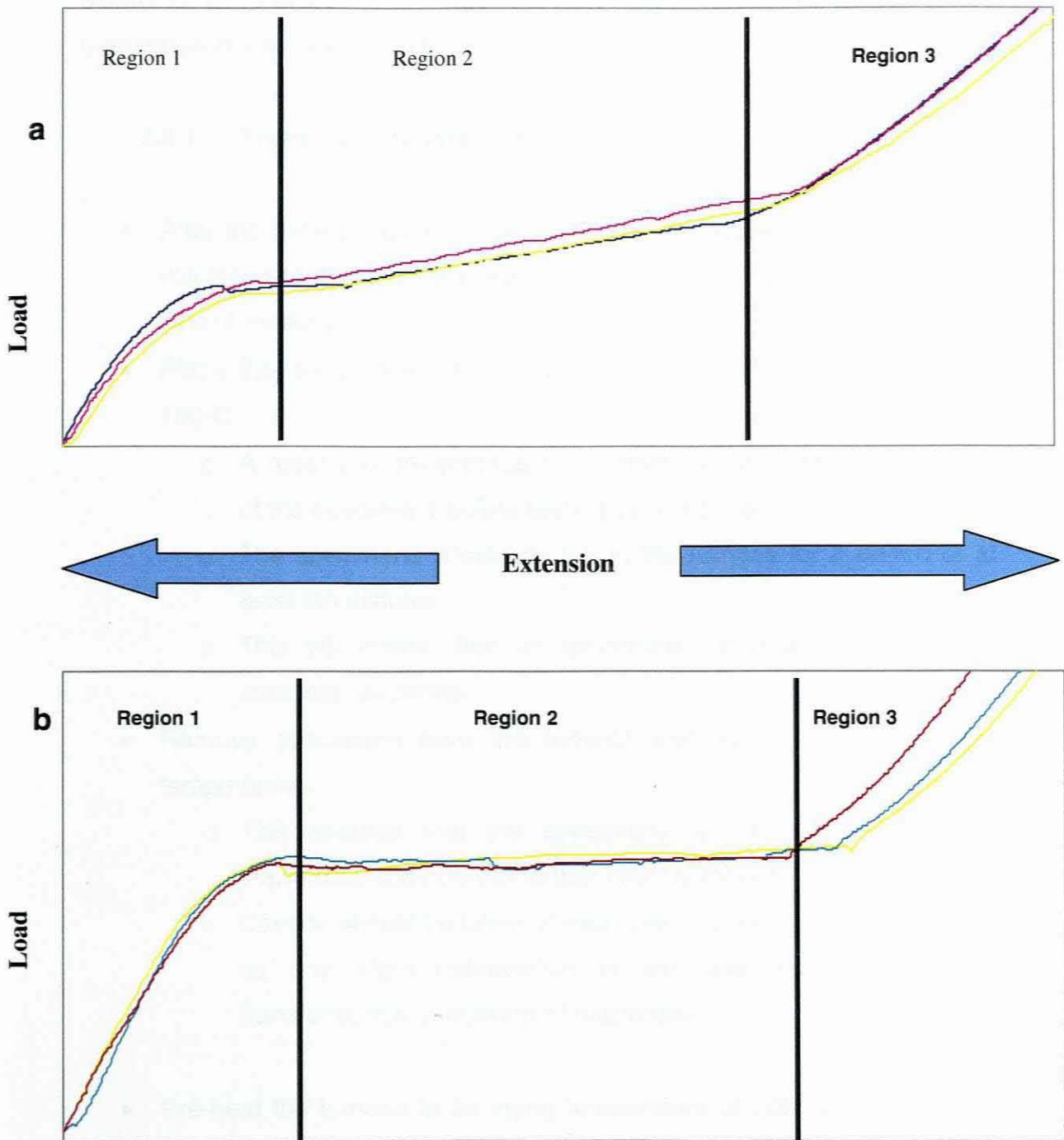


Figure 2.7: Quasi-plastic behaviour of 3mm diameter NiTi shape memory alloy wires when (a) untreated / no heat treatment [47] and (b) aged at temperatures in excess of 200°C

Based on all the gathered results and the preceding discussion a method and experimental protocol for Shape memory alloy wires that need to be embedded in a matrix material is proposed.

2.6.1 Procedure for stabilizing SMA wire

- After the determination of the amount of embedded SMA (percentage volume) into a host matrix one should identify the specimens by some kind of marking.
- Place the specimens into a furnace preheated to a temperature of 100°C.
 - A means to pre-stabilize the material as the metallurgical state of the specimens before testing cannot be accounted for.
 - The specimens should be left in the furnace for a period of at least ten minutes.
 - This will ensure that all specimens transform to the parent structure, austenite.
- Remove specimens from the furnace and allow to cool at room temperature.
 - This ensures that the specimens are all in their twinned martensitic state before further heat treatment.
 - Caution should be taken of excessive handling during this period as any slight deformation of the specimens may induce transformation to detwinned martensite.
- Pre-heat the furnace to an aging temperature of 200°C or 250°C and place all specimens inside the furnace simultaneously.
- Allow the specimens to 'age' for a period of ten hours at this temperature.
- Remove the specimens and cool them in still air or quench them in water
 - The specimens should all behave uniformly after this treatment and should be ready to act as actuators in a active composite

CHAPTER 3

Manufacturing of a SMAHC

3.1 Introduction

The shape memory hybrid composites, with either embedded or bonded shape memory material components, have proved to be unique material systems that provide tremendous potential for creating new paradigms for material-structural interaction [53]. Commercial shape-memory materials can be easily fabricated into various forms such as fibres, wires, ribbons, particles and thin films, therefore making it feasible to manufacture a great diversity of shape-memory hybrid composites with conventional fabrication procedures [53].

Partly due to the technical simplicity in manufacturing, most previous efforts with embedded shape-memory fibres or wires, have been directed at thermoplastic and thermo-set polymer matrix composites, where many engineering applications have been found [52], [53]. For instance, the polymer matrix shape-memory composites have demonstrated varying success: shape and position control, active and passive control of the vibration and acoustic

transmission of materials subjected to dynamic loads, impact damage and creep resistance in structures [24],[34],[35].

The fusion of two distinct different materials (the matrix and the reinforcement) brings forth a mismatch of their thermal expansion coefficients. This results in a tensile or compressive residual thermal stress being introduced into the composite when fabricated at high temperature and then cooled down to room temperature. If the reinforcement, often also referred to as filler, shrinks in the matrix at the temperature of operation or within increasing applied stress, compressive stress may also be introduced, thereby contributing to the tensile properties of the composite. This is exactly what shape memory alloys do when they exhibit such shrinkage when pre-strained at the martensitic state and then heated to the parent phase.

Previously, a few attempts to incorporate embedded NiTi wires directly into a polymer matrix composite proved largely unsuccessful due to manufacturing difficulties and problems associated with interfacial bonding [32]. To avoid the interfacial bonding issue, SMA wires were alternatively incorporated into polymer matrix by using coupling sleeves [26], [27]. Both thermoset and thermoplastic composites have been addressed [28-34]. Comparatively, fibre-reinforced thermoplastics offer some substantial advantages over fibre-reinforced thermosets because of their excellent specific stiffness, high fracture toughness, low moisture absorption and possible fast and cost-effective manufacturing processes. However, the high processing temperatures may be problematic with respect to the embedding of SMA elements. The thermoplastic processing must be performed at higher temperatures, typically, between 150°C and 400°C, whereas, the thermoset processing cycle of the composites is in the relatively low temperature range of room temperature to 170°C. The thermoplastic processing cycle has some effect on the microstructure of the SMA fibres as manifested in the change in transformation temperatures and peak recovery stress: the transformation temperatures of the SMA shift upwards while the peak recovery stress drops as a result of the thermoplastic processing [31].

The thermoset processing only mildly affects the transformation characteristics of SMAs fibres. However, some dynamic properties of SMAs fibres may be significantly affected [39], [40]. Much of the previous research on the SMAs hybrid composites utilized the one-way shape-memory effect, especially in the applications, which require recovery stress of the SMA. Much care should be taken to prevent shape recovery of the pre-strained SMA fibres or wires during the composite cure cycle. Void content is one of the pressing issues in manufacturing the SMAs hybrid composites. Voids in composite materials significantly affect the material integrity and behaviour. Their presence in the SMAs composites will not only lead to property degradation of the host composite material, but the efficiency of activation and the level of interfacial bonding between the SMAs fibres and host matrix will also be sacrificed.

Probably the greatest difficulty with regard to Shape Memory Alloy Hybrid Composites (SMAHC), manufacturing of the composite, received most attention and a variety of composites to be used in both passive and active applications was attempted.

3.2 Manufacturing procedures

3.2.1 Passive Applications

When used passively the shape-memory alloy elements strengthen the matrix composites, absorb strain energy and alleviate the residual stress and thereby improve the creep or crack resistance by stress-induced martensitic transformations.

Furuya et al. [74] used the adaptive mechanism of metal matrix composites when they designed reinforced aluminium matrix composites with embedded NiTi fibres.

The excellent ductility and workability of NiTi shape memory alloys make it very easy to fabricate fibres of several hundred micrometres in diameter with conventional processing methods [53]. Embedding the fibres in the aluminium matrix can be achieved by squeeze casting or compacting via a powder

metallurgical route. Specially, three kinds of fabrication procedures have been developed.

- The NiTi fibres were arranged in a fixed holder in a mould, then molten aluminium (697°C) was poured into the mould, followed by pressurization at 65 MPa. Because the melting temperature of aluminium is not very high, even though a thin layer with a thickness of less than 3 μm of the fibre surface was affected by diffusion interaction, most of the NiTi fibres remained unaffected during the process. The composite was then subjected to heat treatment (500°C, 30 min) to shape memorize the NiTi fibres, followed by ice water quenching to induce martensitic transformation. A specific tensile pre-strain was applied and then the composite was heated to a temperature above the A_f point.
- Aluminium powders and NiTi fibres were placed in a mould and were pressed at 200MPa in air at room temperature to form a green sheet, and then it was sintered in a vacuum furnace at 570°C for 1h. Simultaneously, a shape-memory treatment was made during the sintering process. The porosity of the as-sintered composite was 8%. The high elongation of the aluminium matrix at room temperature (up to 12%) would provide pre-strains of 4% - 5% to the NiTi fibres [53].
- The NiTi fibres were wound around or longitudinally laced on to thin aluminium alloy sheet with rectangular end notches. The fibre-laced prepreg sheets were stacked on a pair of hot-press dies or loaded into a vacuum canister and then were hot pressed at proper temperatures and pressures, as illustrated in figure 3.1. The optimum vacuum hot-pressing conditions for Al-6061 matrix composite were found to be 500°C for 30 min at 54MPa [53]. The material could be both directly water quenched and then aged, or cooled down in the furnace while keeping the pressure constant, followed by a solution treatment. A loading and unloading process was applied to the composite at room temperature to produce various pre-strains. This process resulted in

good macro-scale homogeneity and little internal porosity, and various volume fractions of NiTi fibres could be embedded into the aluminium matrix.

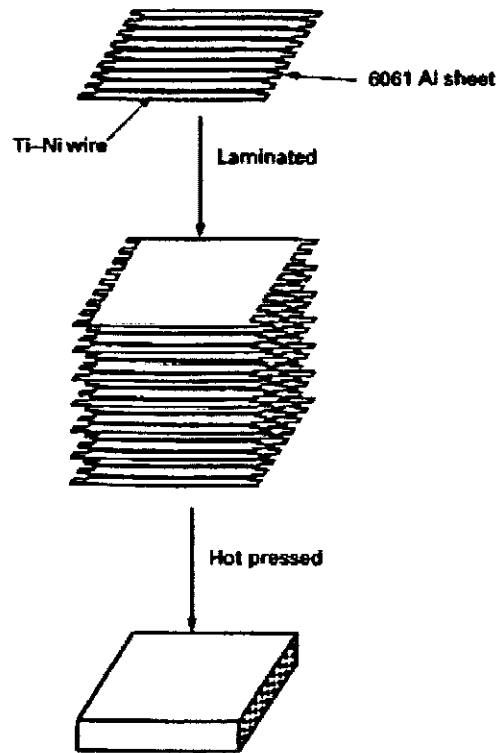


Figure 3.1: Fabrication procedure for SMA wire wound prepreg [53]

It is noted that the abovementioned fabrication methods, whether using squeeze casting or compacting, occur at temperatures much higher than the reverse transformation start temperature (A_s) of NiTi shape memory alloys ($\approx 70^\circ\text{C}$). There are other concerns and questions regarding the manufacturing techniques described above that immediately spring to mind. Although the melting temperature of the NiTi is in the order of 1600°C these high process temperatures might still have an effect on the usefulness of this reinforcement material. Previous trials with this material have shown that contrary to the norm the material tends to remember the deformed shape, and this is related to “training” of the SMA wire. Evidently this restricts the functionality and diversity of the composite only to one type of application. In nullifying the shape memory effect (SME) the only other implementation of its unique characteristics is via the Active Property Tuning method, where it exploits the

changes in the stiffness of the SMA components during their activation. With the SMA wires not being in a pure martensitic state, complex heat treatment and shape memory treatment procedures were introduced to shape memorize the fibres. The whole composite structure had to undergo loading and unloading processes to acquire adequate pre-strain. Another critical parameter that was not reported on in Furya's [74] work was the effects of pressure on temperature. One of the most common occurrences in Engineering reveals that an increase in pressure results in an increase in temperature. Some of the other disadvantages of metal-matrix-composites compared to monolithic metals and polymer matrix composites are:

- Higher cost of some material systems
- Relatively immature technology
- Complex fabrication methods for fibre-reinforced systems (*Fibre-reinforced systems are popular for a variety of applications*)
- Limited service experience
- The composites' performance largely depend on a fairly high volume fraction of SMA wire/fibre

3.2.2 Active Applications

Contributions by Tsoi, et al [45] described the manufacturing of a SMA composite that consisted out of a fibre-reinforced matrix with embedded shape memory alloy wires. To ensure that they produced an overall composite with a pre-strained Shape memory alloy wire, a fixture frame was designed and made by a producer in Switzerland. This enabled the SMA wires to be wound around comb-like pins, 0.5mm apart, situated at both ends of the frame. One of these combs could be moved so that the wires were pre-strained and then held at the required pre-strain value during curing. A picture of the frame is shown in figure 3.2.

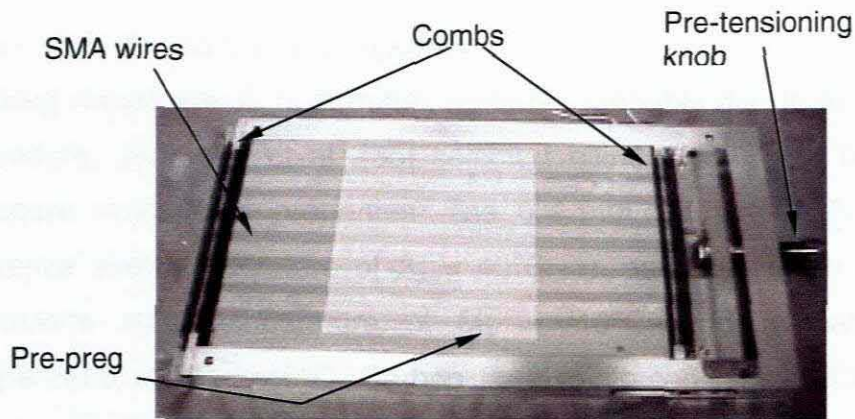


Figure 3.2: A typical SMA Composite frame, designed by EPFL.

These SMA-composites consisted of two layers of Aramid fibre pre-preg and one layer of SMA wires. The pre-preg contained 60% Kevlar 29 fibre and an epoxy resin system. The wires were pre-strained to different values ranging from 0 to 8% before the pre-preg sheets were hot pressed at the following conditions: the curing cycle took place for 12h at 70°C which was then followed by a post cure cycle of 1h at 140°C.

From the image in figure 3.3 it can be seen how the implementation of this fixture jig limits the manufacture of such a composite. The Kevlar composite occupies only close to half the area that was produced by the stretched shape memory alloy wires. Post manufacturing processes were employed to cut the composite to specimen size and alternatively to get rid of the sections of wire which was deformed around the combs.

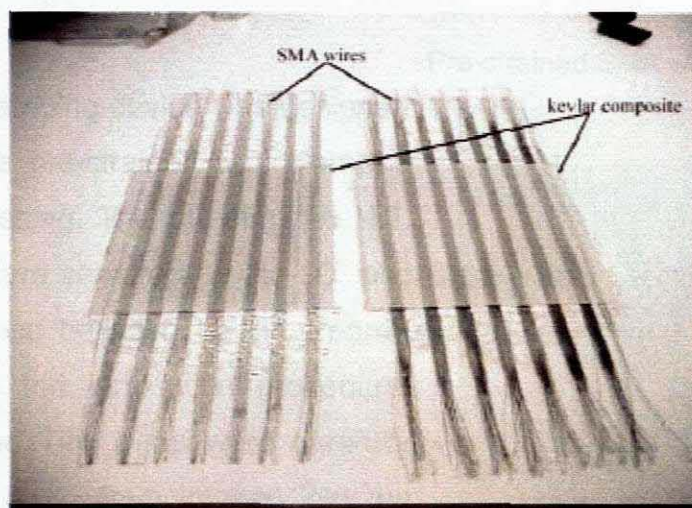


Figure 3.3: The SMA-composite specimens after curing

Other work around SMAs-composites proved just how popular fibre-reinforced prepreg sheets are as host matrix material, probably due to its simple lay-up procedure. Jang, Xu et al. [55] selected nitinol (NiTi) wire because of its attractive mechanical properties. The 0.4 mm diameter NiTi wire had an austenite start temperature of $A_s = 40^\circ\text{C}$, an austenite finish of $A_f = 62^\circ\text{C}$, martensite start temperature of $M_s = -10^\circ\text{C}$, and a martensite finish temperature of $M_f = -40^\circ\text{C}$. Carbon fibre reinforced plastic (CFRP) prepreg with 0.2mm in thickness was cut in sizes of 100× 50 or 200×100 mm and stacked as cross ply. The CFRP host materials consisted of an inner side for the 90° ply and outer side for the 0° ply configuration of carbon fibers, respectively as shown in figure 3.4.

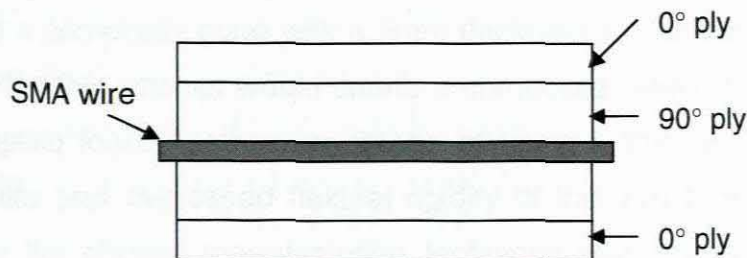


Figure 3.4: Schematic drawing of SMA/CFRP laminates.

The CFRP composite laminate configuration was cross-ply [0/90/0]. The pre-strained NiTi wires with 0.5~7% stain range was obtained by applying tensile load, in advance. Stacked bodies with CFRP prepreg and NiTi wires were laid up in the designed steel mold as shown in figure 3.5.

This special clamping device was designed to maintain the pre-strained wire clamped during hot pressing. The pre-strained NiTi wires, which were centered on the 90° ply, were sandwiched between CFRP prepreg layers. During the lamination procedure, the pre-strained TiNi wires were carefully embedded as a 1~ 4mm interval into the center of 6 sheets of CFRP layers.

Pre-strained SMA wires

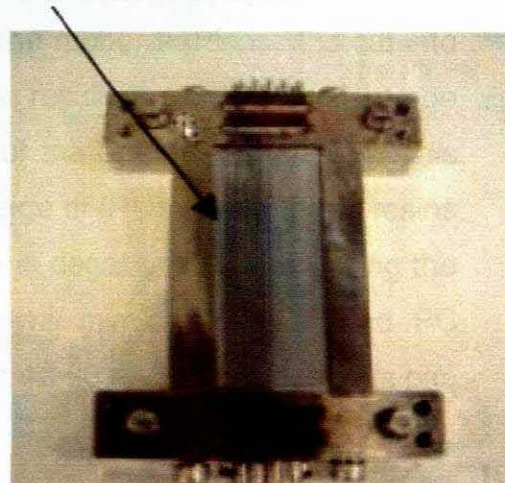


Figure 3.5: Clamping device and mould [55]

Anti-heat vinyl sheets were used to prevent the flow of epoxy resin of CFRP prepreg during heating. Curing was accomplished by controlling the applied pressure in the range of 0.03~0.3 MPa whilst heating the composite between 130~180°C for 2 hours. After the curing, the hot-pressed specimens were allowed to cool to room temperature.

3.3 The Manufacture of a polymeric composite with embedded SMA's

A detailed description follows of the fabrication technique used to produce a SMAHC for use in active applications. The desired application of the proposed SMAHC is to be used in deflection and shape control, hence the decision to manufacture a composite plate with a 5mm thickness for an initial run. It was considered that this attempt would create a composite, which deforms easier upon an applied load. Another advantage of using a thinner section is the added pliability and decreased flexural rigidity of the structure. The biggest influence on the chosen manufacturing technique was the shape memory alloy behaviour at elevated temperatures. The other processes described before clearly stated the high temperatures at which those composites were cured inducing phase transformations.

The rapid prototyping technique, vacuum casting, was used as a method to produce repeatable products (the SMAHC) in a simpler way. Vacuum Casting is considered as the simplest and oldest rapid tooling technique where a rapid prototype (RP) positive pattern is suspended in a vat of liquid silicone or room temperature vulcanizing (RTV) rubber. When the rubber hardens, it is cut into two halves and the RP pattern is removed. The resulting rubber mould can be used to cast up to 20 polyurethane replicas of the original RP pattern. This silicon tool into which we could pour a wide range of (PU) polyurethane resins through a vacuum chamber, ensures the resin is degassed thus removing the majority of air bubbles. Materials available will mimic ABS, PP and PC Elastomers and can have a shore hardness of 40-90 and some materials can be heat resistant up to 150°C.

3.3.1 Designing a RP Master and mould making

As indicated in the previous chapter the final composite was based on a rectangular “dummy plate” (which was the envisaged final part) made of the acrylic sheet PMMA. The width of the plate was subdivided into 9 equal parts, resulting in 8 wires equally spaced and 32mm apart. See figure 3.6. The plate was later altered and decreased to a manageable size that only accommodated 7 SMA wires.

Modelling the master part on the exact final prototype allowed the luxury of not having to cut grooves/ insertions to lay-up the SMA wire into the silicone mould. Shape memory alloys are very malleable and easily deformable in their low temperature state hence the decision to use steel wire of the same diameter (2mm) to produce the impressions in the silicone tool. Holes were drilled axis-symmetrically off the neutral axis. This was done to induce bending in the plate once the shape memory alloy wires contract.

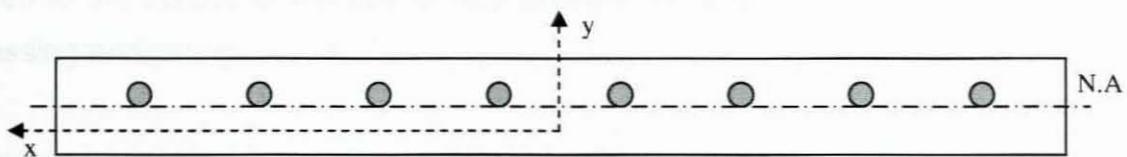


Figure 3.6: Schematic of the plate detailing wire placement

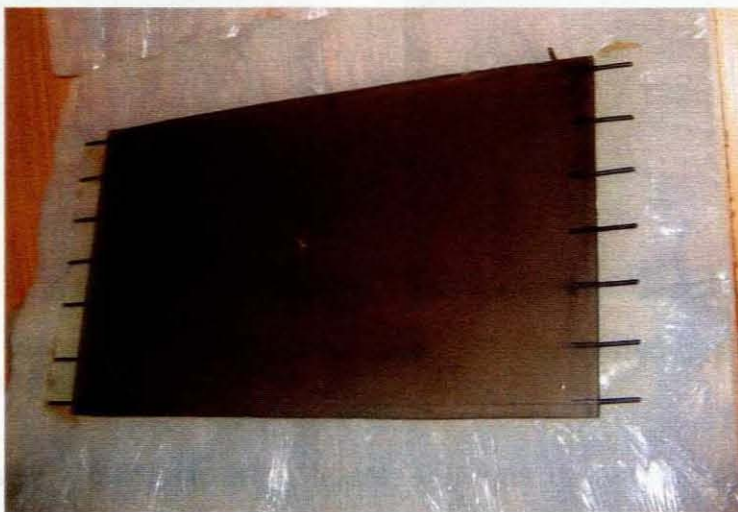


Figure 3.7: Dummy plate with inserts simulating SMA wires

After the creation of the master the part was weighed to help with verification of the weight of the resins. The parting plane and resin feed point (pouring gate) was identified and indicated on the part. A box was built with outer walls 50 millimetres around the outer silhouette of the part. Provision was made at the height of the box to allow for silicone-rising during the degassing stage. The box was made from Melamine face board due to its smooth surfaces, which detaches relatively easily from the silicone and the glue. The base of the box was cut to fit inside the vacuum chamber and random sized squares were glued onto the base using a hot-melt glue gun.

An in-gate was created by using a glue stick that tapered to 6mm diameter. The tapered point was glued to the lowest point of the part and the top to a strip equal in length to the base. Inserts, as shown in figure 3.8, were used to rest the part on and to ensure that the part is fixed to both the top and bottom of the box. This was done to counter any movement of the part during silicone pouring. Packaging tape was used to define the parting plane and was later fixed to the insides of the box to help prevent movement during pouring, degassing and curing.

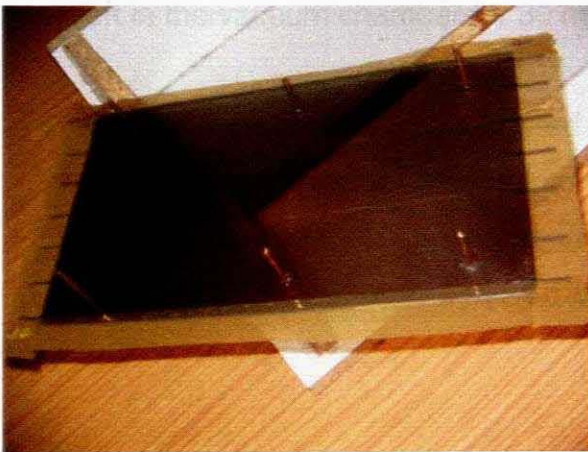


Figure 3.8: Parting plane and supports on boundary of part



Figure 3.9: Completed box with suspended part

The volume of the box (shown in figure 3.9) was determined to obtain the required mass of the silicone. Wacker Silicone is a two-part rubber consisting of a base and hardener. The provided specifications for this silicone showed a density of 1.14g/cm^3 and a pot-life (curing time) of 90 minutes.

The multiplication of the volume with the density provided the mass in grams of silicone needed. The mixed silicone was poured in a large bucket (25ℓ) to help de-gassing, since the silicone can increase in volume up to 10 times.



Figure 3.10: Mixing bucket for silicone



Figure 3.11: Liquid silicone in box

The bucket with silicone was placed inside a vacuum chamber and evacuated for a period of time. At first the silicone level rose rapidly (seemed as though silicone was boiling). When the silicone rose up to the edge of the bucket it was countered with a pressure shot to ensure level drops again. This process was repeated until the silicone stopped rising and the degassed silicone was left in the vacuum chamber for 30 minutes to ensure that all air was removed.

The degassed silicone was poured into the box at one of its corners and the mould (box) was placed back into the vacuum chamber to evacuate the air that was trapped due to the pouring. After a further 30 minutes inside the chamber the mould was removed and left (overnight) at room temperature to further solidify.



Figure 3.12: Vacuum chamber with silicone mould

After full solidification the box was broken and the mould removed. The runner occupying the in-gate was pulled out and a weave (wavy line) was drawn on the side of the mould in-line with the parting line. The weave facilitates easy mould-half alignment. The mould was cut in half all along the weave and deep enough to reach the packaging tape that defined the parting plane. The mould halves were pulled apart and the part (plate) was carefully removed. All the excess tape that was still stuck to the mould was removed to ensure mould integrity. Possible air traps were identified and vent holes were created by piercing small holes into these areas on the top half of the mould. The silicone mould's cavity faces were meagrely cleaned with an applicator that was not harmful to silicone and immediately dried with compressed air.

A stack of plates was used to create the top halves and the bottom halves by using packaging tape around it. The mould was held by 10mm of the expanded foam and used to create the top half. The bottom half was created by using the same process.

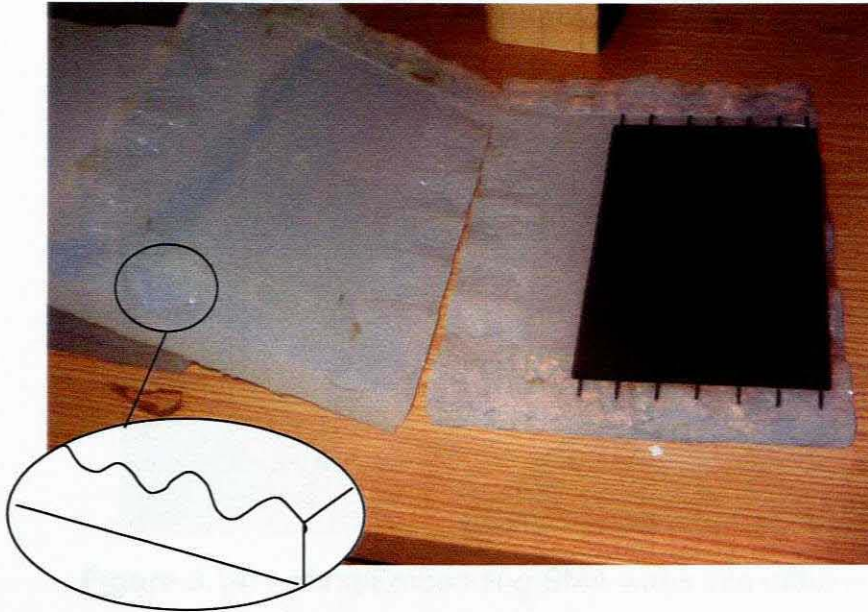


Figure 3.13: Mould halved along cutting weave

3.3.2 Embedding SMA and casting of part

The inner cavity faces of the mould were sprayed an arm length away with a release agent. The prepared pre-strained SMA wires (as documented in Chapter 2) were carefully embedded one by one into the seats (impressions made by the protruding wires on the dummy plate) on the two edges along the width of the plate. The top half of the mould was placed into position whilst ensuring that the wires remained in position and did not deform during the closing of the mould (View the process illustrations on the next page).

A staple gun was used to secure the two halves and the split line was sealed by wrapping packaging tape around it. The mould was further wrapped and 10mm of tape protruded above the mould to catch excess resin and prevent overflow into the vacuum chamber.



Figure 3.14: Lacing/Embedding SMA wires into mould-base

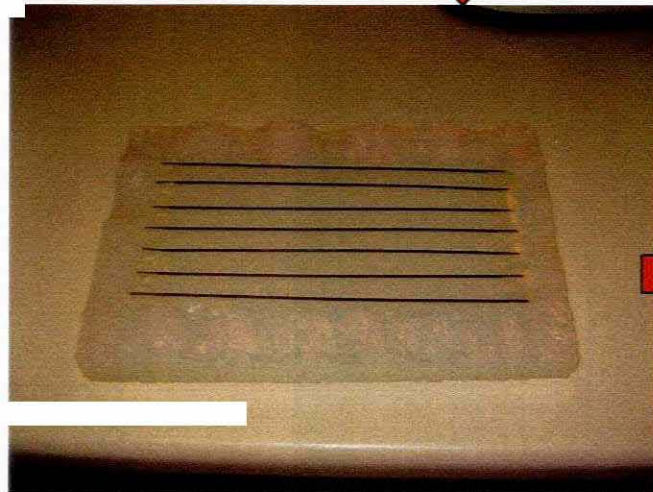


Figure 3.15: Cavity with longitudinally laced SMA wire

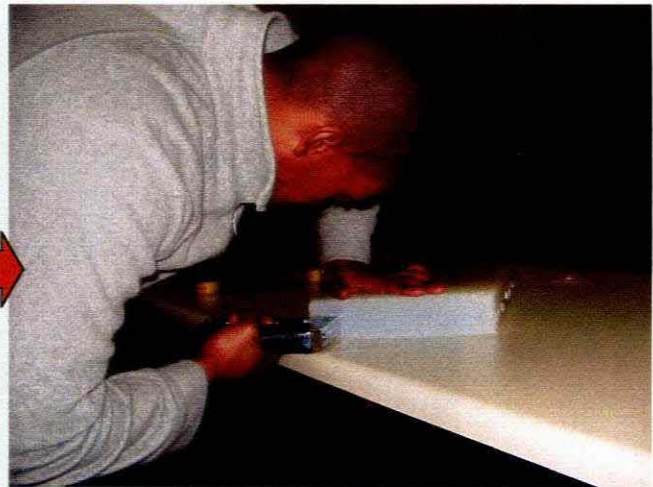


Figure 3.16: Closing mould with staples along split-line

A semi-rigid urethane casting resin was used as a first attempt. This resin from the Smooth-Cast line (provided by Smooth-On) was of Shore Hardness 45D which is a softer semi-rigid plastic. The table provides a technical overview of materials in the flexible to less-flexible range.

| Value Product | Mix Ratio (pbv) | Colour | Shore Hardness | Pot Life | Demold Time | Mixed Viscosity | G/C C | Cu. In./Lb. | Ultimate Tensile | Tear (Die C) | Elong. at break | Shrink in./in. |
|---------------|-----------------|--------|----------------|----------|-------------|-----------------|-------|-------------|------------------|--------------|-----------------|----------------|
| SC 45D | 1A:1 B | Amber | 45D | 5 min. | 20 min. | 500 cps | 1.08 | 26 | 1,500 | 150 pli | 100% | .002 |
| SC 60D | 1A:1 B | Amber | 60D | 3 min. | 10 min. | 300 cps | 1.08 | 26 | 1,800 | 220 pli | 20% | .010 |
| SC 61D | 1A:1 B | Amber | 61D | 7 min. | 60 min. | 300 cps | 1.08 | 26 | 1,800 | 220 pli | 20% | .010 |

Table 3.1: Properties of three Urethane plastics

The resin quantities that were obtained from the mix-ratio provided were poured into two plastic containers. The bigger container contained the resin with the greater viscosity and a smaller cup with the 'thinner' fluid. Slightly more material was mixed to accommodate for losses in the runner and air vents.

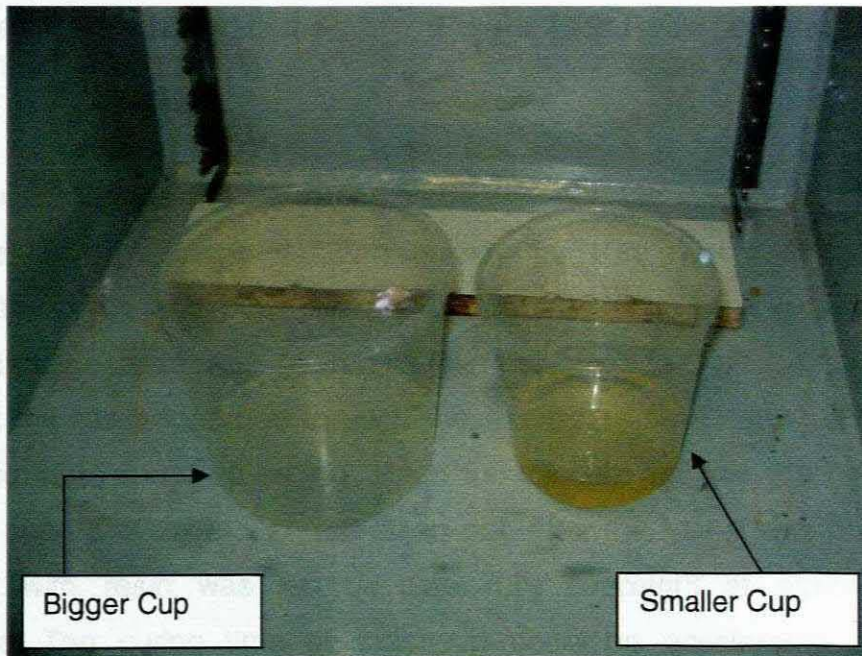


Figure 3.17: Measuring Cups for two-part resin

The resin was degassed for a while before it was loaded into its respective holders in the vacuum chamber. At this time the mould, with a funnel attached to the in-gate (or runner opening), were loaded onto the mould tray inside the chamber and placed in-line with the tipper. The mould was elevated at a slight

angle to allow resin to flow easier through the cavity. The bigger cup was stirred with a mixing paddle to hasten degassing and once the air bubbles decreased the smaller cups' contents was emptied into the mixing bowl (bigger cup). The mixing speed was increased due to the limited time allowed before resin curing. The pot-life for this kind of resin range generally from 3 to 7 minutes.

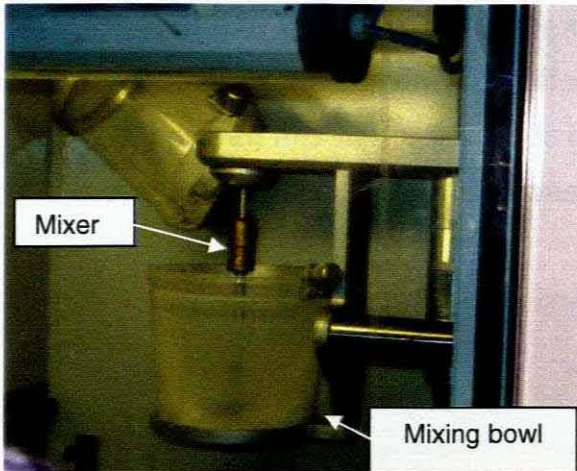


Figure 3.18: Part B resin added to the mixing bowl (part A)

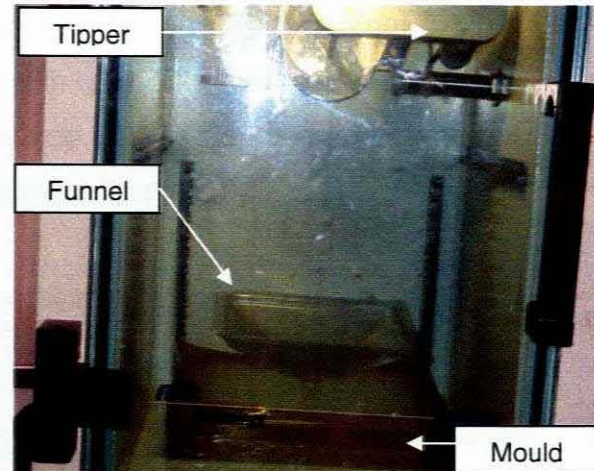


Figure 3.19: Resin poured slowly from the tipper into the funnel

The mixer was stopped and the mixing blade orientated to assist easy casting. A pressure shot (releasing vacuum quickly by 10kpa) was induced to smoothen the resin and burst excess air bubbles. The mixing bowl was swivelled and the resin was poured at a medium pace. Full vacuum was drawn until the resin appeared through the risers (the vent holes) and then released slowly to avoid splashing. Upon full vacuum release the chamber door could open and the mould was taken out. After the funnel was removed the mould with resin was left to cure fully overnight at atmospheric temperature. The curing time of the resin could be accelerated by low temperature heating (70°C) in an oven, but because this would cause temperature induced transformation of the shape memory alloys the former option was chosen. The plastic on top of the mould surface that 'leaked' through the runner and air vents gave one a good account of whether the material solidified adequately.

3.3.3 Part removal and Finishing

The packaging tape was removed from the mould and the staples along the split-line detached. The mould halves were carefully pulled apart and the casting specimen removed. Any vent pieces attached were broken off and the part was inspected for surface finish, flashing and cracks. It was expected that the final part would be quite porous due to the fact that the material did not flow easily into the cavity and stiffened up with time. The end result (see figure 3.20) proved this with a few voids concentrated near the ends of the plate, but nowhere near the severity that was initially expected.

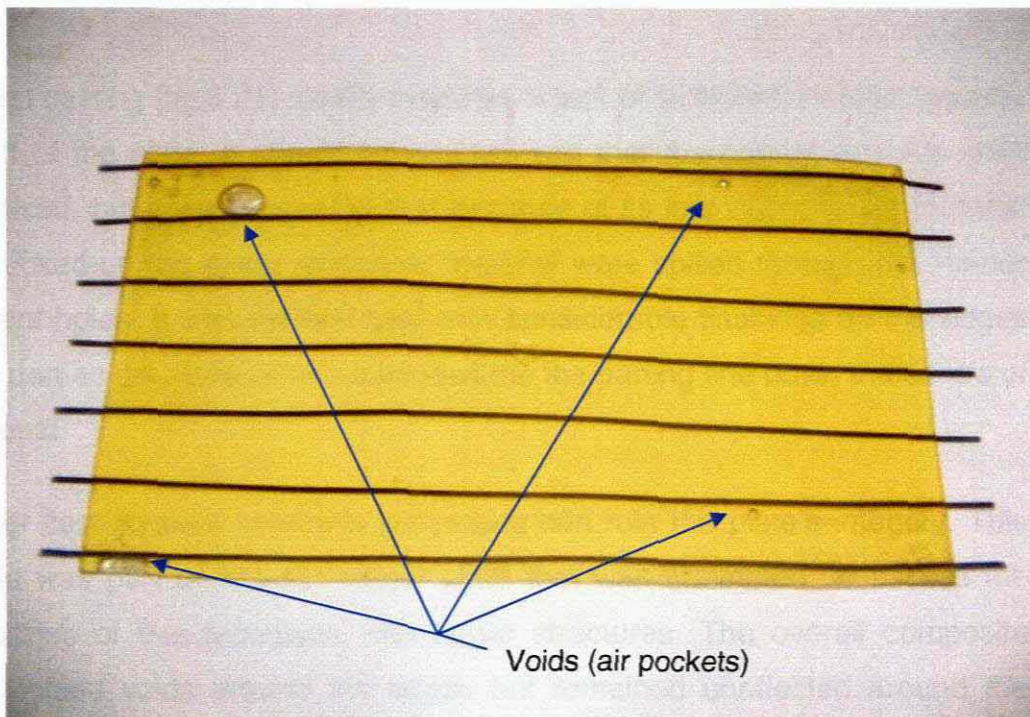


Figure 3.20: Polymer Composite plate with embedded SMA

The same manufacturing method was employed to cast other resins with varying shore hardness. Comparatively the results of two rigid thermosets, from different manufacturers, showed that not all materials are best suited to the vacuum casting process. These materials can surely be vacuum cast, but require that the process is slightly altered to obtain the desired effect.



Figure 3.21: Transparent Urethane from Smooth-On

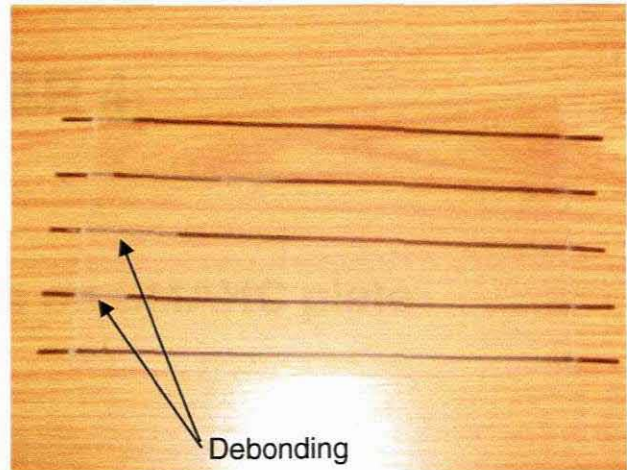


Figure 3.22: Similar Urethane from Axson

The first casting (fig.3.21) clearly indicates a lack of sufficient material towards the left of the plate. It should be emphasized that the correct quantity resin was mixed, but it was observed that because of its low viscosity the material was sucked-up too easily and most material were spilled through the runner and vent holes. It was the first cast with considerable flashings on the edges of the part as the material escaped towards the parting line down the centre of the mould.

Another cast showed how post processes can ruin the plate's integrity. This sample was part of a much bigger plate that was attempted, to assess the capabilities of this technique with larger structures. The overall composite plate yielded voids around the edges but remained unaffected around the locations of the SMA wires. The sample size was cut with a machine saw and because NiTi are hard materials the cutting action caused some debonding. This necessitated the recommendation that composites would be cut using only a diamond saw.

CHAPTER 4

Experimental Analysis on SMAHC plate

4.1 Introduction

This chapter introduces testing techniques employed to measure the effect of embedded SMA wire on the overall structural properties of a composite plate. An experimental protocol was developed to study the macroscopic behaviour of the SMA-polymer hybrid composite plates. The protocol investigated:

- a) Active and Passive Deflection of the SMA-polymer hybrid composite;
- b) The change in flexural rigidity of the SMA-polymer hybrid composite as a function of ambient temperature conditions; and
- c) The time taken for the deformed SMA-polymer hybrid composite plate to return to an un-deformed configuration.

4.2 Active and Passive Deflection Testing

Passively, the shape-memory alloy wires are used to strengthen the polymer matrix composites, to change the composite's stiffness and to close or repair possible cracks that may occur during the SMAHC's working life. Actively, the embedded SMA wires are usually activated by Joule heating and hence undergo the reverse martensitic transformation to austenite, giving rise to a change of stiffness in the SMAHC that influences its vibration frequency and

amplitude, acoustic transmission, structural tuning and change in the shape of the SMAHC.

The changes in these physical and kinematic material properties of the SMAHC are thus accomplished through: (i) the change in stiffness (inherent modulus) of the embedded SMA elements or, (ii) activating the pre-strained SMA elements to generate a stress (tension or compression) which “will tailor the structural performance and modify the modal response of the whole composite system just like tuning a guitar string” [53].

This experiment was conducted on Shape Memory Alloy Hybrid Composite Plates of varying thickness. Four rectangular plates were manufactured using the techniques described in Chapter 3 (with dimensions as indicated in the previous chapter, 260 x 150mm), and analysed using the methods detailed in this section. To check the accuracy of the manufacturing technique each specimen was measured for a nominal thickness along each of its axes (See Appendix B). These dimensional measurements showed that the manufacturing technique is adequate and the thickness deviation (of the order 0.01mm) is acceptable. The nominal thickness for the respective plates was found to be 4.04 mm, 4.05 mm, 6.7 mm and 7.7 mm.

4.2.1 Conceptualising the Theoretical Model for passive testing

Plates and shells are initially flat and curved structural elements, respectively, for which the thicknesses are much smaller than the other dimensions. Plates may be classified into three groups: thin plates with small deflections, thin plates with large deflections, and thick plates. The composite plate used within this study falls into the category of thin plates according to the criterion often applied to define a thin plate; the ratio of the thickness to the smaller span length should be less than $\frac{1}{20}$ [56].

The experimental set-up was constructed according to boundary conditions and generally employed assumptions of classical plate theory. A schematic of the experimental set-up that was devised is shown in figure 4.1.

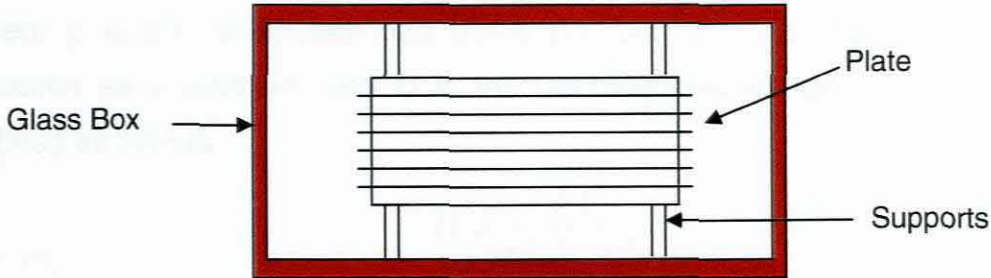


Figure 4.1: Top view of simply supported plate

The set-up was designed using a glass box that was constructed in the same way as detailed in the previous chapter with a base and outer walls. Two end supports, 12 mm in diameter, were machined to match the width of the plate. The T-shaped supports were placed symmetrically on the extremity of the container (box). The plate was positioned in the centre and loaded as illustrated in the next figure.

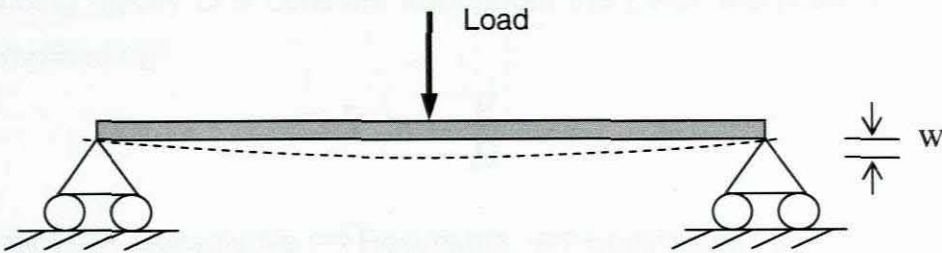


Figure 4.2: Plate with loading condition

The tests were conducted to obtain the required force leading to the in-plane displacement, w , at the mid-span. Many approaches exist for the problem presented here, but they all invariably were derived from the governing equation for the deflection of plates. The governing equation is summarized as follows:

4.2.2 The governing equation for deflection of plates

The small transverse (out-of-plane) displacement w of a thin plate is governed by the Classical Plate Equation,

$$\nabla^2 D \nabla^2 w = p$$

where p is the distributed load (force per unit area) acting in the same direction as z (and w), and D is the bending/flexural rigidity of the plate defined as follows,

$$D = \frac{Et^3}{12(3-\nu^2)}$$

in which E is the Young's modulus, ν is the Poisson's ratio of the plate material, and t is the thickness of the plate.

Furthermore, the differential operator ∇^2 is called the Laplacian differential operator Δ ,

$$\Delta \equiv \Delta^2 = \begin{cases} \left\{ \frac{\partial^2}{\partial r^2} + \frac{1}{r^2} \frac{\partial^2}{\partial \phi^2} + \frac{1}{r} \frac{\partial}{\partial r} \right. & \text{cylindrical coordinate} \\ & \text{(circular plates)} \\ \left. \frac{\partial^2}{\partial x^2} + \frac{\partial^2}{\partial y^2} \right. & \text{cartesian coordinate} \\ & \text{(rectangular plates)} \end{cases}$$

If the bending rigidity D is constant throughout the plate, the plate equation can be simplified to,

$$\nabla^4 w = \frac{p}{D} \quad (1)$$

Kinematics \Leftrightarrow Constitutive \Leftrightarrow Resultants \Leftrightarrow Equilibrium = Plate Equation

Where $\nabla^4 = \nabla^2 \nabla^2 = \Delta \Delta$ is called the biharmonic differential operator

An alternate form of this equation by expansion is:

$$\frac{\partial^4 w}{\partial x^4} + 2 \frac{\partial^4 w}{\partial x^2 \partial y^2} + \frac{\partial^4 w}{\partial y^4} = \frac{p}{D} \quad (2)$$

The theory of bending of rectangular plates was later derived from these formulae. The standard formulae obtained from the theory, however, may be presented in simple form and are relatively easy to apply. We now consider a

rectangular plate with only two opposite simply supported edges carrying a uniformly distributed load on a section of the plate

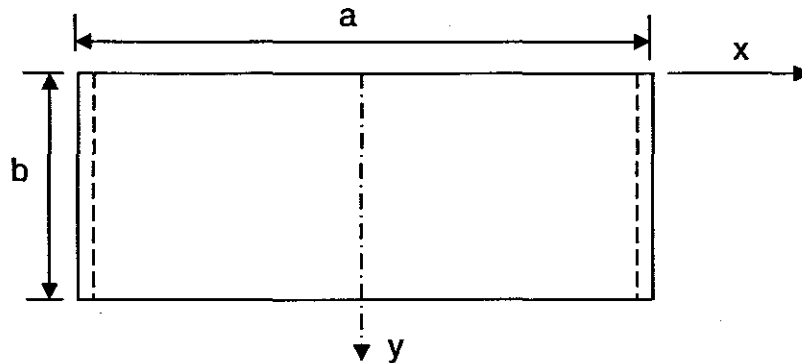


Figure 4.3: Top view of the plate with boundary conditions

The load P in equation 2 is represented by a load that is applied along the line passing through $x = \frac{a}{2}$ parallel to the y -axis. Clearly the loading described in

this problem deforms the plate into a cylindrical surface possessing its generating line parallel to the y -axis. We thus have $\frac{\partial w}{\partial y} = 0$ and $\frac{\partial^2 w}{\partial x \partial y} = 0$

that would reduce equation (2) to

$$\frac{d^4 w}{dy^4} = \frac{p}{D}$$

This expression is of the same form as the beam equation. Hence the solution proceeds as in the case of a beam.

4.2.3 Testing the deflection of passive SMAHC plates

The input parameters to the tensile tester included a loading rate of 2 mm/min and a pre-load of 0.7 N before results were recorded. The end-of-test condition was that all plates were deformed to a displacement of 8 mm and the subsequent force required to produce that deflection was recorded. This

data was used in the maximum deflection equation (for simply supported beams) and manipulated to provide the Flexural Rigidity, EI .

The load displacement behaviour of a 4mm plate is graphically presented in figure 4.4. From the graphs it is evident that a load of more than 2 N was required to achieve the default displacement of 8 mm.

The set-up for this experiment was found to be problematic. If we consider the figure 4.4 as two parts sectioned along 2.8 mm we observe that the graphs display different trends. The first section shows that during the first and third tests a load of 1.7 N was needed to deflect the plate to 2.8 mm displacement, however only a load of 0.7 N (the pre-load) was recorded for the second test at the corresponding stage. This was due to the start-of-test set-up where the central loading mechanism (plunger) was lowered to touch the surface of the plate. It was found that the plunger was not perpendicular to the plate, hence the questionable contact over the entire mid-span. The second part to this figure displays similar trends for all the three tests.

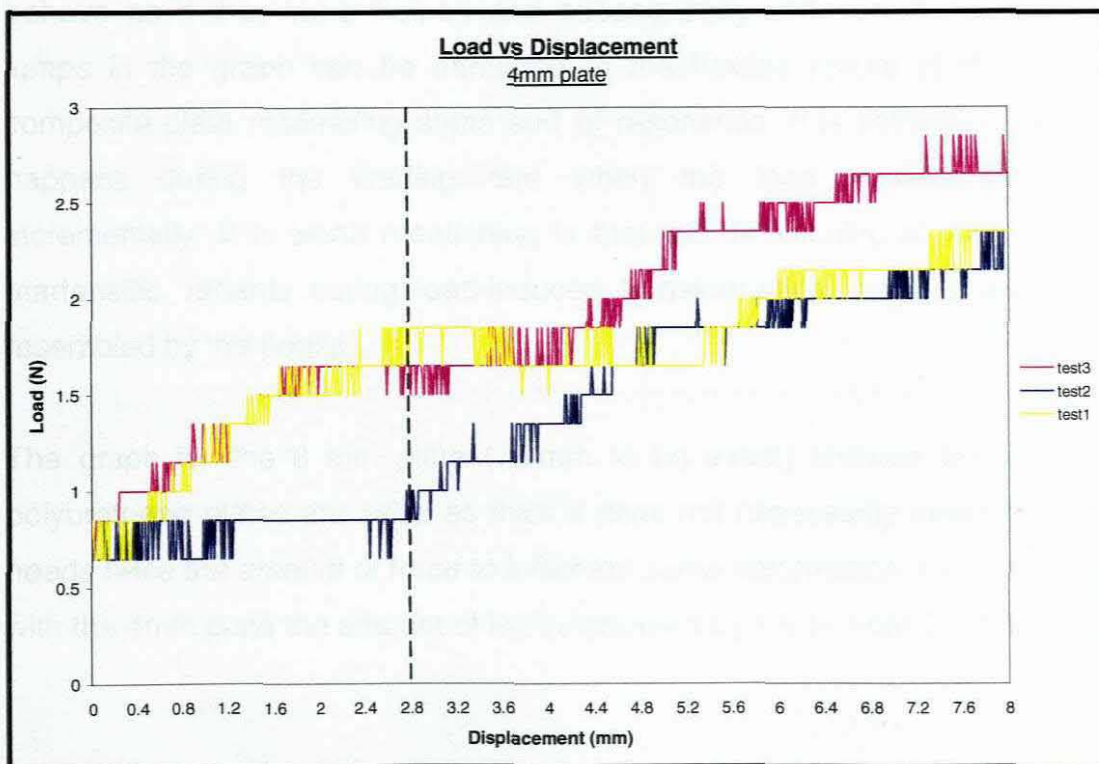


Figure 4.4: Trends for a 4mm plate deflected by 8 mm

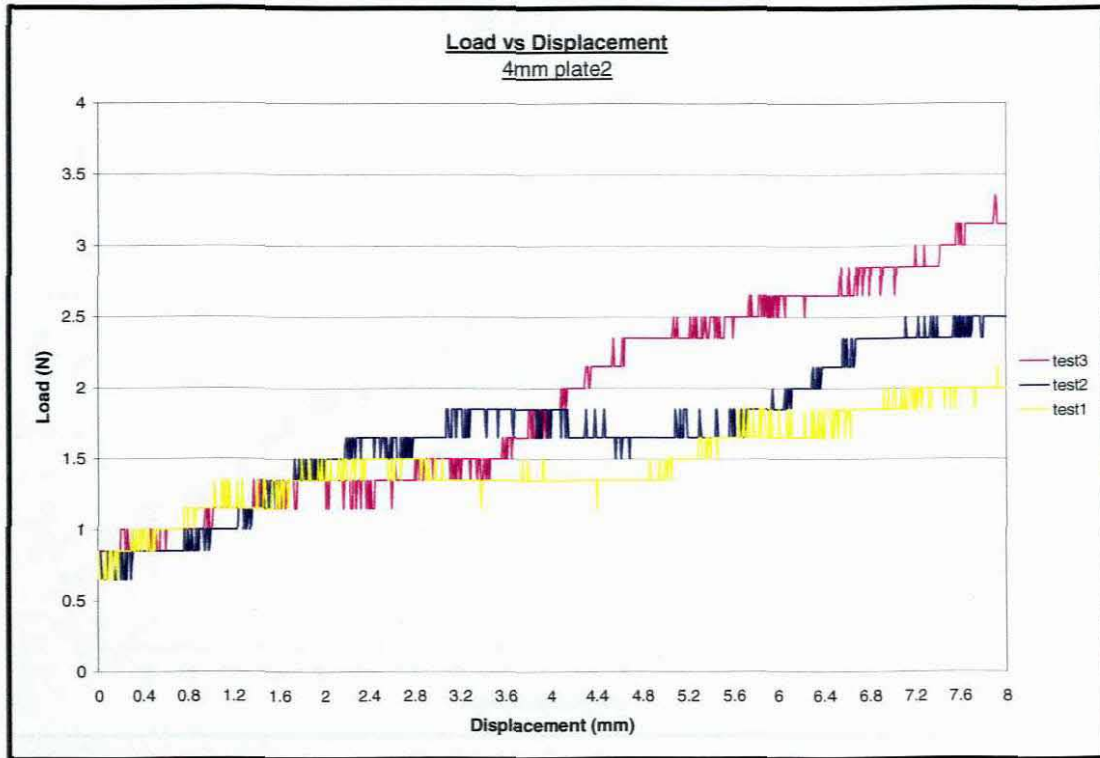


Figure 4.5: Trends for the second 4mm plate deflected by 8 mm

The curves show that after a few repeated tests the shape memory alloys behave as if they were trained and subsequently stiffened the plate. The jumps in the graph can be attributed to the flexible nature of the overall composite plate resembling some sort of resonance. It is assumed that this happens during the loading rate when the load moves downward incrementally. It is worth mentioning is that the de-twinning of the different martensitic variants during load-induced transformation, could possibly be resembled by the peaks.

The graph for the 8 mm plate (7.7mm to be exact) showed that if these polyurethane plates are twice as thick it does not necessarily mean that one needs twice the amount of force to inflict the same deformation. In comparison with the 4mm plate the amount of load increased by 1.5 N, from 2.2 N to 3.7 N

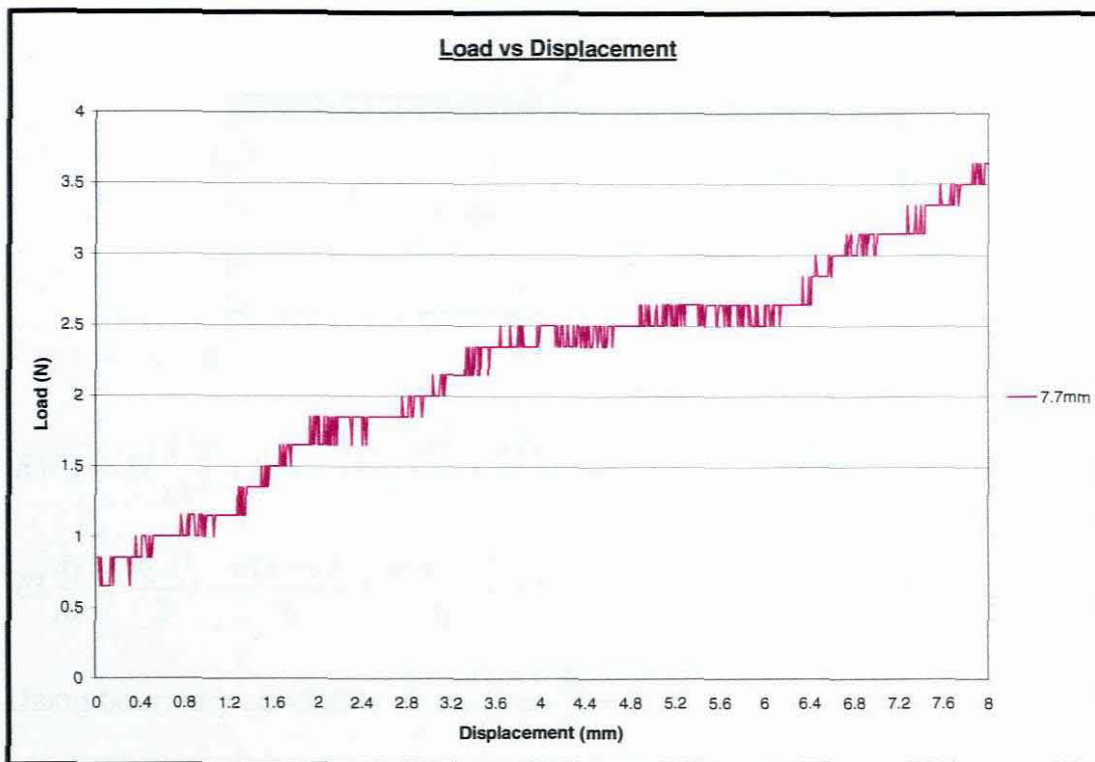
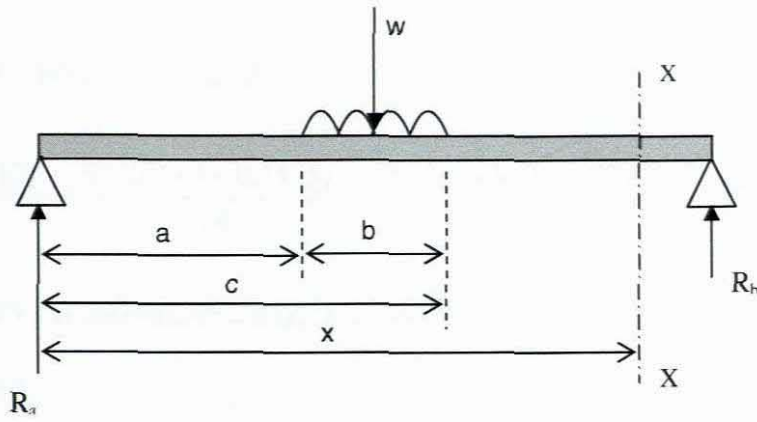


Figure 4.6: Load –displacement behaviour for 8mm plate

Another key observation is that these graphs, apart from the jumps, display the possibly similar load extension behaviour of a neat SMA wire. The shorter transformation is noticeable, but during these tests the SMA is loaded axially and the effect of the surrounding matrix has to be taken into account. One can only make such a deduction based on overwhelming evidence and it is recommended that numerous loading cycles be used for future work.

The data that were obtained from these deflection tests were imposed on the beam deflection equation from where the flexural rigidity / stiffness (the beams resistance to bending) was calculated. A typical calculation for the beam problem is described by the following formulation using the Macauly's Method:



$$BM_{xx} = EI \frac{d^2 y}{dx^2} = R_a \cdot x - \frac{w(x-a)^2}{2} + \frac{w(x-c)^2}{2} \quad \dots \text{BM equation}$$

$$EI \frac{dy}{dx} = \frac{R_a \cdot x^2}{2} - \frac{w(x-a)^3}{6} + \frac{w(x-c)^3}{6} + C \quad \dots \text{Slope equation}$$

Using boundary conditions @ $x = l \Rightarrow \frac{dy}{dx} = 0$

$$0 = \frac{R_a \cdot l^2}{2} - \frac{w(l-a)^3}{6} + \frac{w(l-c)^3}{6} + C$$

$$0 = \frac{1.14 \cdot (0.26)^2}{2} - \frac{91.2(0.26 - 0.1175)^3}{6} + \frac{91.2(0.26 - 0.1425)^3}{6} + C$$

$$C = -0.0192$$

Substituting into slope equation, we get:

$$EI \frac{dy}{dx} = \frac{R_a \cdot x^2}{2} - \frac{w(x-a)^3}{6} + \frac{w(x-c)^3}{6} - 0.0192$$

$$EIy = \frac{R_a \cdot x^3}{6} - \frac{w(x-a)^4}{24} + \frac{w(x-c)^4}{24} - 0.0192x + B \quad \dots \text{Deflection equation}$$

Using boundary conditions @ $x = l \Rightarrow y = 0$

$$0 = \frac{1.14(0.26)^3}{6} - \frac{91.2(0.26 - 0.1175)^4}{24} + \frac{91.2(0.26 - 0.1425)^4}{24} - 0.0192 \cdot (0.26) + B$$

$$B = 0.0025$$

Therefore the deflection equation for the above loading condition is:

$$EIy = \frac{R_a \cdot x^3}{6} - \frac{w(x-a)^4}{24} + \frac{w(x-c)^4}{24} - 0.0192x + 0.0025$$

For maximum deflection y_{\max} @ $x = \frac{l}{2}$

$$EIy = \frac{1.14(0.13)^3}{6} - \frac{91.2(0.13 - 0.1175)^4}{24} + \frac{91.2(0.13 - 0.1425)^4}{24} - 0.0192(0.13) + 0.0025$$

$$EIy = 0.000417 - 0.000000092 - 0.0025 + 0.0025$$

$$EIy = 0.000417$$

Giving a flexural rigidity of $EI = \frac{0.000417}{0.008} = 0.052 \text{ N.m}^2$

The calculation clearly showed that the two terms containing the integrating constants, C and B , vanished and that the moment due to the distributed load in the centre of the beam had very little effect on the final result. The general deflection equation would then reduce to:

$$EIy = \frac{R_a \cdot x^3}{6} - \frac{w(x-a)^4}{24}$$

The calculations for each plate thickness yielded the following results (shown in table 4.1) showcasing the rigidity (N.m^2) of each plate. (Consult Appendix E on the detailed calculation of each plate).

| Plate size | Load (N) | udl (m) | w | y (m) | EI (Nm^2) |
|------------|----------|---------|--------|-------|----------------------|
| 4.03 | 2.28 | 0.025 | 91.20 | 0.008 | 0.052 |
| 4.04 | 2.35 | 0.025 | 94.00 | 0.008 | 0.054 |
| 6.7 | 2.95 | 0.025 | 118.00 | 0.008 | 0.068 |
| 7.7 | 3.43 | 0.025 | 137.20 | 0.008 | 0.079 |

Table 4.1: Experimental data imposed on deflection equation

The two values for the thinner plates (i.e. 4 millimetres) have an almost negligible difference in flexural stiffness, which also validates the chosen methodology. The measurements (Seen in Appendix B) along the thickness of two supposedly identical plates are justified as the small variance in thickness accounts for the slightly bigger force required to deflect the second plate.

4.2.4 Testing of an active SMAHC

The same tests were repeated to evaluate the behaviour of the plates at an elevated temperature. It was decided to expose the plates to 75°C in the MK mini oven via convective heating. Each plate was kept at this temperature for 5 minutes before it was taken and positioned under the tensile tester. A preliminary test indicated that even when exposed to open air the composite did not lose its heat that quickly, which prompted the decision to record the temperature fluctuations at regular intervals during the test. As a result a thermocouple was attached to the surface of the plate to record the drop in temperature during the test.

Ideally these tests should be conducted using a steady state temperature, which will provide improved grounds for comparison. Even though these results could hardly be used in a quantitative analysis of the behaviour it was still useful in giving an idea of what to expect when these plates are heated. A test was later introduced that used a steady temperature via convective heating.

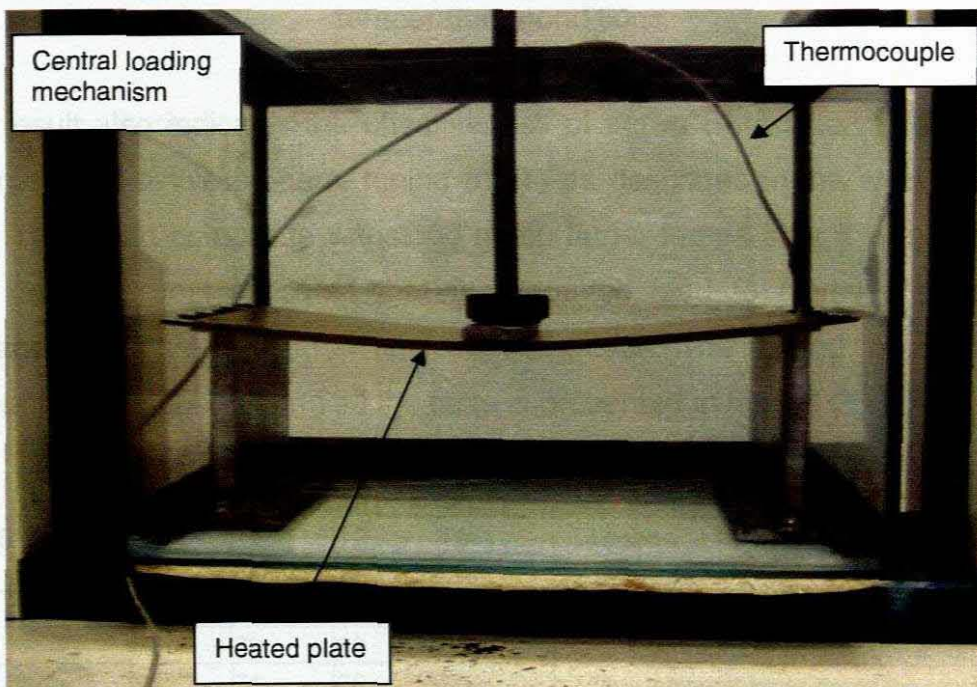


Figure 4.7: Experimental setup for deflection tests

The load-displacement behaviour of these tests shows how remarkably the actuation of the shape memory alloys enhances the flexural rigidity of the SMAHC plates (see Fig 4.8).

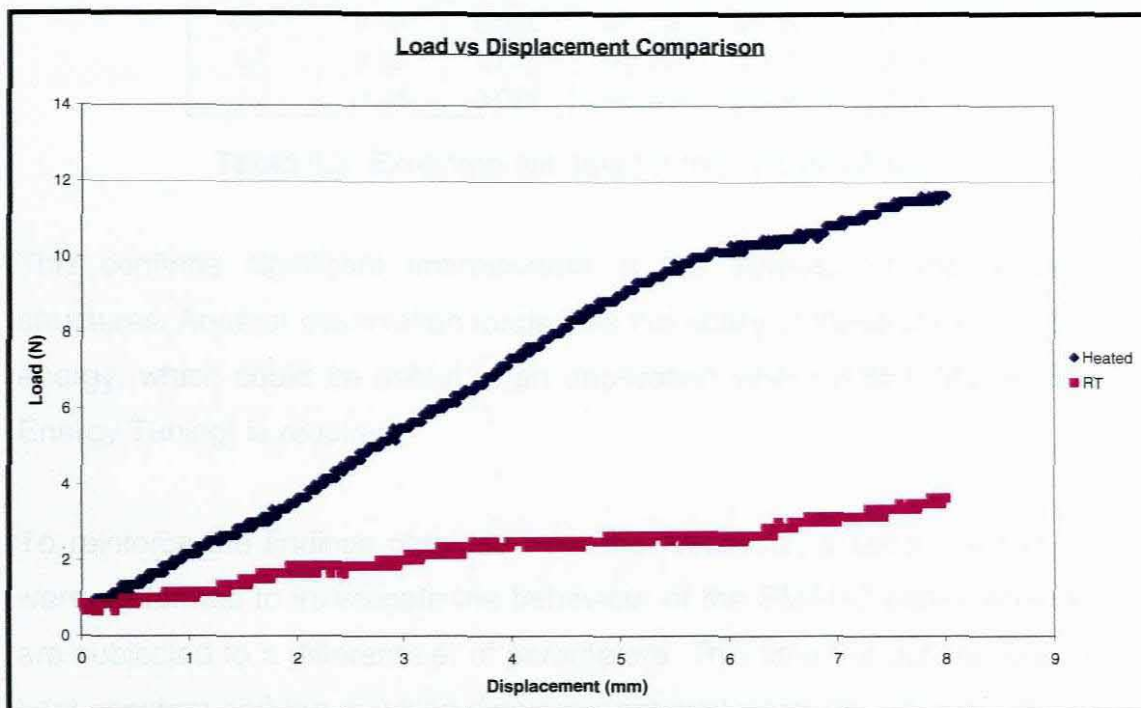


Figure 4.8: Comparison of 8mm plate under different temperature conditions

This result also indicates the effectiveness of active SMA when used in the application of active property tuning (APT) as described in the work by Wei et.al. The smart composite withstood much larger forces after it was heated. This particular test indicated that the required load to cause the default displacement increased three times in magnitude. The extend to which the temperature dropped during all the tests is presented in table 4.2

| Plate Size (mm) | Temperatures in deg C | | | |
|-----------------|-----------------------|----|----|----|
| | Ts | T1 | T2 | Te |
| 4.03 | 78 | 75 | 73 | 69 |
| 4.04 | 79 | 76 | 72 | 70 |
| 6.7 | 76 | 73 | 69 | 67 |
| 7.7 | 74 | 71 | 68 | 66 |

Legend
 Ts = Start temperature
 T1 = temperature at 2mm deflection
 T2 = temperature at 5mm deflection
 Te = temperature as deflection reached 8mm

Table 4.2: Temperature fluctuation during loading experiment

The results from the heated-plate experiments were also used in the deflection equation and yielded values in flexural stiffness of 0.099 N.m^2 , 0.125 N.m^2 , 0.224 N.m^2 and 0.254 N.m^2 .

| Plate size | Load (N) | udl (m) | w | y (m) | EI (N.m^2) |
|------------|----------|---------|--------|-------|-----------------------|
| 4.03 | 9.5 | 0.025 | 380.00 | 0.008 | 0.099 |
| 4.04 | 9.53 | 0.025 | 381.20 | 0.008 | 0.125 |
| 6.7 | 9.65 | 0.025 | 386.00 | 0.008 | 0.224 |
| 7.7 | 11.65 | 0.025 | 466.00 | 0.008 | 0.254 |

Table 4.3: Experimental data for the heated plate

This confirms significant improvement in the stiffness of the respective structures. Another observation made was the ability of these plates to absorb energy, which could be useful in an application where ASET (Active Strain Energy Tuning) is required.

To reinforce the findings obtained from the first tests, a second set of tests were performed to investigate the behaviour of the SMAHC plates when they are subjected to a different set of parameters. This time the applied load was kept constant and the resulting displacement evaluated. The incremental load was substituted with a weight on the centre span of the plate.

4.3 The change in flexural rigidity as a function of ambient temperature

The “memory” from all previous tests was erased and the plates flattened by heating the plates to 75°C inside the oven. In order to compare the macroscopic change in the plate due to temperature the same base (unheated) experiment was conducted. The flat plate was positioned on the end supports as previously giving an effective span of 232 mm between the supports. A 20 mm-square bar was cut to 150 mm length and used as the weight in the experiment. The bar weighed at a mass of 475 g.

The weight was placed in the centre of the plate and the deflection was measured. The bar was then removed and the vertical deflection again recorded to obtain the recovery.

The oven was switched on and allowed to reach 75°C. *This convection oven always heated the elements to around 82°C and then regulated the temperature in the chamber to 75°C.* Each plate was kept at this temperature for 12min to ensure that the whole plate flattened through the heat expansion. The SMAHC plate was loaded and the resulting deflection measured. As with the base experiment the load was removed and the remaining displacement checked.

The results gained from these experiments provided an insight into the smart behaviour of these semi-rigid polyurethane plates with embedded SMA. This testing method also made it possible to capture data of the remarkable recovery of restrained SMA. It identified two key factors that should be considered when an active structure is designed.

- The NiTi shape memory alloy used throughout this thesis could be pre-strained even more before it is embedded into the host structure. This would enable much higher recovery forces that could be exploited in an application such as the active surface.
- The shape memory effect and shape recovery is best exhibited under load and temperature.

The table below contains the results indicating the possibility of obtaining enhanced shape control. These were preliminary tests, which were also checked against the first series of tests. The results were also imposed on the deflection equation to investigate how the flexural stiffness was altered.

| Plate size | Tests without heating | | | | Tests with heating at 75C | | | |
|------------|-----------------------|--------|------------------|--------|---------------------------|--------|------------------|--------|
| | Cycle1 | Cycle2 | Cycle1 | Cycle2 | Cycle1 | Cycle2 | Cycle1 | Cycle2 |
| | y in mm | | y after recovery | | y at 75°C | | y after recovery | |
| 4.03 | 22 | 22 | 12 | 12 | 4.7 | 5 | 0 | 0 |
| 4.04 | 22 | 21 | 12 | 13 | 4.5 | 4.8 | 0 | 0 |
| 6.7 | 17.8 | 17 | 10.8 | 11 | 3 | 2 | -4 | -3 |
| 7.7 | 14.5 | 14.5 | 7 | 8 | 2.5 | 2 | -1 | -2 |

Table 4.4: Deflection of SMAHC plate at an elevated temperature

The behaviour of the thicker plates, upon removal of the weight, is best described by the accompanying figure.

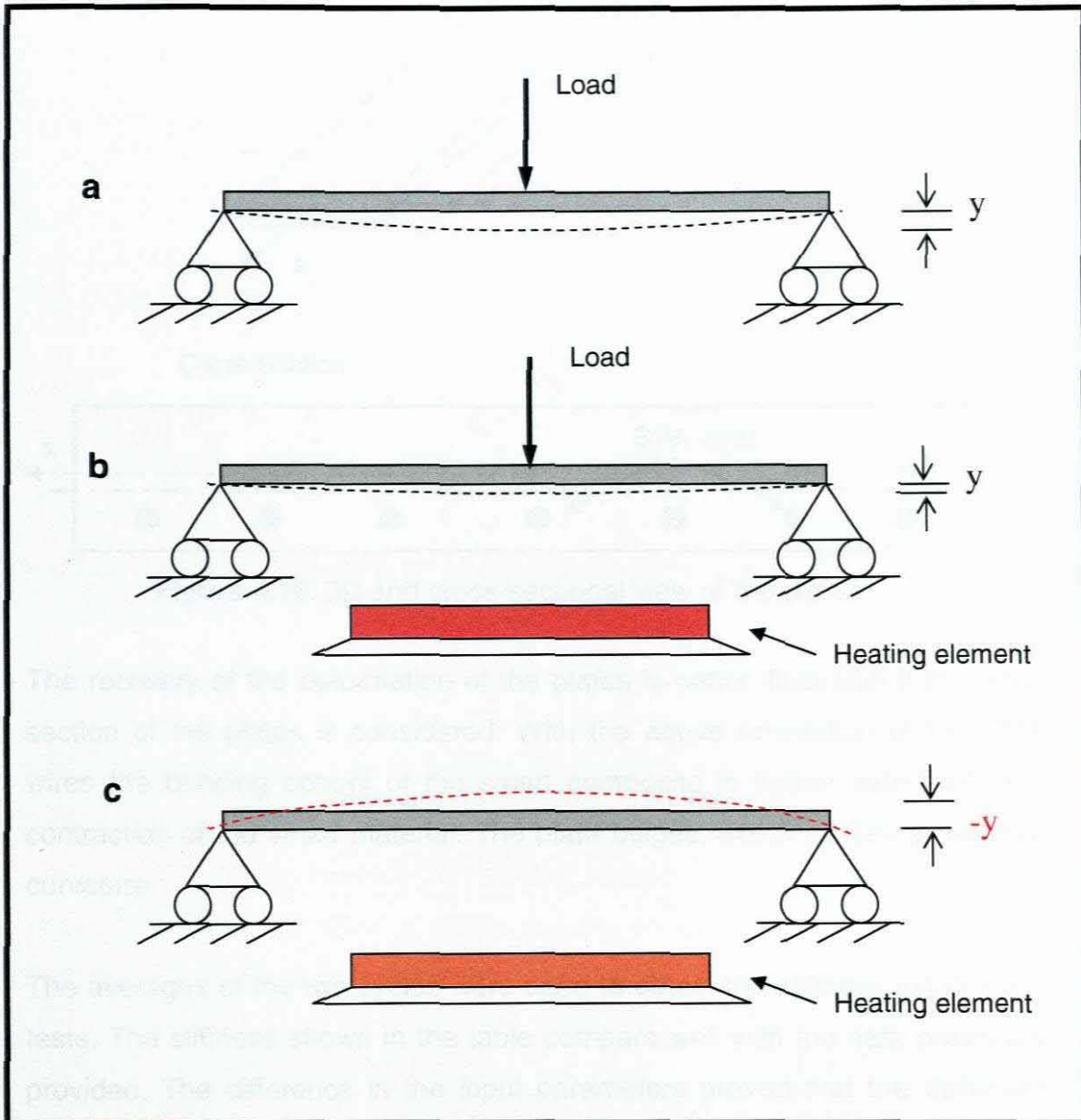


Figure 4.9: Schematics of the deflection tests conducted with (a) no heating, (b) induced load and temperature, (c) induced temperature

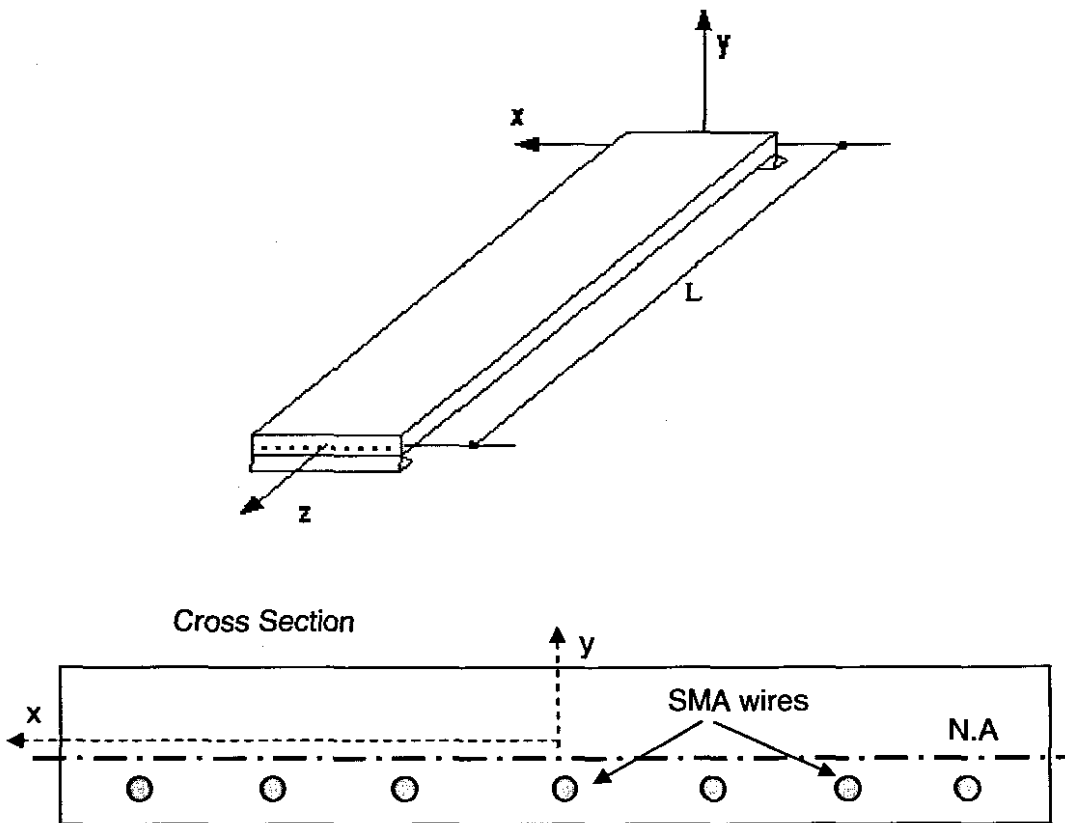


Figure 4.10: 3D and cross-sectional view of the plates

The recovery of the deformation of the plates is better illustrated if the cross section of the plates is considered. With the above orientation of the SMA wires the bending control of the smart composite is further aided with the contraction of the smart material. The plate bulges, which causes a negative curvature.

The averages of the two cycles were used to obtain the stiffness using these tests. The stiffness shown in the table compare well with the data previously provided. The difference in the input parameters proved that the deflection equation could successfully be used to obtain any of the variables. For the tests in the oven the load was kept constant and the different deflections were substituted into the equation. As expected the constant heat provided by the oven kept the plates stiff, hence the higher values for the rigidity, EI .

The flexural rigidity of the deformed plates at room temperature correlates well with the corresponding values that were obtained using digitally measured data from the tensile testing machine.

The bigger differences common to the thicker plates could be ascribed to measurement errors, such as the height gauge used in this experiment and the probability of the error of parallax.

| Plate sizes (d) | Machine tests | | Oven Tests | |
|-----------------|---------------------------------------|---------------------------------------|---------------------------------------|---------------------------------------|
| | Room temp | Elevated temp | Room temp | Elevated temp |
| | Flexural Stiffness (Nm ²) | Flexural Stiffness (Nm ²) | Flexural Stiffness (Nm ²) | Flexural Stiffness (Nm ²) |
| 4.03mm | 0.052 | 0.099 | 0.039 | 0.180 |
| 4.04mm | 0.054 | 0.125 | 0.040 | 0.186 |
| 6.70mm | 0.068 | 0.224 | 0.049 | 0.365 |
| 7.70mm | 0.079 | 0.254 | 0.059 | 0.405 |

Table 4.5: Stiffness results for the various plates

4.4 Analysing the composite's recovery after deformation

Further tests into the behaviour of the Shape Memory Alloy Hybrid Composite were conducted to quantify the transformation of the constrained SMA. The host material used in this study does not have a high glass transition temperature and is a semi-rigid plastic that could easily border on the shore hardness scale for rubber. A heating test on this thermoset plastic revealed that 80°C and higher softens the material drastically and that the material became silky. This necessitated the use of convective heat rather than the direct method of resistive heating. It was feared that serious debonding between SMA wires and host would occur.

4.4.1 Objective

- To establish the time consumed for a SMAHC plate to transform back to its original shape.
 - Investigate the effect of plate thickness on transformation time

4.4.2 Methodology

The methodology below was followed ensuring that the same experimental procedure was repeated throughout all tests.

Step 1 Ensure that the SMAHC plate is horizontal to the x plane (i.e. flat) Excess handling of the plate and exposure to a fluctuating environmental temperature might induce small deformation *whether twisting, bending, or stretching (thermal expansion).*

Conduct one heating and cooling cycle. Expose the specimen (plate) to the typical transformation temperature for the NiTi wire used in the study i.e. 75°C, by placing the plate inside the oven on the wooden support base. Heat the specimen for 15 min. The sample becomes soft (passes its transition temperature) and flattens during this time. Also expect that the plate will display some curvature as the orientation of the pre-strained wires aid *bending.*

Step 2 Turn the oven off, and allow the specimen to cool as the temperature decreases. This may take another 15 minutes.

Step 3 Remove the specimen (plate) from the oven and allow it to cool further in still air (RT, 22°C). This step requires 20 minutes, but can be hastened by quenching the plate in a water bath. The plate should now be free from the recovery stresses *produced by the induced thermal load. Check that the plate has its original dimensions (with respect to size and shape).*

Step 4 All specimens should undertake this cycle to ensure that all the plates are 'stabilized'.

Step 5 Set the oven to 75°C and allow it to heat up to this temperature. Give 5 minutes for the temperature to settle. Position the support base on the oven grid.

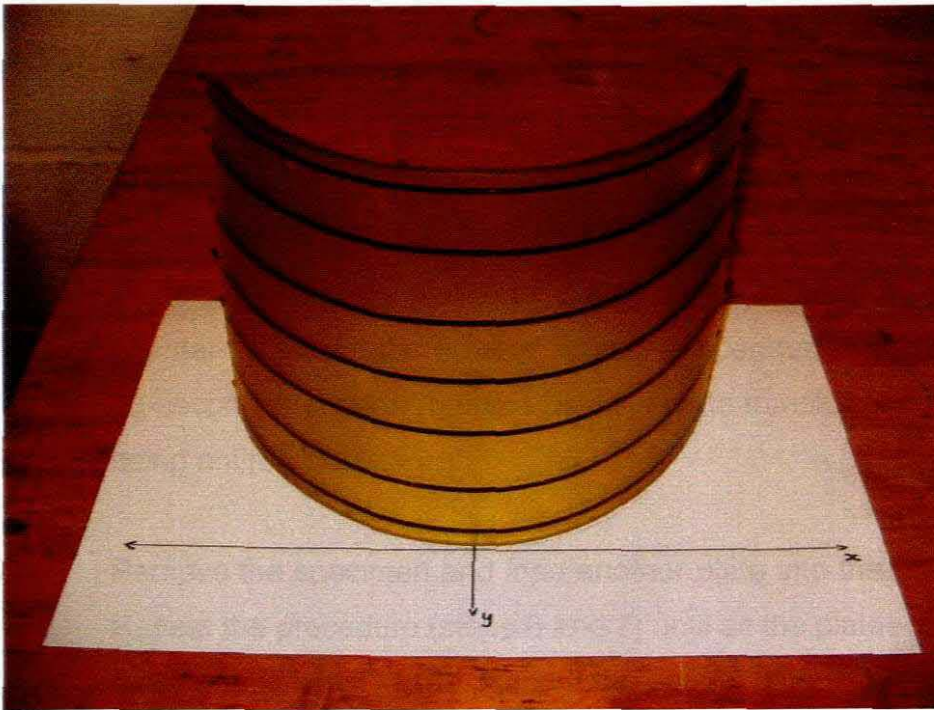


Figure 4.11: Curved 4mm SMAHC plate

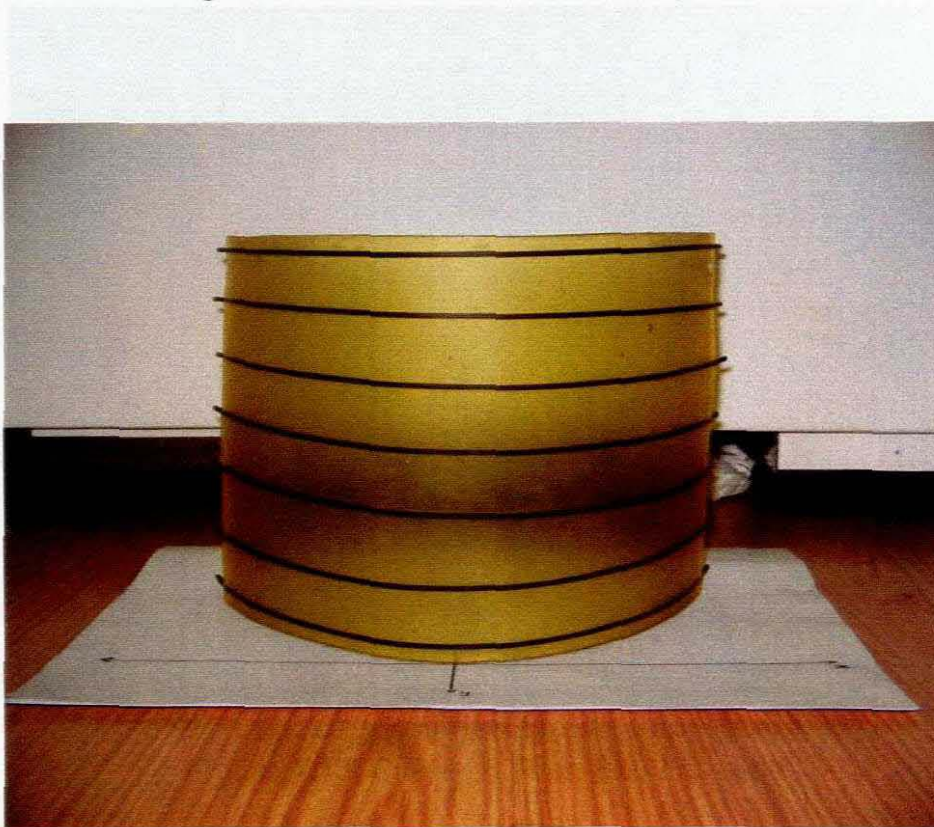


Figure 4.12: Curved 4mm SMAHC plate

All specimens are deformed into a pre-determined shape before actuation. Each plate was rolled to a set positive (convex) curvature. It was important to check for conformability and consistency on a set curve that was produced on an x-y axis. All the plates were checked for their shape on this curve (see figures 4.11 – 4.13)

Step 6 Place the first plate (the 4mm plate) on the base in its convex orientation. Close the lid and record temperature and time, at 30-second intervals. Continue until the plate transformed back to being entirely flat.

Step 7 Remove the specimen and load another plate into the chamber. Repeat the procedure (steps 6 and 7) until all the plates reverted back to their initial shape. Record the data and findings.

Figure 4.14: Curved 7.7mm SMAHC plate

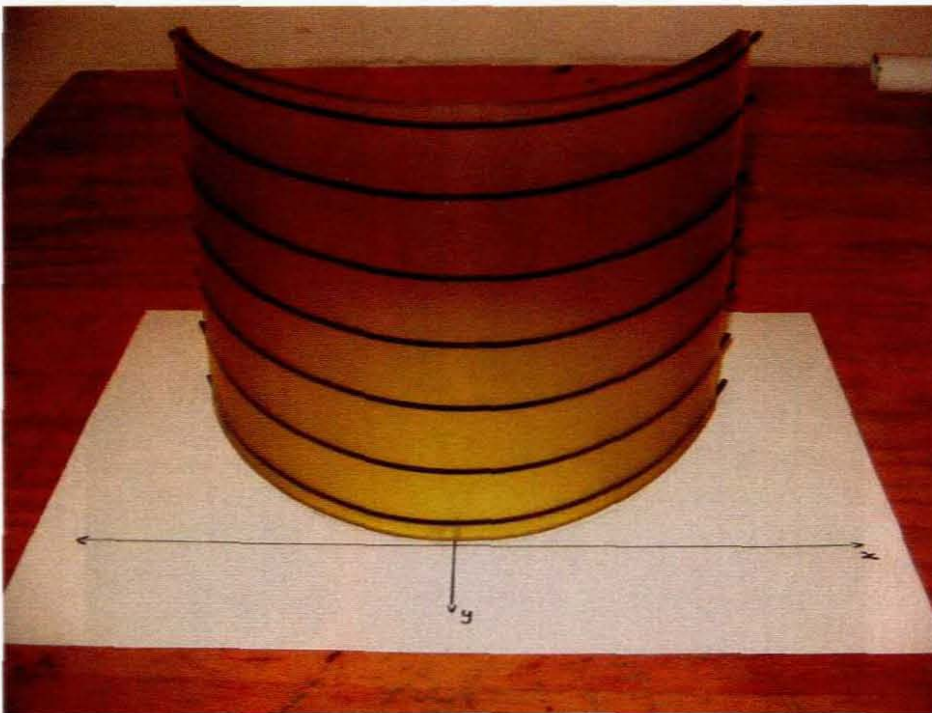


Figure 4.13: Curved 6.7mm SMAHC plate

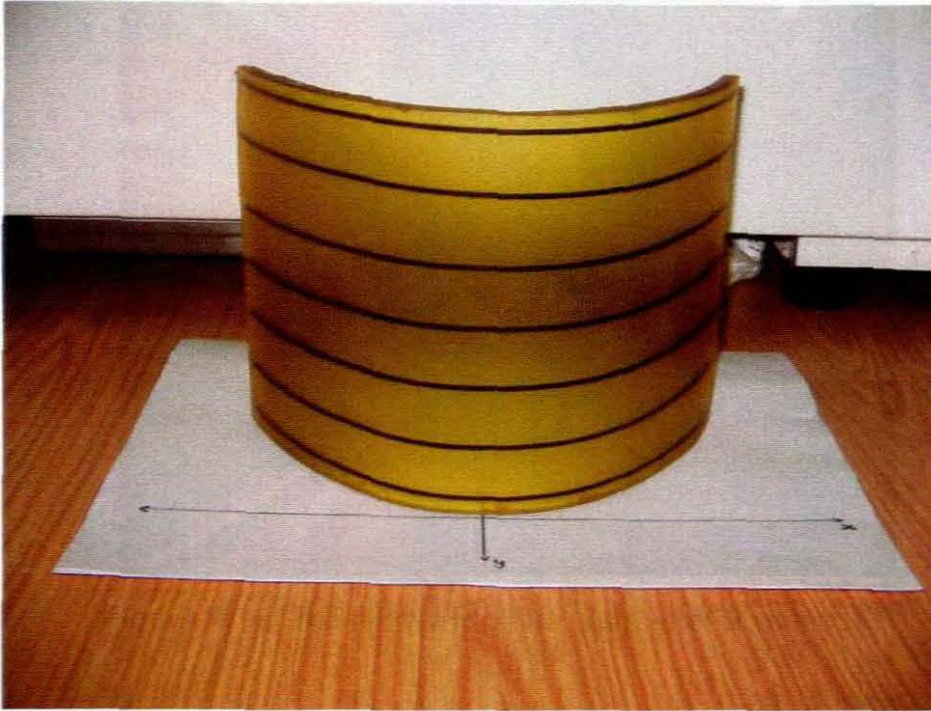


Figure 4.14: Curved 7.7mm SMAHC plate



Figure 4.15: A 4mm plate at the start of the experiment, $t = 0$ sec



Figure 4.16: The recovery of the plate after 90 seconds.

4.4.3 Results and discussion

The tests provided an idea of how long the shape memory alloys take before they transform to their original configuration when exposed to an elevated environmental temperature. All specimens were subjected to 3 cycles of the same test described in the methodology. The results of these tests are displayed in table 4.6

| | PLATE 1 | PLATE 2 | PLATE 3 | PLATE 4 | | | |
|--------------|----------|---------|----------|---------|----------|---|-----|
| Cycle | Time (s) | Cycle | Time (s) | Cycle | Time (s) | | |
| 1 | 142 | 1 | 150 | 1 | 270 | 1 | 396 |
| 2 | 146 | 2 | 154 | 2 | 274 | 2 | 394 |
| 3 | 146 | 3 | 149 | 3 | 268 | 3 | 388 |
| Average time | 144.7 | 151 | 270.7 | 392.7 | | | |

Table 4.6: Data for the time elapsed (in seconds) during the tests of flattening the plates.

The average values of the results for the first two plates supported the decision to cast two identical plates to investigate repeatability in the manufacturing process. The measurements of plate thickness (Appendix B) indicated a small variance in thickness, which ultimately led to an increase in transformation time. The SMAHC plate was also placed in the oven in its

manufactured state to observe if any traces of recovery stress existed that could be used for active shape control.

The SMAHC systems were placed in the mini oven as displayed in the figure below. A videocamera was used to capture images of the deflections at different times in the heating of the plates. Thermocouples were used to measure the temperature of the upper and lower surfaces of the beams.

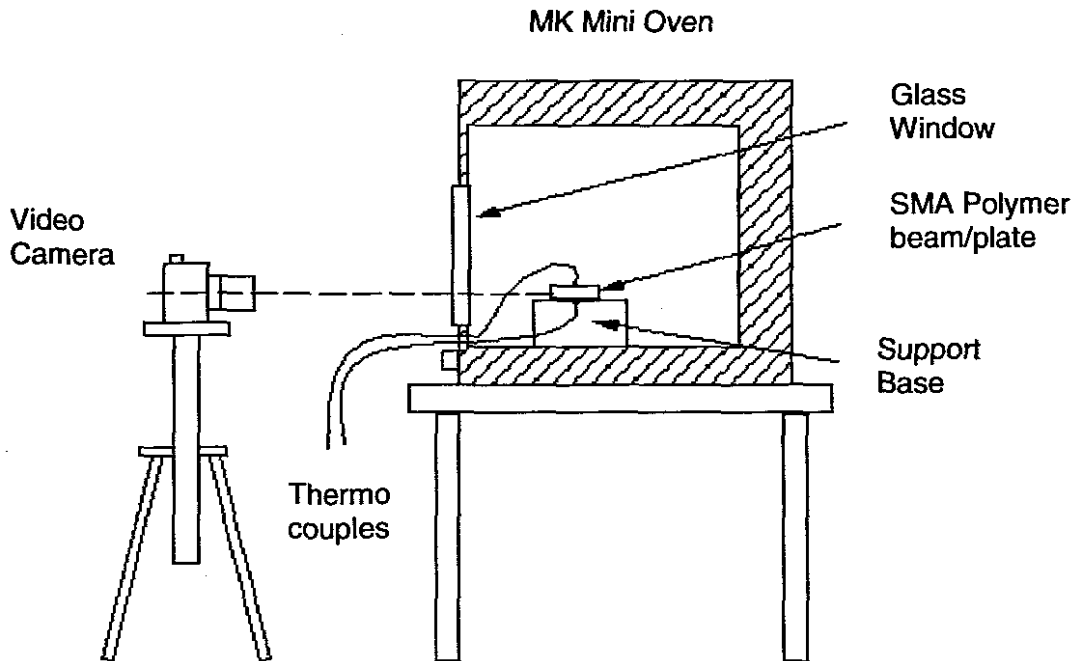


Figure 4.17: Experimental set-up for imaging SMA plate deflections.

An interesting behaviour was noted during the duration of each test that was later verified from the videos of each experiment. Initially the beam was at zero curvature due to negligible residual stress development at the SMA polymer curing (at room temperature) stage. The development of a positive curvature in the beam is related to the movement of the neutral axis during the experiment. At low temperature in the beginning of the experiment, the neutral axis is near the geometric centreline and there is a temperature gradient across the beam; the top surface is hotter than the bottom surface by about 10°C. Balance of the thermal expansion across the thickness of the beam creates a small downward deflection (negative curvature) of the beam (See figure 4.19). As the temperatures increased further, the top of the beam reached the glass transition temperature of the urethane first.

When this occurs, the material near the top of the beam relaxes and drops in stiffness by about two orders of magnitude. The neutral axis moves rapidly away from the geometric centreline and the thermal gradients across the beam thickness begin to pull the beam upward leading to a positive curvature.



Figure 4.18: SMAHC plate in the horizontal position.



Figure 4.19: The SMAHC plate bulging (negative curvature).



Figure 4.20: End of experiment showing very slight positive curvature.

CHAPTER 5

Conclusions

5.1 Conclusions

This document presented the work undertaken in the development of an active surface through the use of shape memory alloys. This active surface can be used in a variety of applications that require the change of the shape of structural members such as submarine sterns, aerospace-vehicle control surfaces, i.e. aircraft wings, etc. The active surface is achieved when the flexible composite structure's shape gets altered through the activation of the embedded SMAs.

An experimental protocol was developed to treat or stabilize shape memory alloys that are used as actuators within composite structures. It was reported that shape memory alloys exhibit complex behaviour during their quasi-plastic material response. The complex behaviour included variability in yield values and the transformation region/range. Two treatment methods were employed to obtain similar behaviour (uniform mechanical properties) between neat SMA wires.

The manufacturing of the shape memory alloy hybrid composite (SMAHC), to be used in an active surface, was achieved using a novel approach. Nickel-Titanium (NiTi) wires were embedded into a very low-modulus matrix through a vacuum casting process and the use of room temperature curing. A methodology was introduced to analyse or test the composite for shape control.

5.1.1 Experimental Investigation

The remarkable behaviour shape memory alloys exhibit is categorized into two unique material responses, ascribed to thermo-elastic martensitic forward and reverse phase transformations, being the shape memory effect and the pseudo-elastic effect. The shape memory alloy actuator used in this study harnesses the shape memory effect, hence the investigation into an important aspect of the shape memory effect, the quasi-plastic material response. Shape memory alloys exhibit this behaviour, under different loading conditions, when in their low temperature martensitic state. In our case the behaviour was analysed under tensile loading conditions. These tests gave a good indication of the material's mechanical properties and provided the opportunity to compare the quasi-plastic response of individual shape memory alloy wires.

It was evident that "packaged" SMA material display distinct variability within regions of tensile testing. The introduction of two methods, to enhance the reliability by providing a more homogeneous material, produced interesting results.

The key aspects of the experiments conducted on the 2mm and 3mm NiTi shape memory alloy were summarized as follows:

- The results confirmed and supported the views that often appear in literature i.e. that the nature of the behaviour exhibited by shape memory alloys is quite complex. Some of these complexities include:
 - Non-homogeneous transformation regions
 - Variable elastic yield values
 - Inconsistent measures of strain

- Probably the single biggest outcome was how aging affected the material. The Aging procedure erased the hardening-like behaviour that the material displayed in tests conducted by Philander in 2004. (See Fig. 2.7)
- Other findings that were reported in the unpublished work by Doctor Mukhuwana that might become critical parameters in future work are:
 - Thermo mechanical cycling increases the transformation strain.
 - The thermo mechanical cycling also decreased the initial elastic strain.
 - Thermo mechanical cycling decreased the initial yield loads.
 - When NiTi Shape memory alloys undergo thermo mechanical cycling it removes variability in both initial elastic strains and yield loads.

5.1.2 The manufacturing of the composite

Process and manufacturing difficulties that were reported in the literature were all considered in the project's planning and decision-making stage. This led to the fabrication of shape memory alloy hybrid composite (SMAHC) by using a vacuum casting process. Nickel-Titanium rods, 2mm in diameter, were embedded in a silicone mould and a very low-modulus (flexible) casting urethane were mixed and poured over the wires. Unlike the methodology used by Tsoi et al. [45] who built fixture jigs to constrain the shape memory alloy wires to the required amount of pre-strain, an easy lay-up technique was used which allowed the part to cure at room temperature. This manufacturing technique negated the danger of inducing the forward transformation of martensite to austenite, which is often caused by high temperature curing (evident in most work, [27], [28], [37], [38], [43-46], [52], [54]). The success rate with these castings was not that high initially, as problems like irregular flow and increased void formation surfaced. Overall this method displayed enough positives like the good repeatability of the thickness cast given by a 0.01mm deviation.

5.1.3 The implementation of a testing technique for shape control

In Chapter 4 an experimental protocol was developed to study the behaviour of the SMA-polymer hybrid composite plates as active surfaces. The protocol investigated:

- Active and Passive Deflection of the SMA-polymer hybrid composite;
- The change in flexural rigidity of the SMA-polymer hybrid composite as a function of ambient temperature conditions; and
- The time taken for the deformed SMA-polymer hybrid composite plate to return to an un-deformed configuration.

The testing techniques that formed the protocol were used to evaluate the effect of the actuated shape memory elements on the shape of the overall composite.

The specimen thickness showed the anticipated behaviour of the overall matrix with respect to time. It took much longer for the thicker (6.7 mm and 7.7 mm) plates to transform back to their original position (i.e. flat) after they were formed and heated.

The deflection tests provided encouraging results that served as good foundation work for ongoing research. These tests quantified the contribution of NiTi shape memory alloys to the overall structural properties and particularly the plate's flexural rigidity.

| % Increase in stiffness due to temp | | |
|-------------------------------------|-----------------|-------|
| | Tensile machine | Oven |
| 4.03mm | 90.4 | 361.5 |
| 4.04mm | 131.5 | 365.0 |
| 6.70mm | 229.4 | 644.9 |
| 7.70mm | 221.5 | 586.4 |

Table 5.1: The percentage increase in flexural rigidity of a SMAHC beam subjected to elevated temperatures

One particular aspect of using NiTi shape memory alloy wire actively in a host matrix material was also proven in this work through the use of Active Property Tuning. The results in table 5.1 show significantly high levels of improvement of rigidity in the respective composite plates.

With further refining and the acquisition of more precision equipment the active shape behaviour can be more accurately predicted.

5.2 Recommendations

When pre-strained shape memory alloys are actuated within composite structures the material tends to contract bringing about recovery stresses. As noted in the literature survey, a considerable number of studies have been previously undertaken both experimentally and analytically to clarify the roles of the shape recovery force generated by SMA wire actuators. However, experimental models of previous researchers were limited to cantilever beams.

In more realistic structures, which are subjected to in-plane forces due to external and thermal loading, compressive loads should be considered as a very important factor. The flexible members in various engineering structures are primarily loaded in axial compression or tension. To this extend the need exists to analyse shape memory alloy elements in compression and to evaluate structures that are subjected to a compressive load.

The host material used for the composite should be carefully chosen. It was found during their fabrication that not all resins are suited to a vacuum casting process. The low viscosity materials are probably more suited to pressure casting where the trapped air gets displaced by applied pressure instead of vacuum. The optimum pouring angle should be obtained for medium flow cast instead of piercing the mould full of vent holes. This would also decrease post process surface finishing. The host material should also preferably have a glass transition (T_g) temperature considerably higher than that of the shape

memory alloys to enable resistive heating without running the risk of melting the material and defusing the bond.

A heating chamber can be manufactured and fitted to both the tensile and fatigue testing machines in order to expand on the current work. This will enable the execution of different load and cyclic tests with steady state temperatures and yield further data contributing in this field.

References:

- [1]. Jonnalagadda, K. D., Sottos, N.R., Qidwai, M. A., Lagoudas, D.C. **Transformation of embedded shape memory alloy ribbons**, *J. of Intell. Mat. Sys. and Struct*, 9, 379-390, 1998
- [2]. Van Humbeeck, J., **Non-medical applications of shape memory alloys**, *Materials Science and Engineering*, A273-275, 134-148, 1999.
- [3]. Birman, V., **Review of Mechanics of Shape Memory Alloy Structures**, *Applied Mechanics Review*, 50(11), 629-645, 1997
- [4]. www.memory-metalle.de/basics.html
- [5]. Boyd, J.G. and Lagoudas, D.C, **A thermodynamic constitutive model for shape memory materials, Part 1. The monolithic shape memory alloy**, *Int. J. of Plast*, 12, 805-842, 1996
- [6]. Shaw, J. A., **A Thermal mechanical model for a 1D Shape Memory Alloy Wire with Propagating Instabilities**, *International Journal of Solids and Structures*, 39, 1275, 2002
- [7]. Shaw J. and Kyriakides, S., **Thermo mechanical aspects of NiTi₂**, *J. Mech. Phys. Solids*, 43, No.8, 1243, 1995.
- [8]. Lagoudas D. C, Bo Z, Qidwai M. A. **A Unified Thermodynamic Constitutive Model for SMA and Finite Element Analysis Of Active Metal Matrix Composites**, *Mech of Comp Mat and Struct*, 3, 153-79, 1996.
- [9]. Qidwai M.A and Lagoudas D.C. **On thermomechanics and transformation surfaces of polycrystalline shape memory alloy materials**, *Int. J. Plasticity*, 16, 1309 – 1343, 2000.
- [10]. Webb, G. V, Kurdila, A. J & Lagoudas, D. C. **Hysteresis modelling of SMA actuators for control applications**. Final Paper sent to JIMSS, 1998.

-
- [11]. Bidaux, J. E, Bataillard, L, Manson, J. A., and Gotthardt, R. **Phase transformation behaviour of thin shape memory alloy wires embedded in a polymer matrix composite**, In *Proceedings of 3rd European Conf. on Advanced Materials and Processes*, Paris, France, 1993.
- [12]. Krumme, J. F. **Connect. Technol.**, Vol 3 (No. 4), April 1987, p 41
- [13]. Paine, J.S.N, Rogers, C. A. **The Effect of thermo plastic composite processing on the performance of embedded Nitinol Actuators**, *J. of Thermoplastic composite materials*, 4, 102 – 122, 1991.
- [14]. Simon, M. et al., **Radiology**, Vol 172, 1989, p 99-103
- [15]. Harrison, J. D., and Hodgson, D. E., **Shape Memory Effects in Alloys**, J. Perkins, Ed., Plenum Press, 1975, p 517
- [16]. Product Brochure, Raychem Corporation, Menlo Park, CA
- [17]. Hodgson, D. E., **Proceedings of Engineering Aspects of Shape Memory Alloys**, (Lansing, MI) 1988.
- [18]. Shaw, J. A, **Simulations of localized thermo-mechanical behavior in a NiTi shape memory alloy**, *International Journal of Plasticity*, 16, 541-652, 2000.
- [19]. Auricchio, F. and Sacco, E. **Thermo-mechanical modelling of a superelastic shape memory alloy wire under cyclic stretching-bending loadings**, *International Journal of Solids and Structures*, 38, 6123-6145, 2001.
- [20]. Tanaka, K., Kobayashi, S. & Sato, Y., **Thermomechanics of transformation pseudoelasticity and shape memory effect in alloys**, *International Journal of Plasticity*, 2, 59-72, 1986.

- [21]. Brocca, M., Brison, L.C & Bazant Z.P, **Three-dimensional constitutive model for shape memory alloys based on microplane model**, Journal of the Mechanics and Physics of Solids, 50, 1051-1077, 2002.
- [22]. Huo, Y. and Müller, I., **Non-equilibrium thermodynamics of pseudoelasticity**, Continuum Mechanics and Thermodynamics, 5, 163-204, 1993.
- [23]. Shaw J. and Kyriakides, S., **On the nucleation and propagation of phase transformation fronts in NiTi alloy**, Acta mater., 45, No.2, 683-700, 1997.
- [24]. Shaw J. and Kyriakides, S., **Initiation and propagation of localized deformation in elasto-plastic strips under uniaxial tension**, International Journal of Plasticity, 13, No.10, 837-871, 1998.
- [25]. Chang, J.L. and Read, T.A. **Trans. AIME**, Vol 191, p 47, 1951.
- [26]. Rogers, C.A, and Robertshaw, H.H., **Shape Memory Alloy Reinforced Composites**, Engineering Science Preprints, 25, Society of Engineering Science, Inc.,ESP25.8027, 1988.
- [27]. Liang, C., Jia, J., and Rogers, C., **Behavior of shape memory alloy reinforced composite plates part ii: Results**. In Proceedings of the 30th Structures, Structural Dynamics and Materials Conference, number AIAA-89-1331-CP, 1504-1513, 1989.
- [28]. Chaudry, Z., and Rogers, C.A., **Response of composite beams to an internal actuator force**. In Proceedings of the 32nd Structures, Structural Dynamics and Materials Conference, number AIAA-89-1331-CP, 1504-1513, 1989.

- [29]. Baz A, and Ro, J. **Thermodynamic characteristics of Nitinol reinforced composite beams**, *Composites Engineering*, 2, 527-542, 1992.
- [30]. Paine, J and C. Rogers, C. **Characterization of interfacial shear strength between sma actuators and host composite material in adaptive composite material systems**, In *Adaptive Structures and Material Systems*, volume ASME AD-35, 63-70, 1993.
- [31]. Furuya, Y., Sasaki, A., and Taya, M., **Enhanced Mechanical Properties of TiNi Shape Memory Fiber/Al Matrix Composite**, *Materials Transactions, The Japan Institute of Metals*, 34, No. 3, 224-227, 1993.
- [32]. Hughes, D. and Wen, J.T., **Preisach Modeling and Compensation for Smart Material Hysteresis**, *SPIE Active Materials and Smart Structures*, 2427, 50-64, 1994.
- [33]. Lagoudas, D. C., D. Moorthy, M. A. Qidwai and J. N. Reddy. **Modeling of the thermomechanical response of active laminates with SMA strips using the layerwise finite element method**. *Journal of Intelligent Material Systems and Structures* 8(6), 476-488, 1997.
- [34]. Boyd, J.G., and Lagoudas, D.C., **Thermomechanical response of Shape Memory Composites**, *International Journal of Intelligent Materials and Structures*, 5, 333-346, 1994.
- [35]. Lagoudas, D.C., Boyd, J.G and Bo, Z., **Micromechanics of Active Metal Matrix Composites with Shape Memory Alloy Fibers**, *ASME Journal of Material Science and Technology*, 116, No.3, 337-347, 1994a.

- [36]. Lagoudas, D.C., Bo, Z., and Qidwai, M.A., **Micromechanics of Active Metal Matrix Composites with Shape Memory Alloy Fibers**, *Inelasticity and Micromechanics of Metal Matrix Composites*, 116, No.3, 163-190, 1994b.
- [37]. Hebda D.A., and White, S.R., **Structural behavior of sma composite beams**, *Adaptive Material Systems*, volume AMD-206, 111-119, ASME 1995.
- [38]. Hebda D.A., Whitlock, M.E., Ditman, J.B., and White, S.R., **Manufacturing of adaptive graphite/epoxy structures with embedded nitinol wires**, *Journal of Intelligent Materials and Smart Systems*, vol 6, 220-228, 1995.
- [39]. Gao, X., Burton, D.S., and Brinson, L.C., **Finite Element simulation of a self-healing shape memory composite**, *To be submitted to Journal of Mech. Materials*. 2004.
- [40]. Lee H.J., and Lee, J.J., **A numerical analysis of the buckling and post buckling behaviour of laminated composite shells with embedded shape memory alloy wire actuators**, *Smart Materials and Structures*, 9, 780-787, 2000.
- [41]. Ghomshei M.M., Khajepour, A., Tabandeh, N., Behdinan, K., **Finite element modeling of shape memory alloy composite actuators: Theory and Experiment**, *Journal of Intelligent Material Systems and Structures*, 12, 761-773, 2001.
- [42]. Sun S.S., Sun, G., Han, F., Wu, J.S., **Thermoviscoelastic analysis for a polymeric composite plate with embedded shape memory alloy wires**, *Journal of Composite Structures*, 58, 295-302, 2002.
- [43]. Turner T.L., Lach, C.L., and Cano, R.J., **Fabrication and characterization of SMA hybrid composites**, *Smart Materials and Structures*, SPIE 4333, 4333-60, 2001.

-
- [44]. Turner T.L., **Experimental validation of a thermoelastic model for SMA hybrid composites**, Smart Materials and Structures, Modeling, Signal Processing and Control in Smart Structures, SPIE 4326, 4326-24, 2001.
- [45]. Tsoi, K.A., Stalmans, R., Schrooten, J., **Transformational behaviour of constrained shape memory alloys**, Acta Materialia, vol 50, 3535-3544, 2002.
- [46]. Masuda A., Qing-Qing, N, Sone, A., Zhang, R., and Yamamura, T., **Preliminary characterization and modeling of SMA-based textile composites**, to be submitted to Smart Materials and Structures, 2003.
- [47]. Philander O., **The development of a computational design tool for use in the design of SMA actuator systems**, Doctorate dissertation, Cape Peninsula University of Technology, 2004.
- [48]. Webb G.V, Kurdila, A.J, and Lagoudas, D.C., **Hysteresis modelling of SMA actuators for control applications**, Final paper sent to Journal of Intelligent Material Systems and Structures, 1998.
- [49]. Peng, X. and Yeng, Y., **A comprehensive description of Shape Memory Alloys with Two phase Constitutive model**, International Journal of Solids and Structures, 38, 6925, 2001.
- [50]. http://www.smartmaterials.info/materials/comparison/qualitative_comp
- [51]. Gandhi, M.V. and Thompson, B.S., **Smart Materials and Structures**, London: Chapman and Hall, 1992.
- [52]. Paine, J.S.N and Rogers, C. A. **Review of Multi-Functional SMA Hybrid Composite Materials and their Applications**, Adaptive structures and Composite materials, AD-Vol 45, 37 – 45, ASME, 1994.

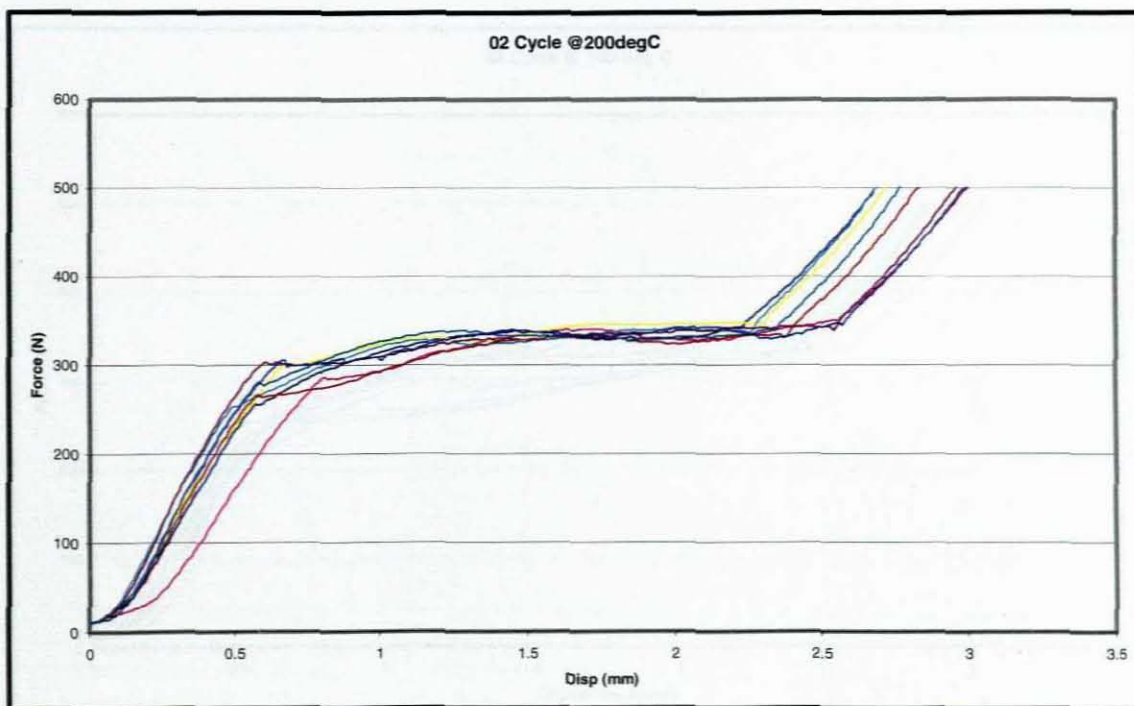
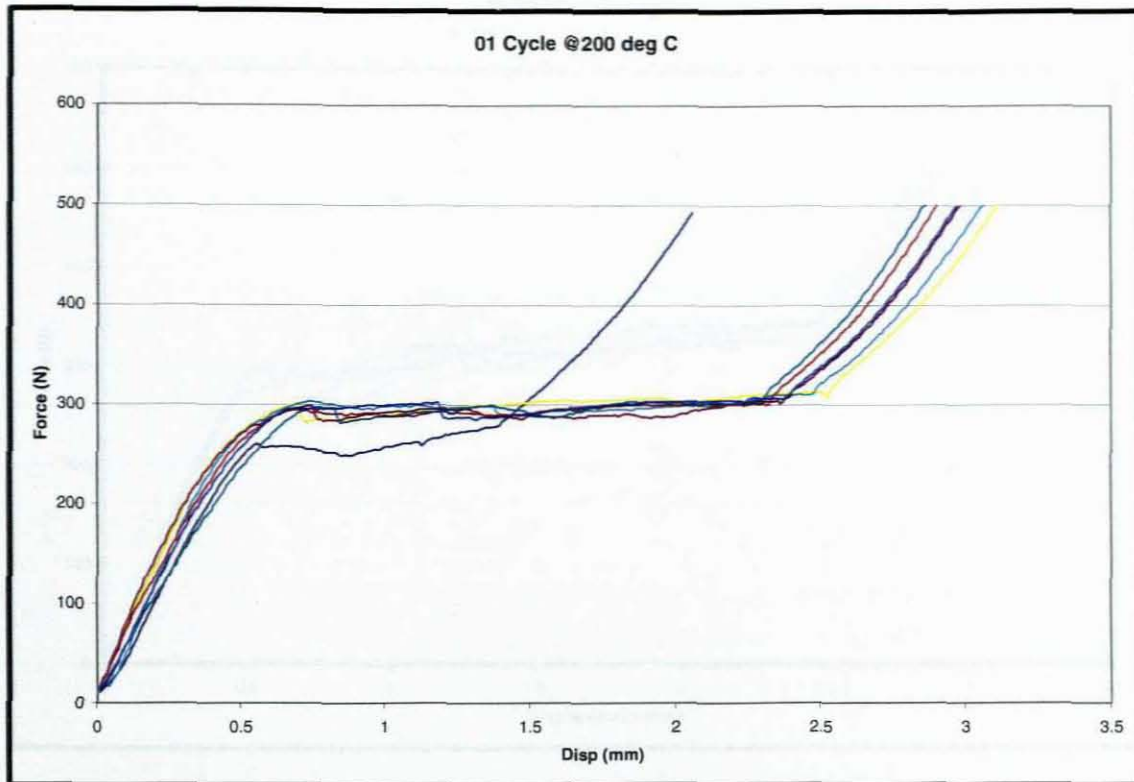
- [53]. Wei, Z.G, Sandstrom, R., Miyazaki, S., **Shape memory materials and hybrid composites for smart systems**, Journal of Material Science, Vol 33, 3763 – 3783, 1998.
- [54]. Vokoun, D., Kafka, V., Hu, C.T, **Recovery stresses generated by NiTi shape memory wires under different constraint conditions**, Smart Materials and Structures, 12, 680-685, 2003.
- [55]. Jang, B., Xu, Y., Oishi, R, Nagai, H **Thermomechanical Characterization and Development of SMA Embedded CFRP Composites with Self-Damage Control**, Int. J. of Mat. and Pro. Tech. 16, 1-3, 117-124, 2001.
- [56]. Hearn, E.J, 1997: **Mechanics of Materials 2**, Butterworth - Heinemann, Oxford, UK.
- [57]. Davidson F M, Liang C and Lobitz D. **Investigation of torsional shape memory alloy actuators** *Proc. SPIE 2717* 672–82, 1997
- [58]. Jardine A P *et al.* **Shape memory TiNi actuators for twist control of smart wing designs** *Proc. SPIE 2717* 160–5, 1997
- [59]. Rediniotis OK, Lagoudas DC, Garner L, Wilson N. **Experiments and analysis of an active hydrofoil with sma actuators**. AIAA Paper No. 98-0102; 36th AIAA Aerospace Sciences Meeting, Reno, Nevada, 1998.
- [60]. T. W. Duerig, K. N. Melton, D. Stockel, and C. M. Wayman, 1990: **Engineering Aspects of Shape Memory Alloys**, Butterworth-Heinemann, Boston, MA.
- [61]. Sachdeva RC, Miyazaki S. **Superelastic Ni-Ti alloys in orthodontics**. In Engineering Aspects of Shape Memory Alloys, 452 – 469, 1990

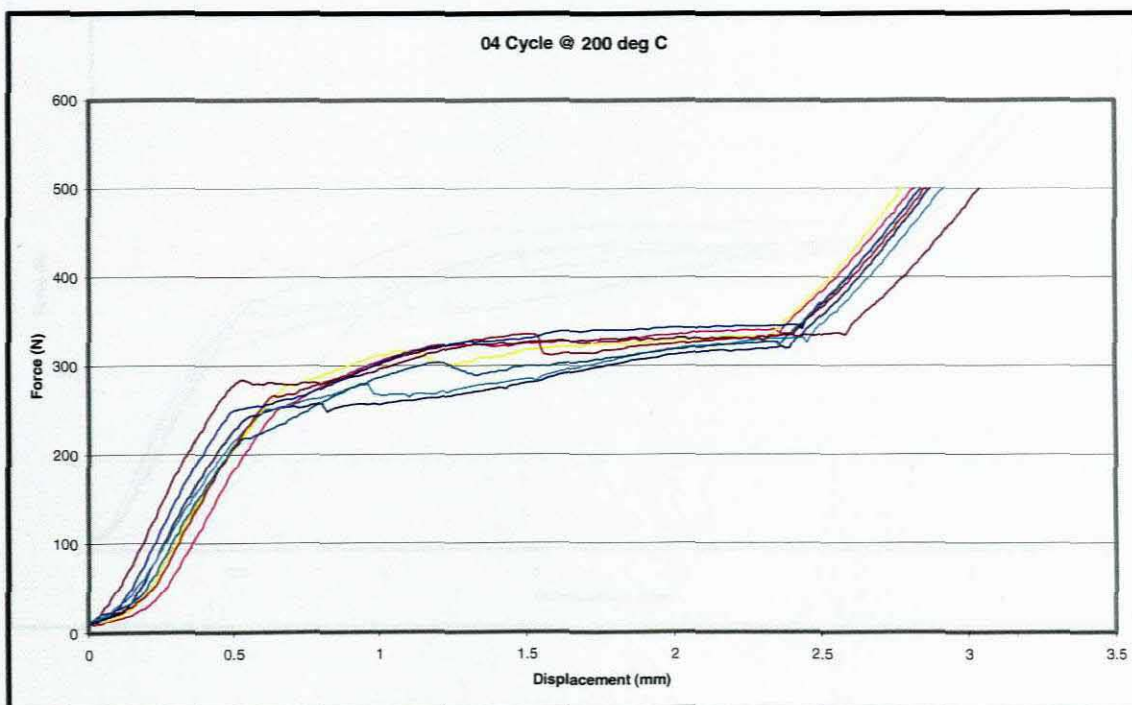
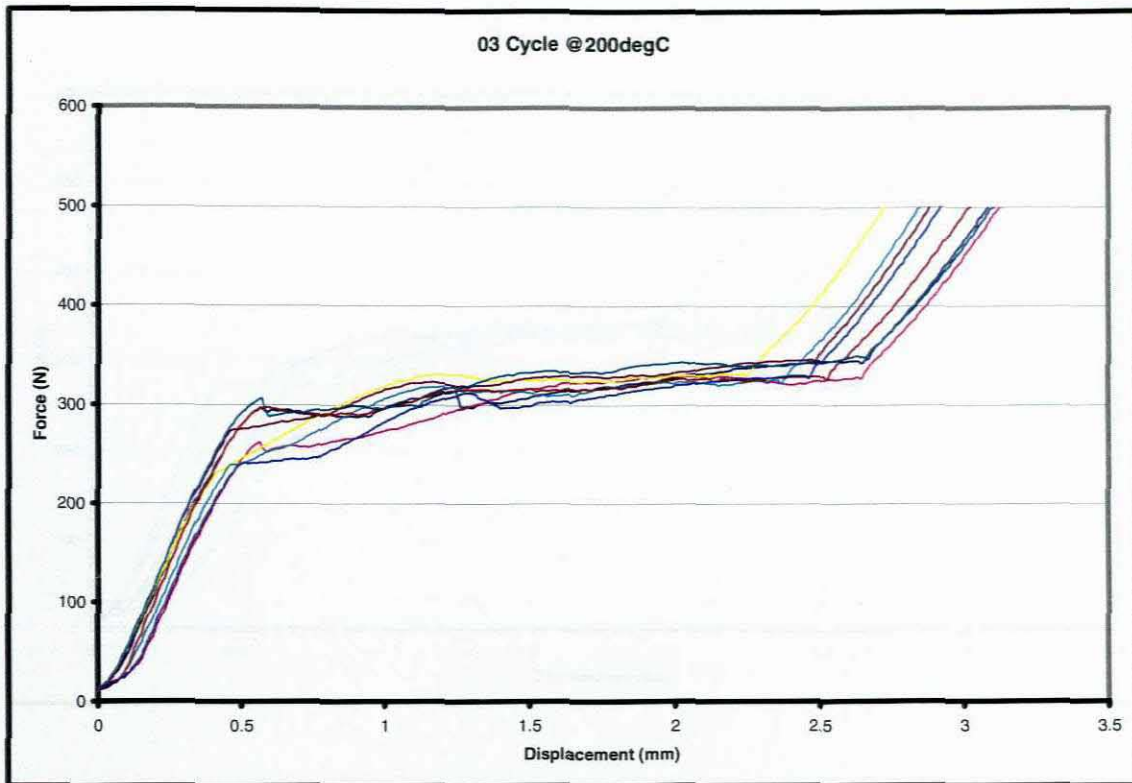
- [62]. Wasilewski RJ, Butler SR, Hanlon JE, Worden D. **Metallurgical Transformation**. 2, 229, 1971
- [63]. Miyazaki, S., Otsuka, K., and Suzuki, Y. **Transformation Pseudoelasticity and Deformation Behavior in Ti-Ni Alloy**, *Scripta Metallurgica*, 15, 287-292, 1981
- [64]. Wayman CM, 1964: **Introduction to crystallography of martensitic transformations**. Mac-Millan, New York.
- [65]. Muller I, Huibin XU. **On the pseudoelastic hysteresis**. *Acta Metallurgica Materialia*;39, 263-271, 1991.
- [66]. Salzbrenner, R.L., and Cohen, M., 1979, **On the Thermodynamics of Thermoelastic Martensitic Transformations**, *Acta Metallurgica*, 27, 739-748, 1979
- [67]. Adler PH, Yu W, Pelton AR, Zadno R, Duerig TW, Barresi R. **On the tensile and torsional properties of pseudoleastic NiTi**. *Scripta Metallurgica et Materialia*; 24, 943-947, 1990.
- [68]. Graesser, E.J., and Cozzarelli, F.A., **Shape-Memory Alloys as New Materials for Seismic Isolation**, *Journal of Engineering Mechanics*, 117, No. 11, 2590-2608, 1991.
- [69]. Leo, P.H., Shield, T.W., Bruno, O.P., **Transient heat transfer effects on the pseudoelastic behavior of shape-memory wires**. *Acta Metallurgica et Materialia*, 41, 2477–2485, 1993.
- [70]. Sittner, P., Takakura, M., Tokuda, M., 1995. **The stabilization of transformation pathway in stress induced martensite**. *Scripta Metallurgica et Materialia* 32 (12), 2073–2079, 1995.

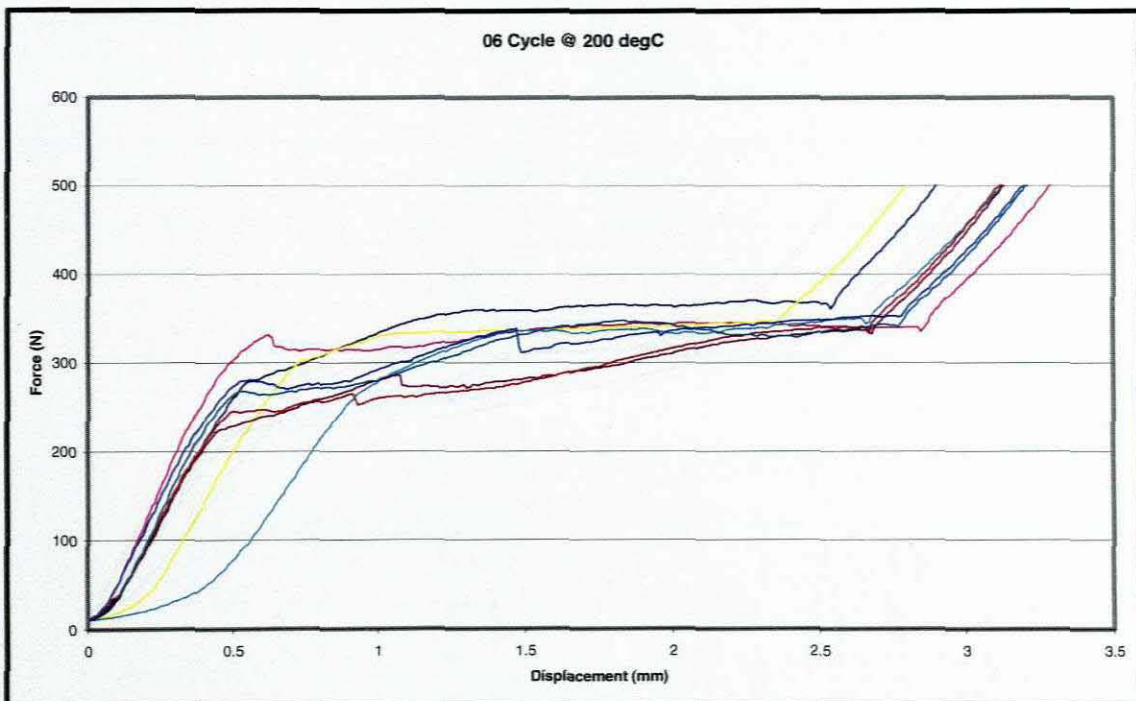
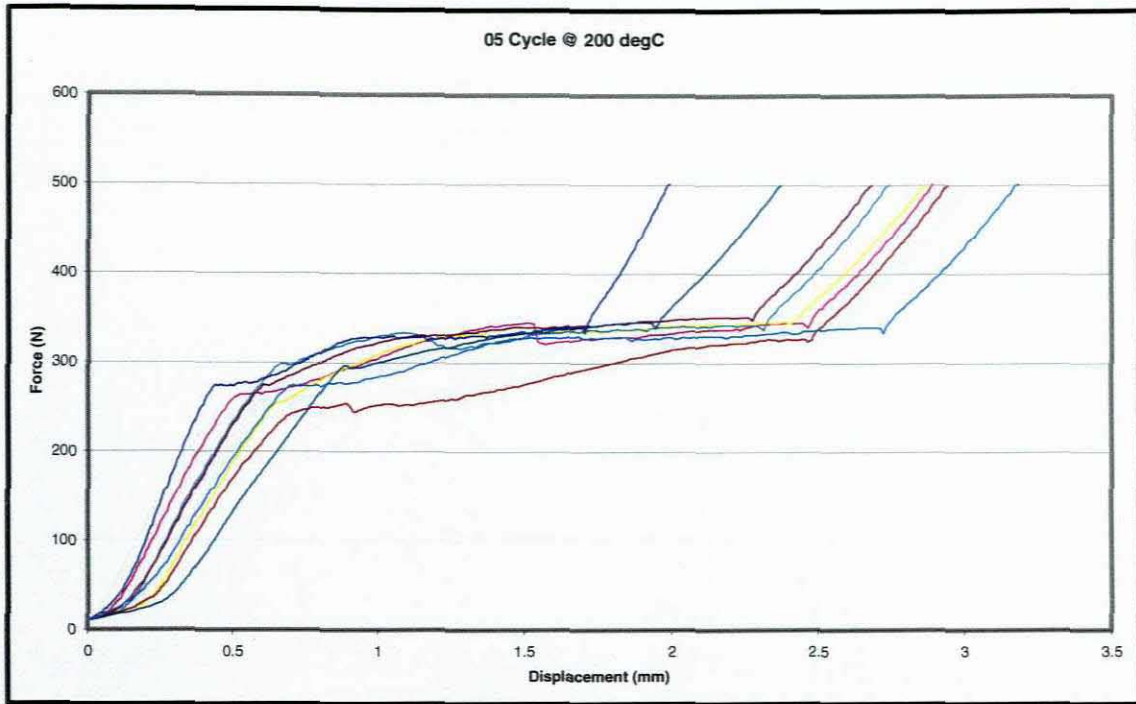
- [71]. Gall, K., Sehitoglu, H., Chumlyakov, Y., Kireeva, I., **Tension-compression asymmetry of the stress-strain response in aged single crystal and polycrystalline NiTi**. *Acta Materialia* 47 (4), 1203–1217, 1999.
- [72]. Zhang, X., Sun, Q.P., Yu, S.,. **A non-invariant plane model for the interface in CuAlNi single crystal shape memory alloys**. *Journal of the Mechanics and Physics of Solids* 48, 2163–2182, 2000.
- [73]. Lim JT, McDowell DL. **Mechanical behavior of a Ni-Ti shape memory alloy under axial-torsional proportional and nonproportional loading**. *Journal of Engineering Materials and Technology*; 121, 9-18, 1999.
- [74]. Furuya, Y., Sasaki, A., and Taya, M., **Enhanced Mechanical Properties of TiNi Shape Memory Fiber/Al Matrix Composites**, *Materials Transactions, The Japan Institute of Metals*, 34, No. 3, 224-227, 1993.

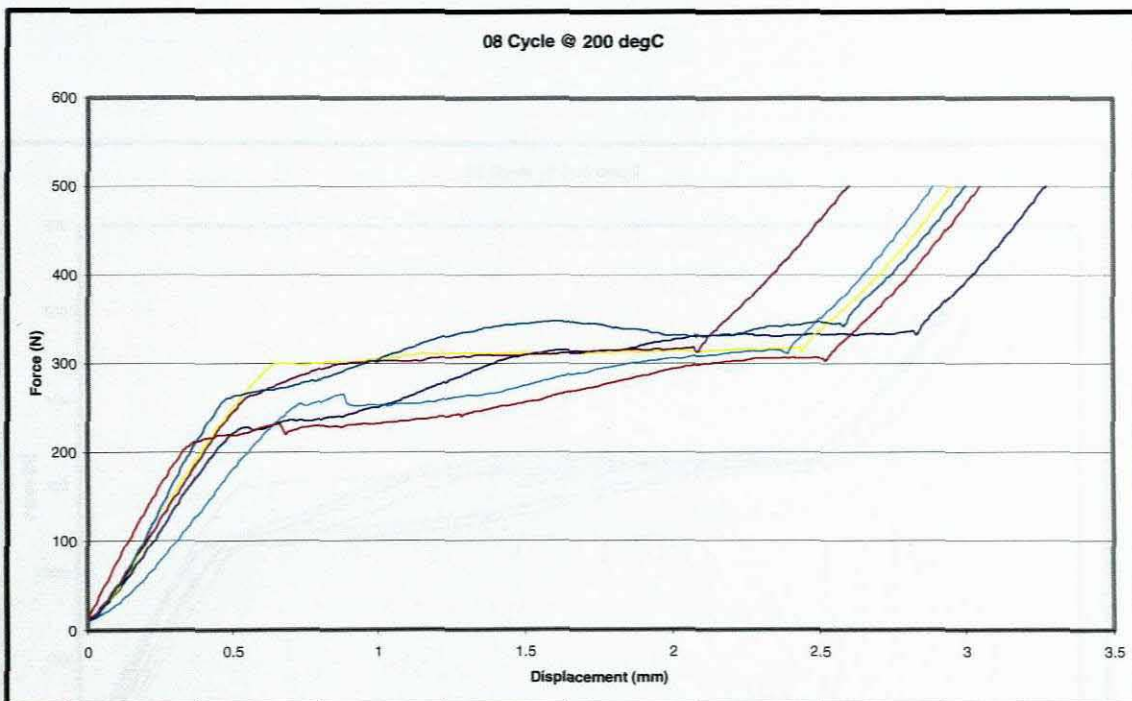
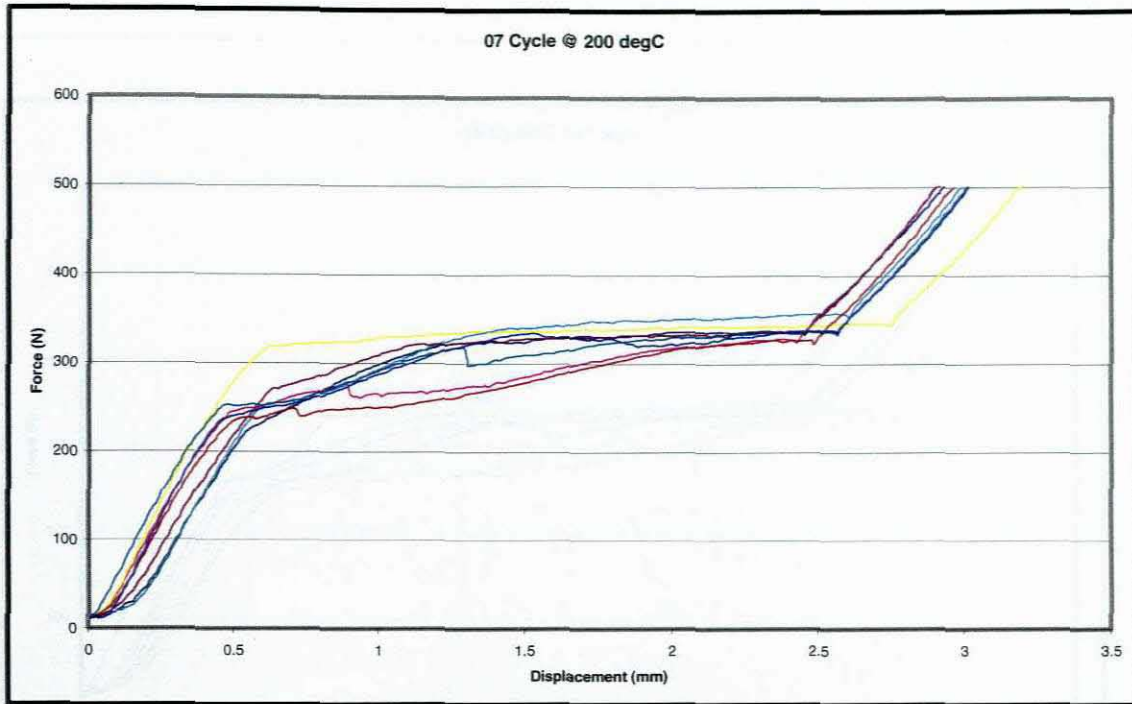
Appendix A

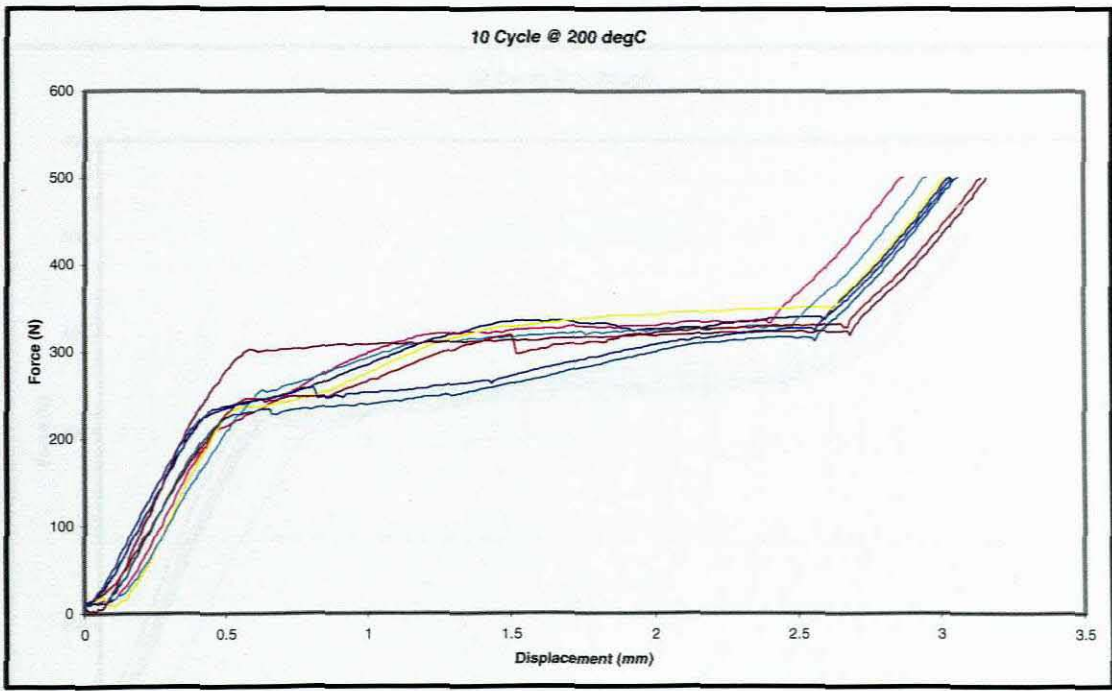
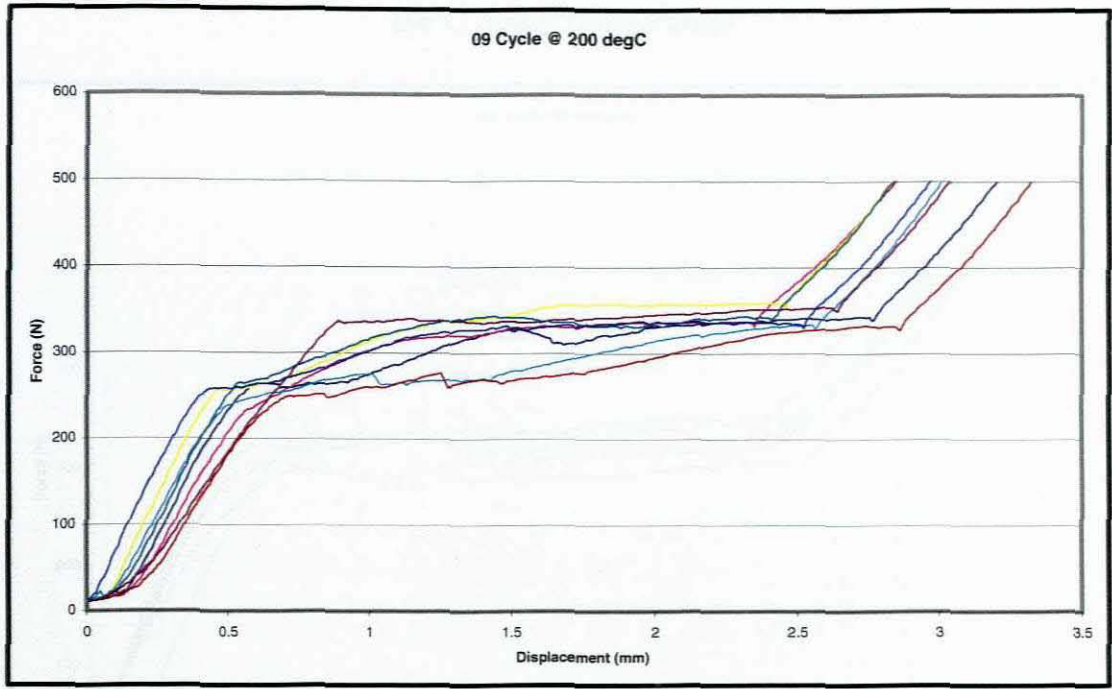
**Load-Extension Behavior
of NiTi SMA rods subjected
to Thermo-Mechanical
Cycling and Aging**



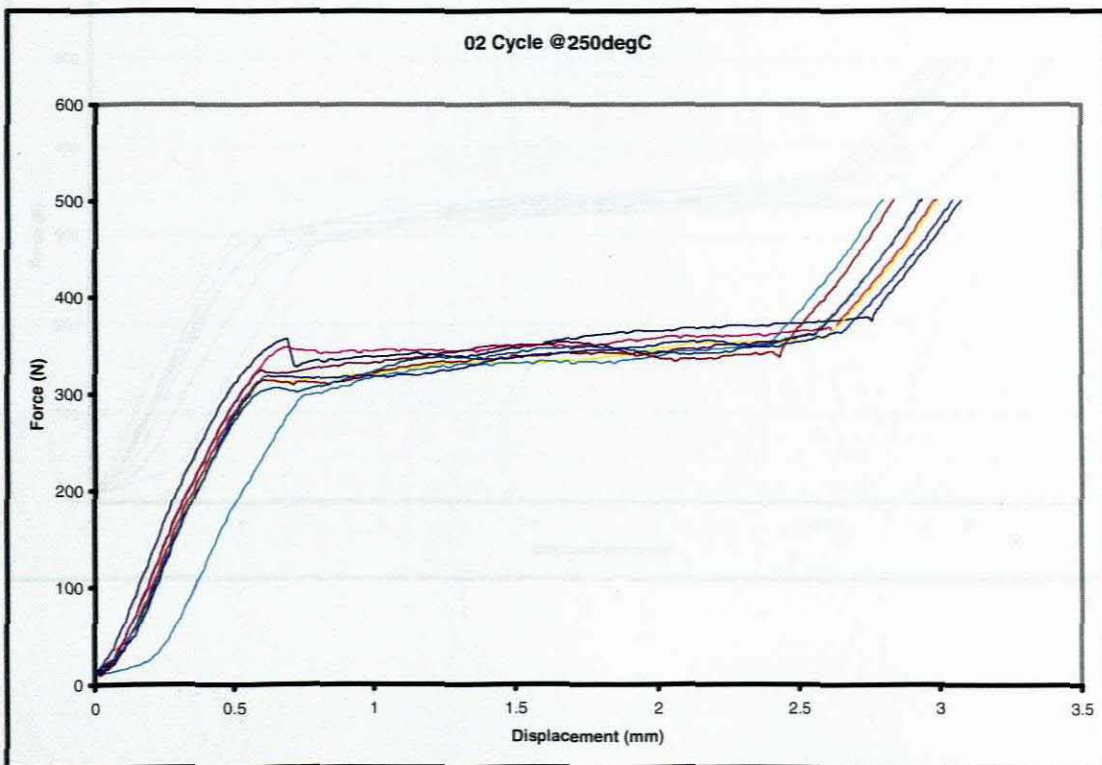
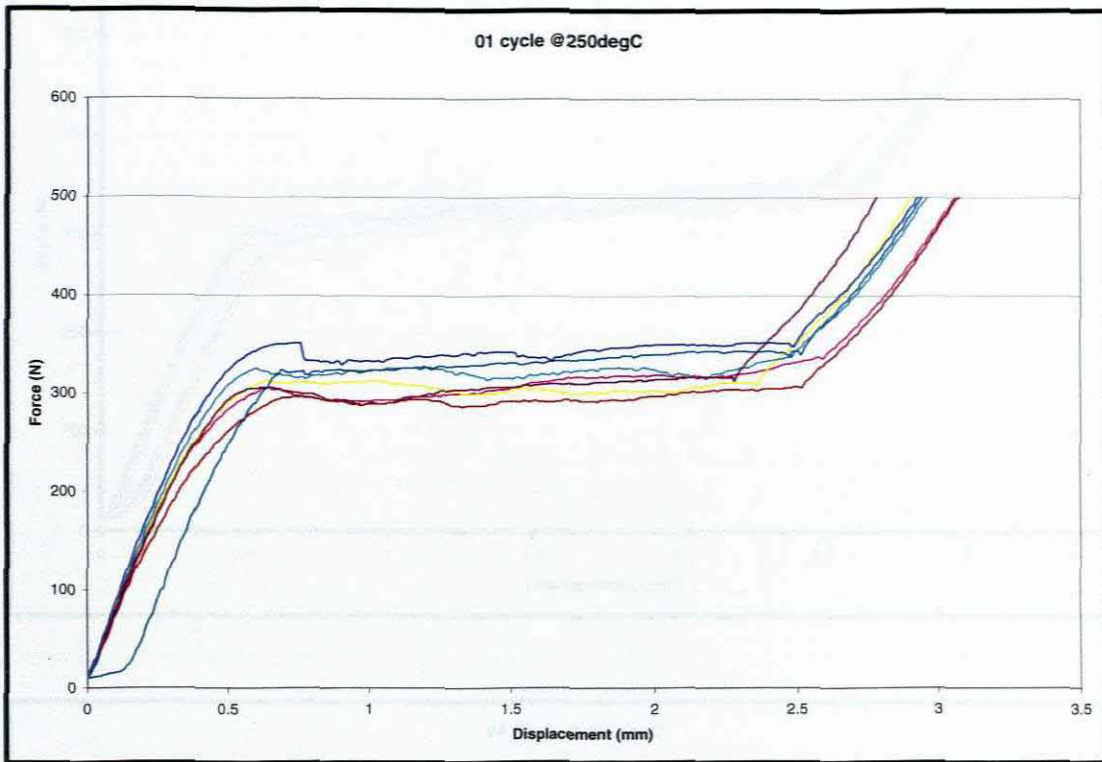


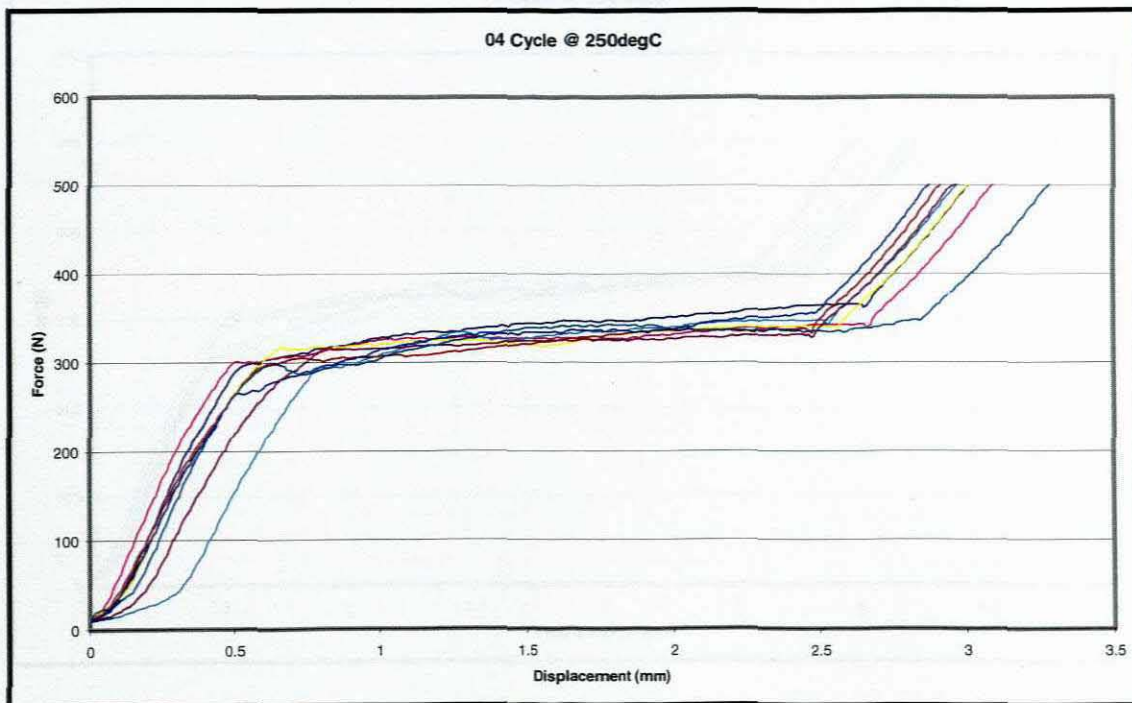
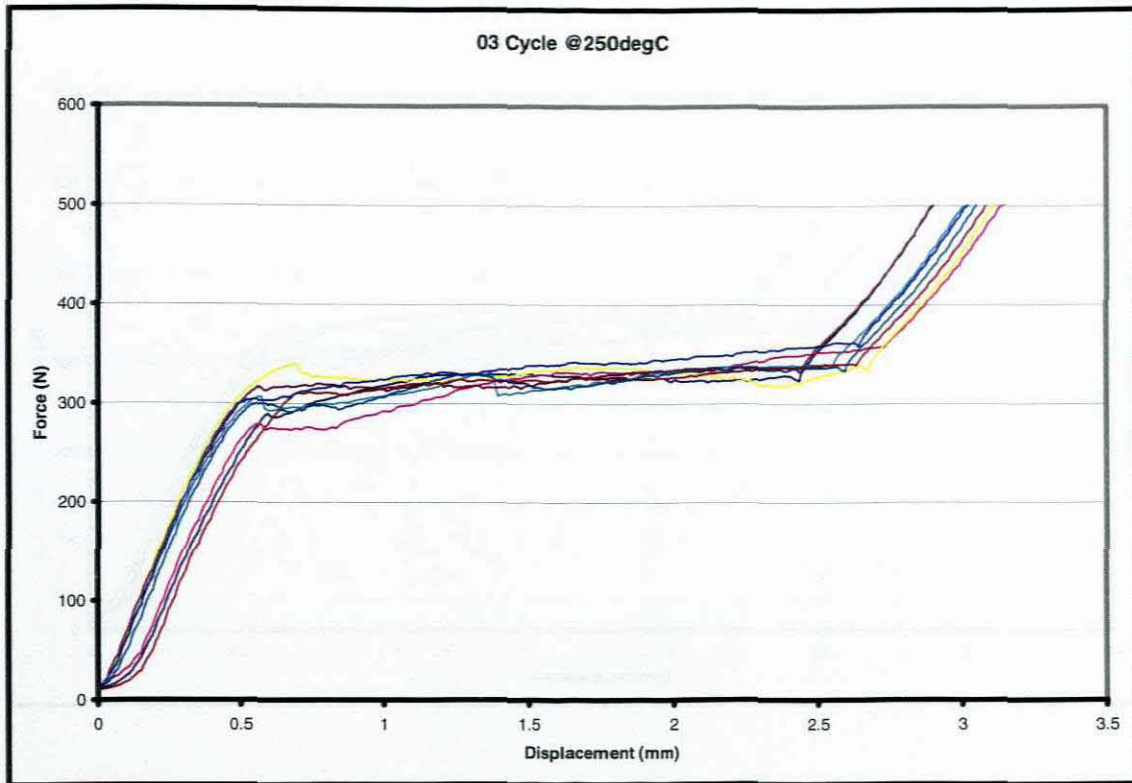


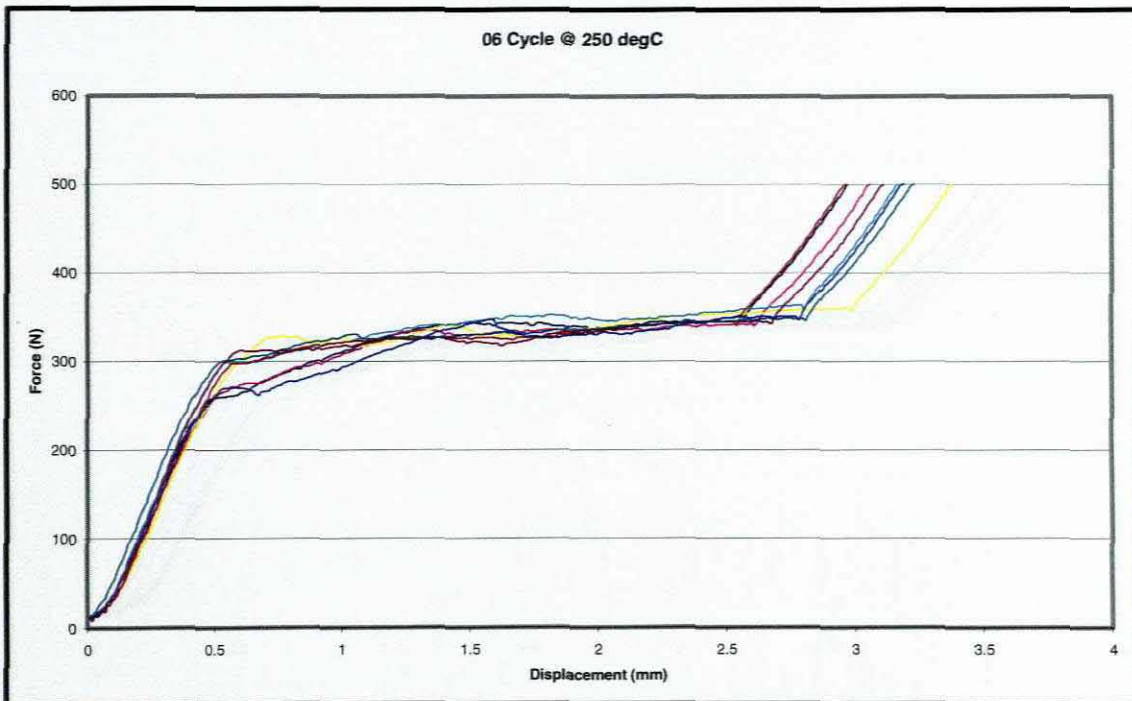
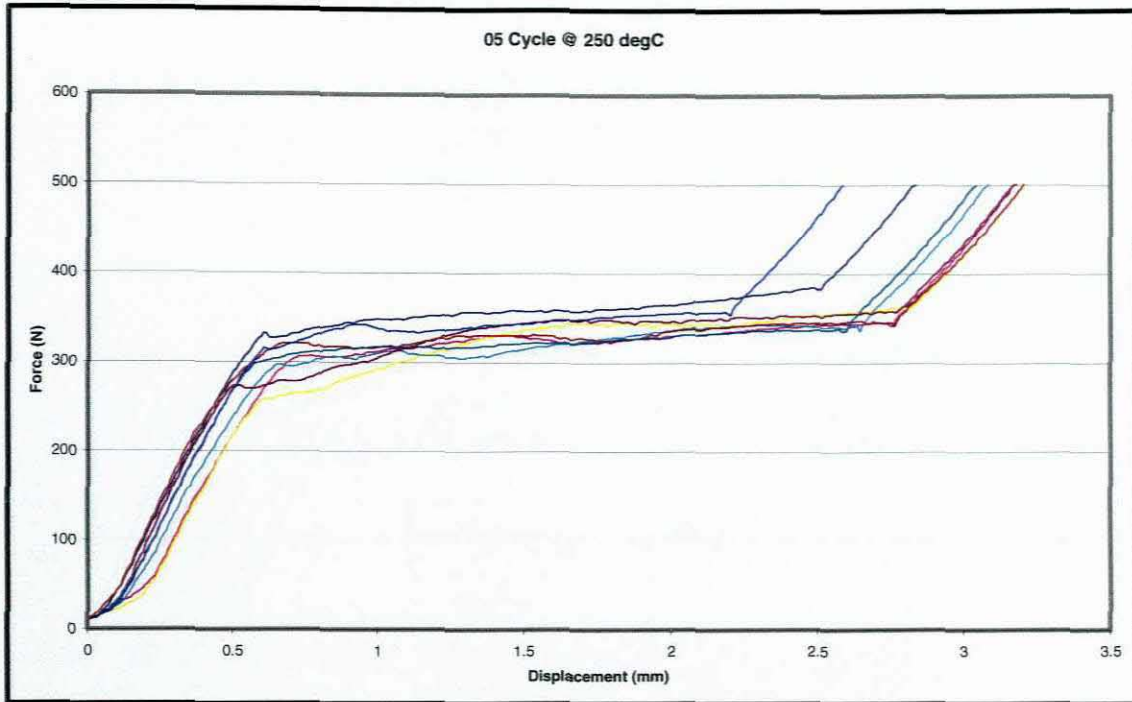


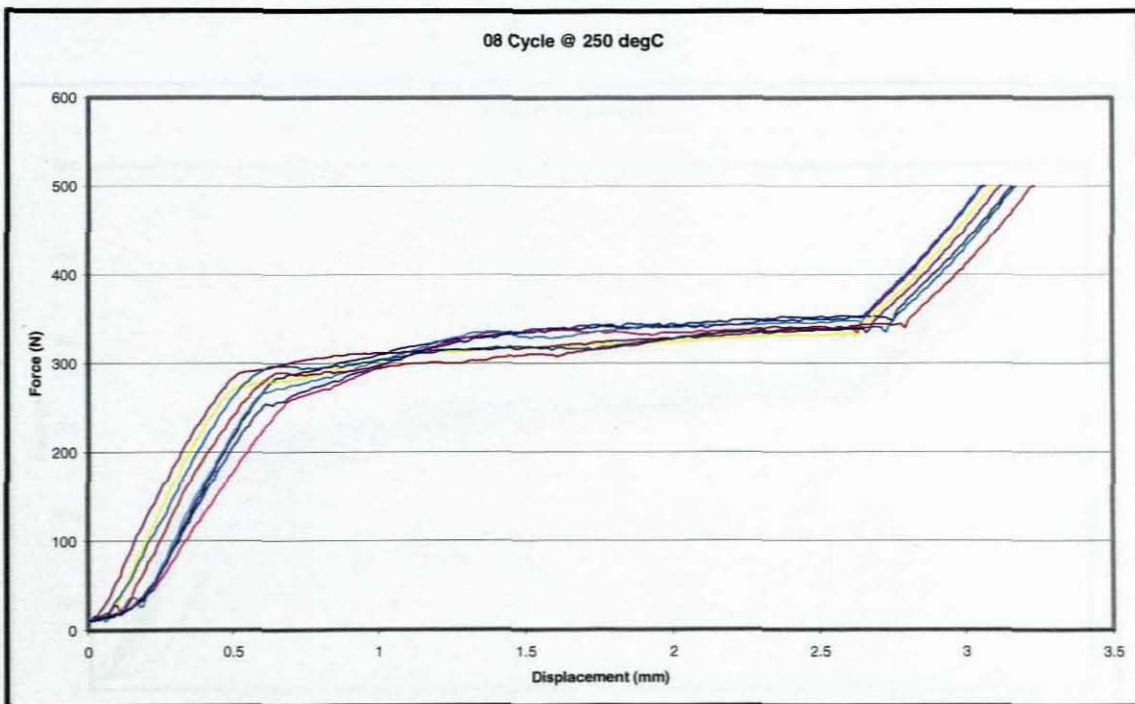
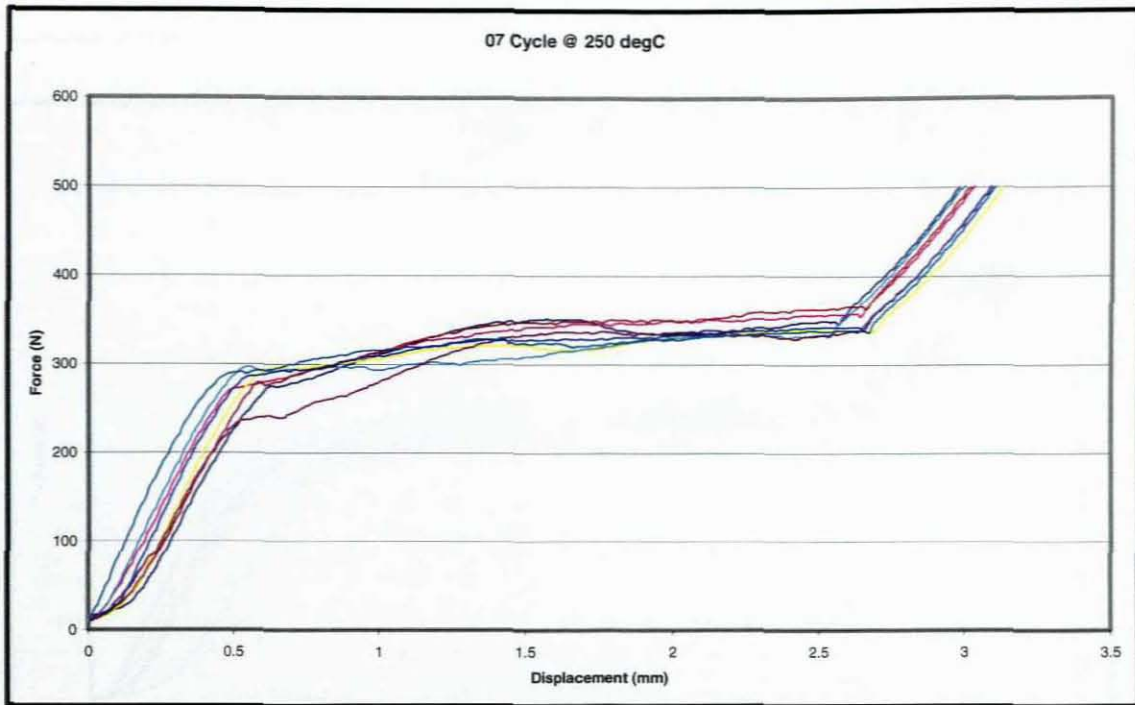


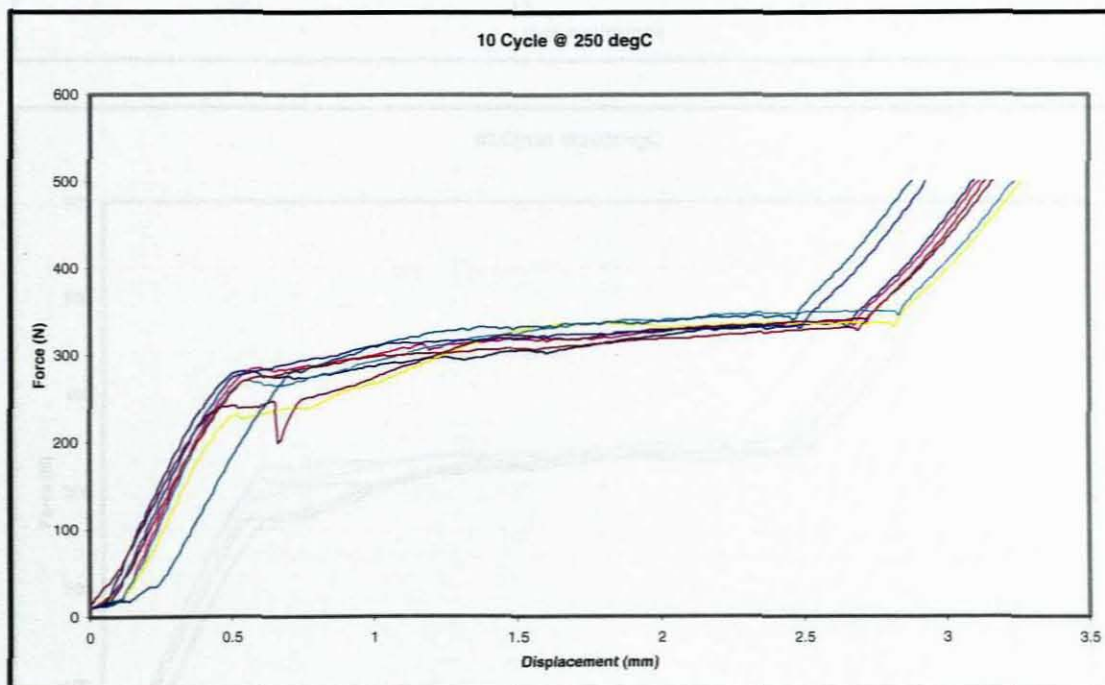
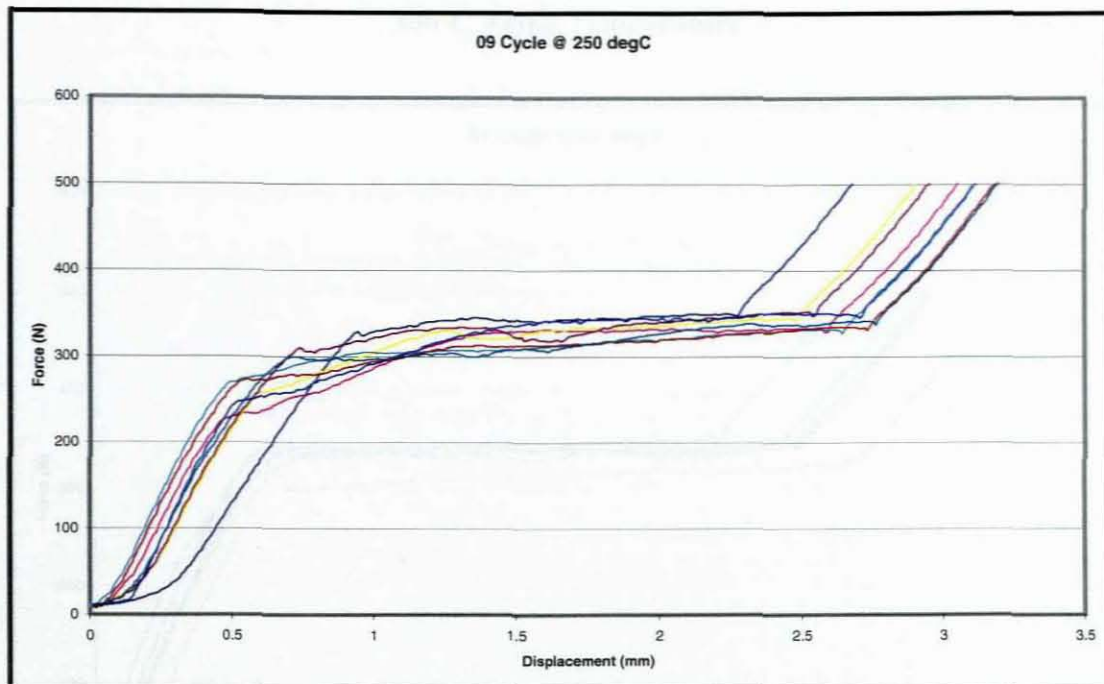
250°C Aging Temperature



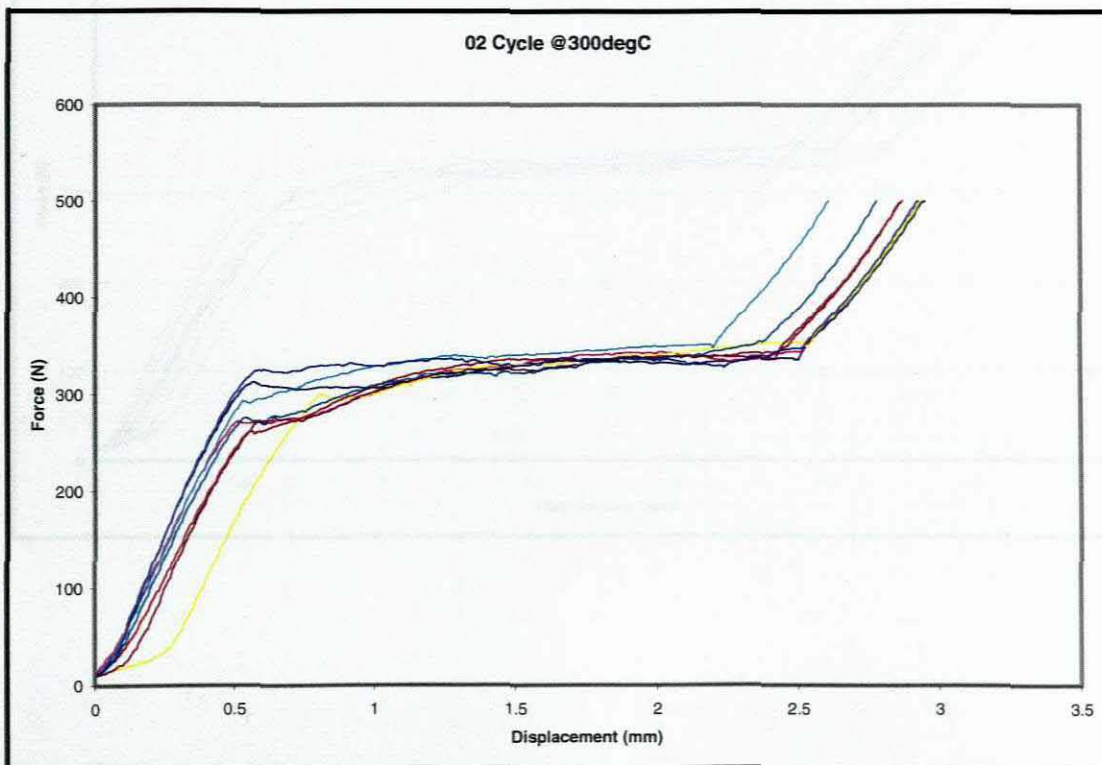
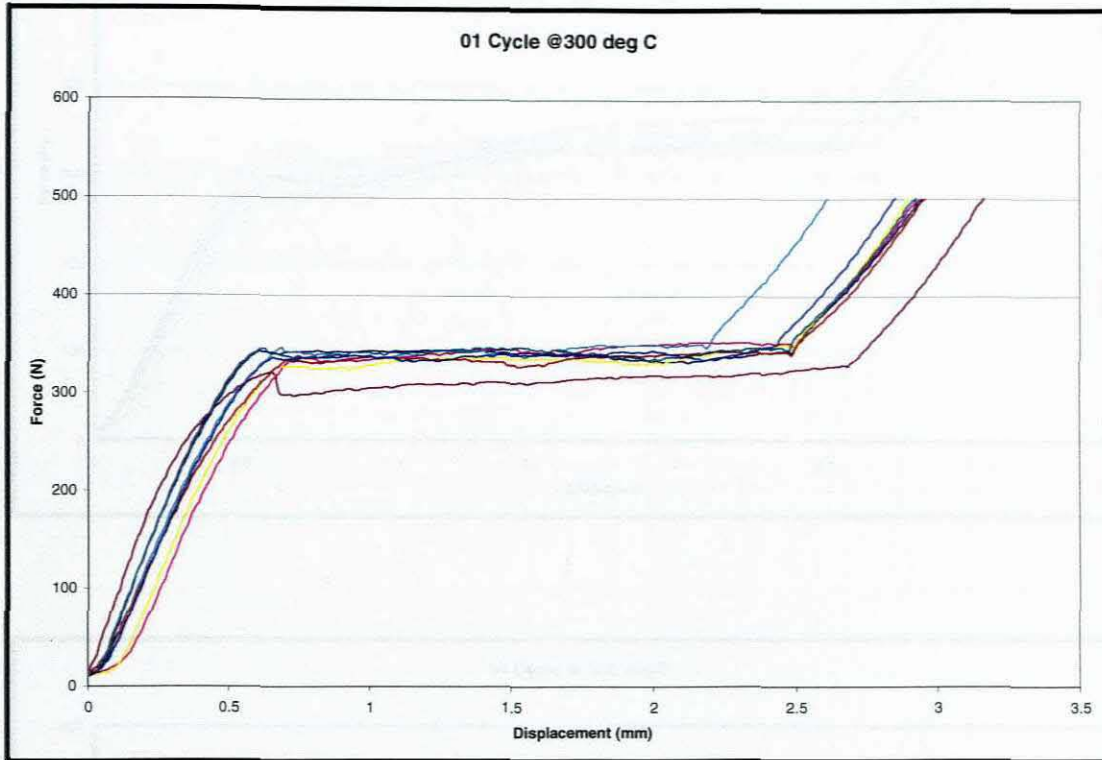


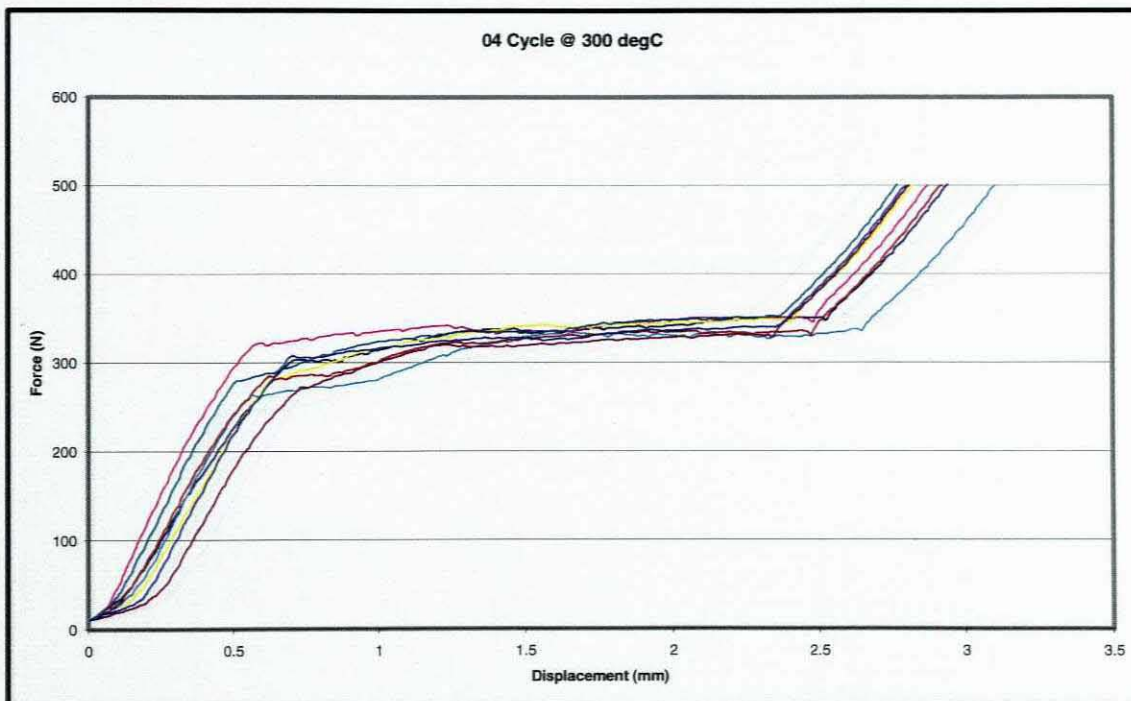
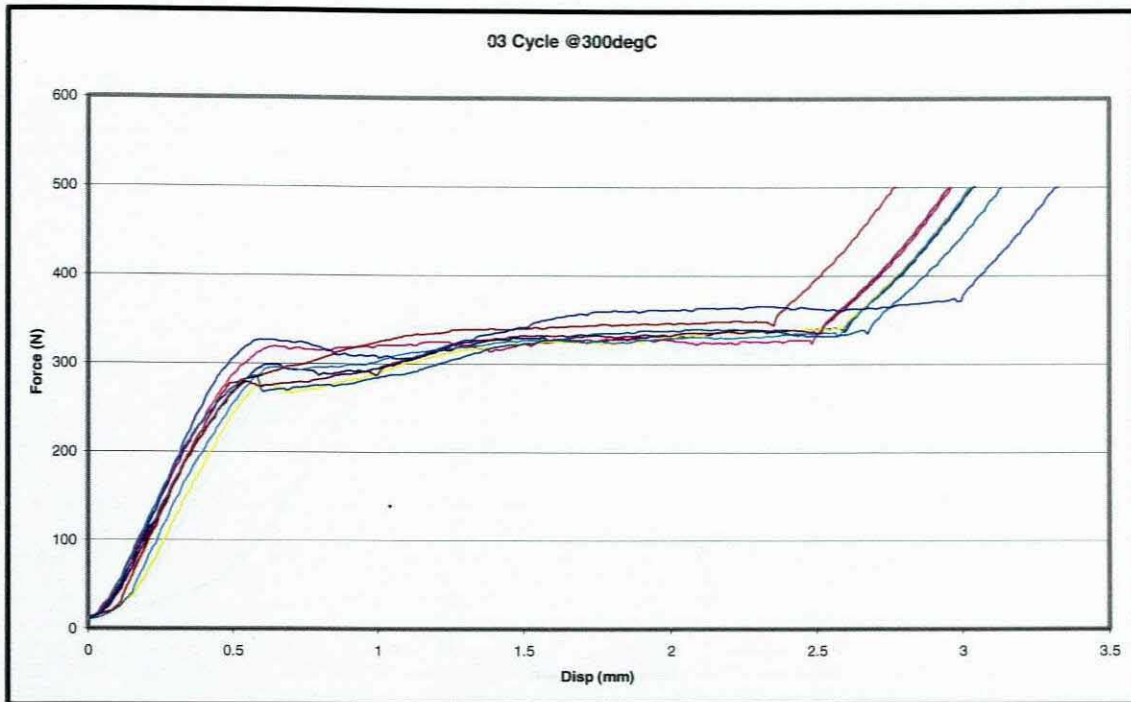


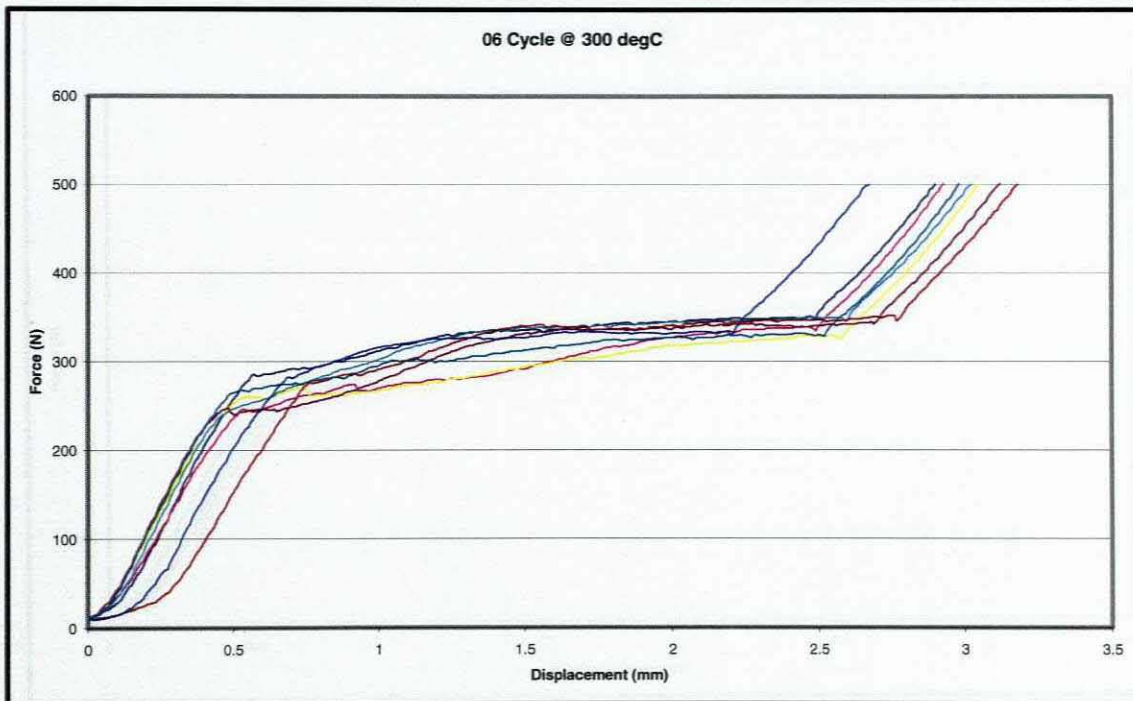
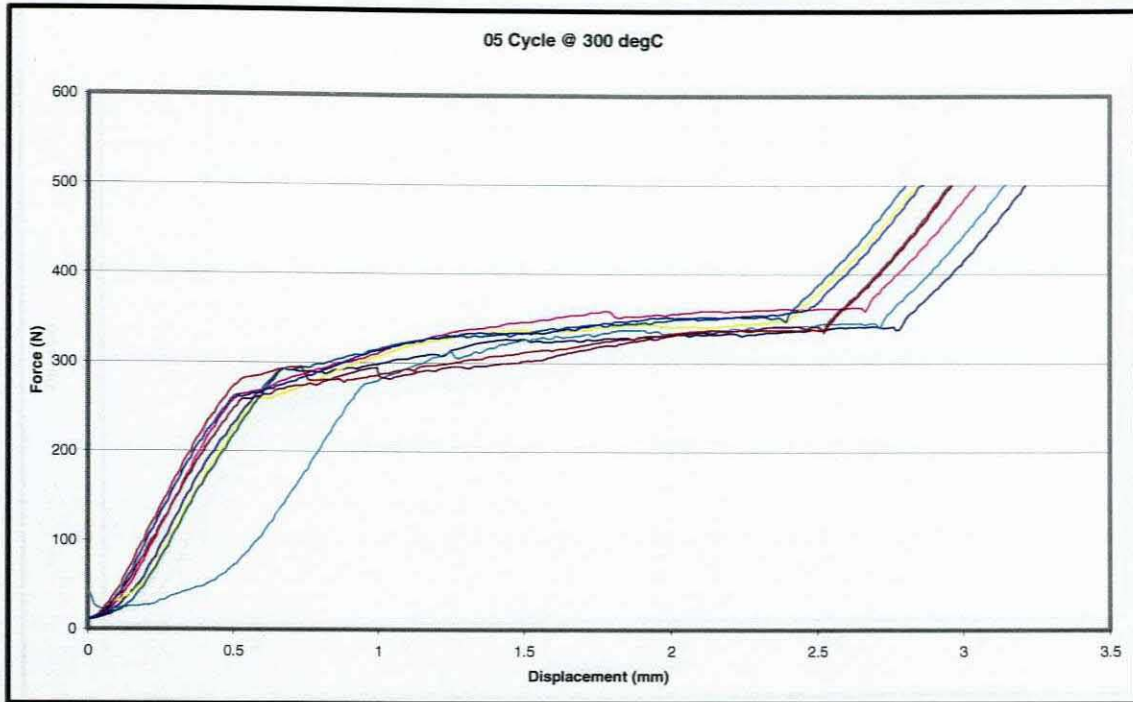


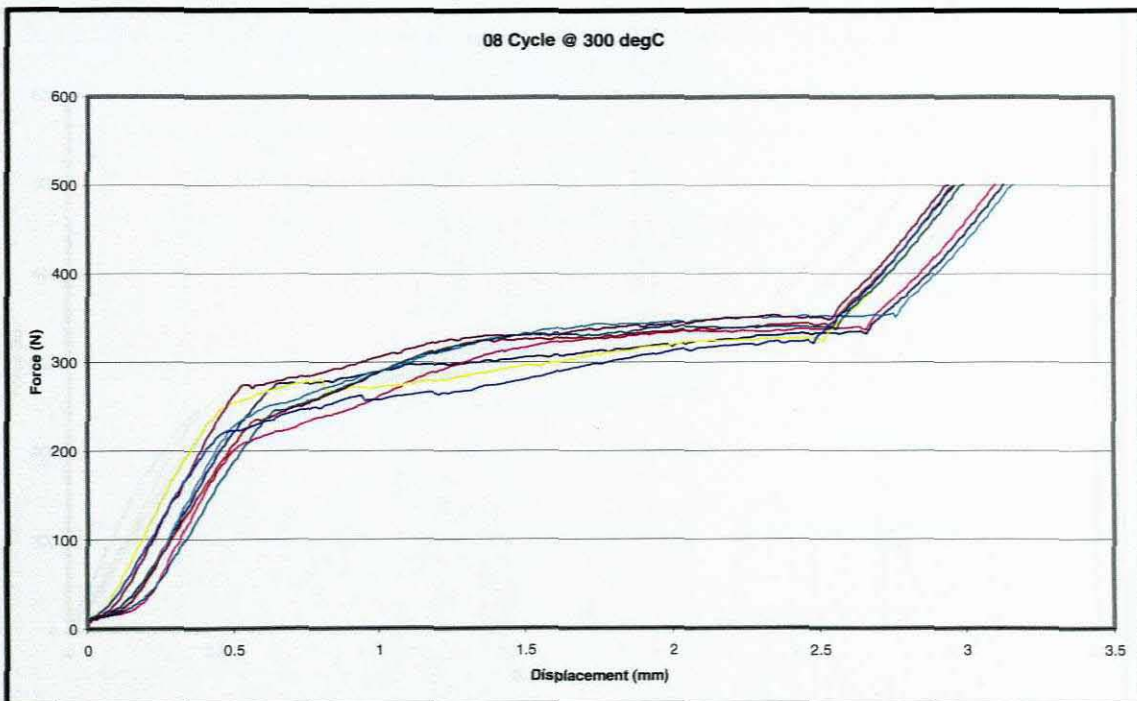
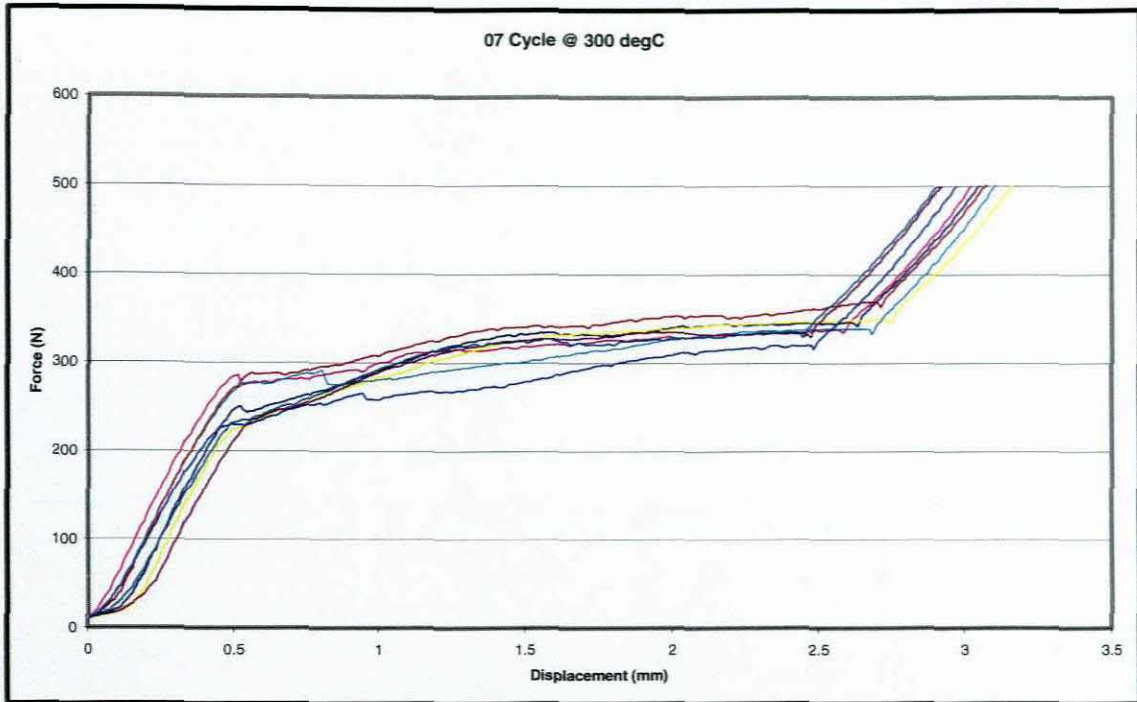


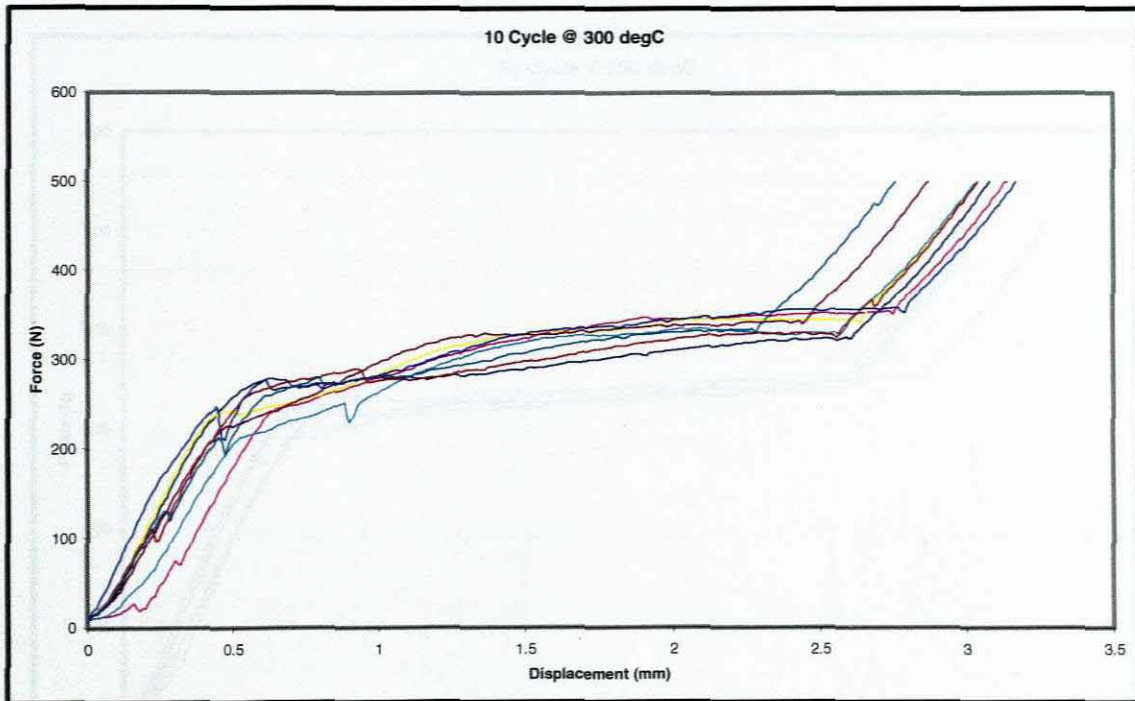
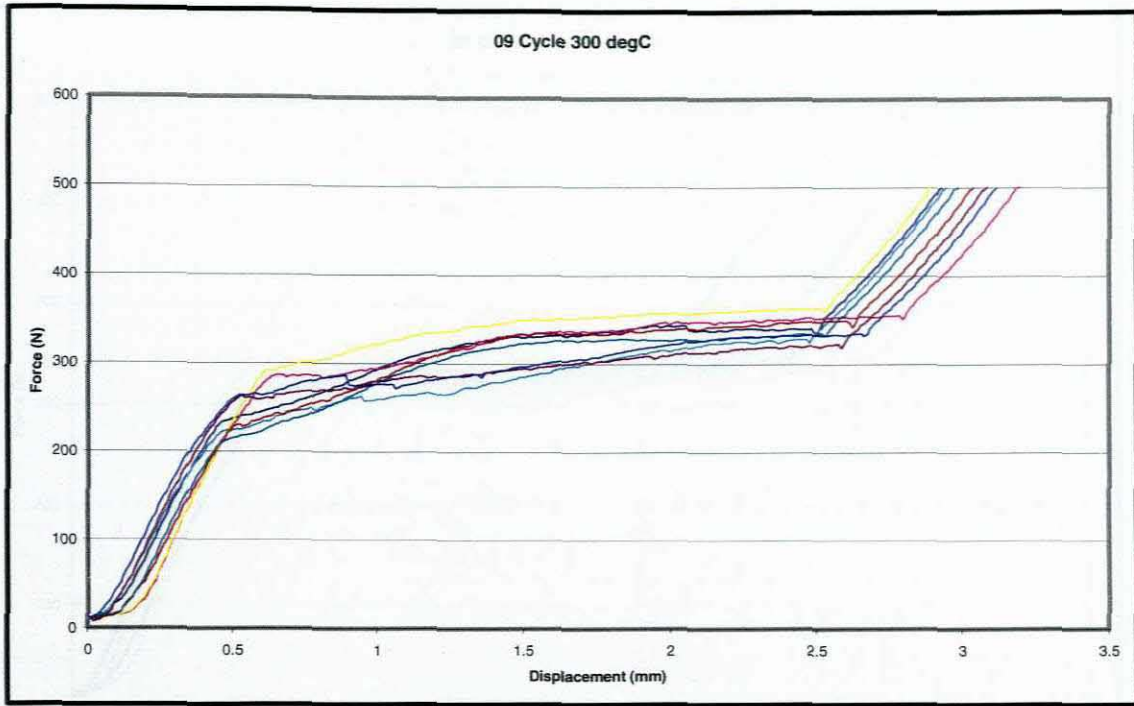
300°C Aging Temperature



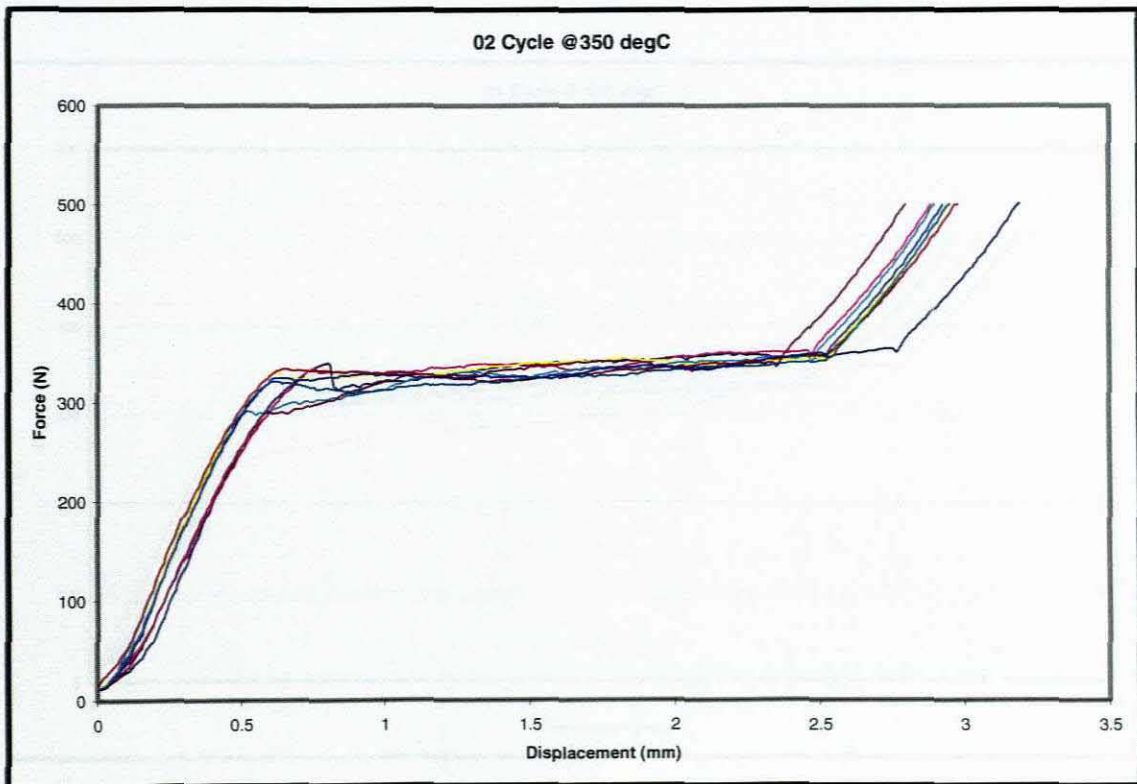
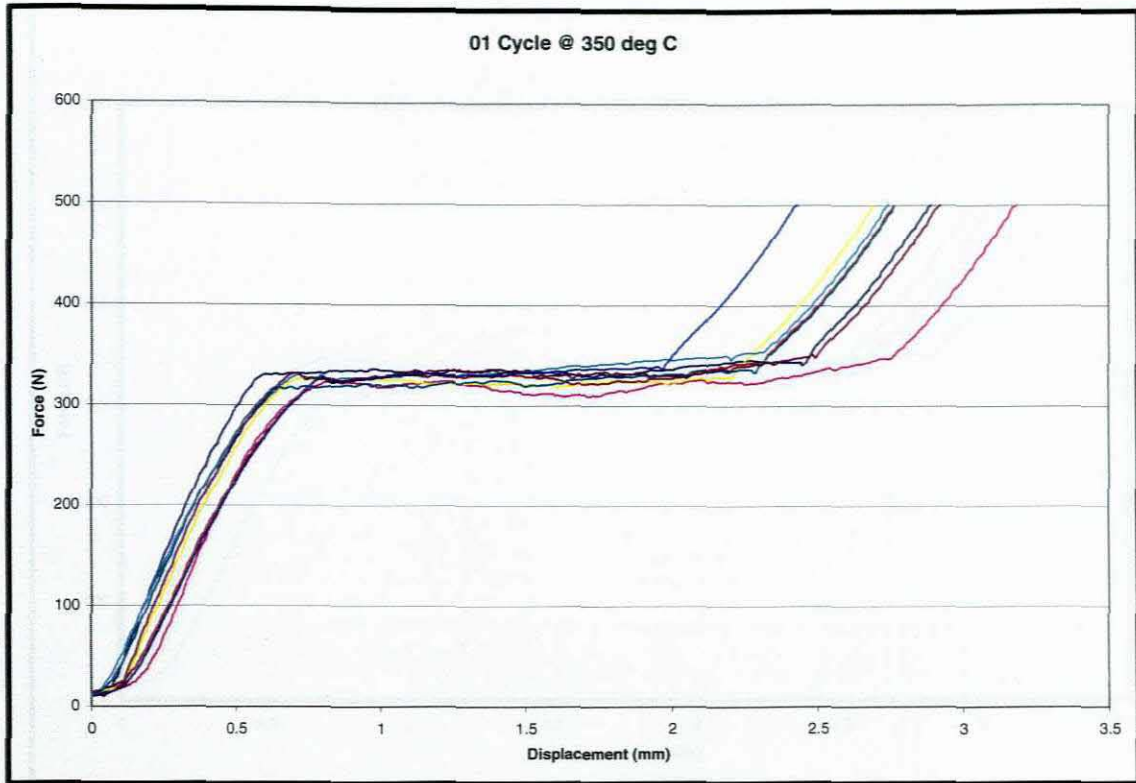


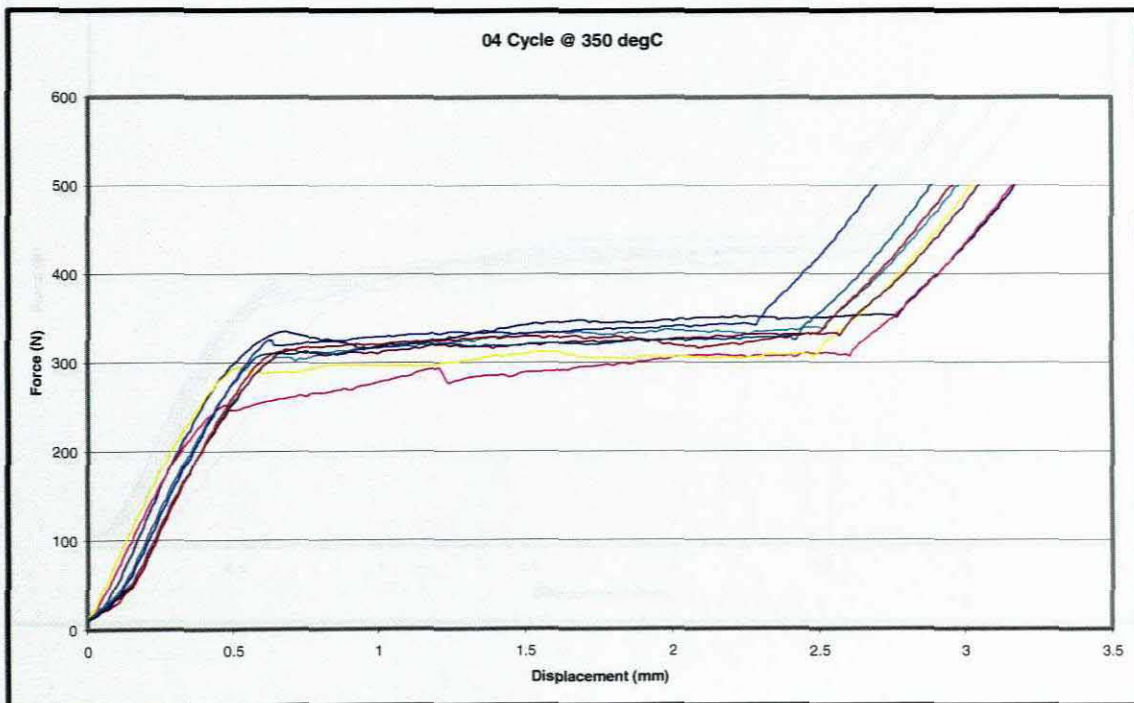
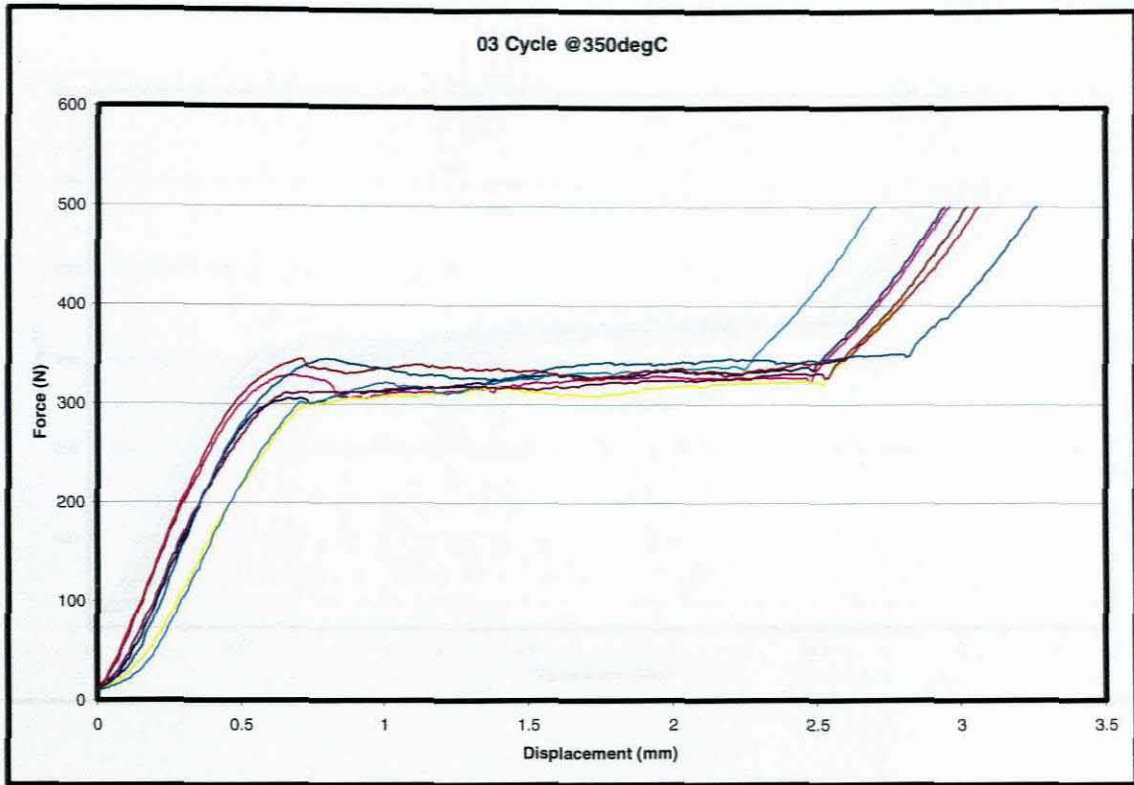


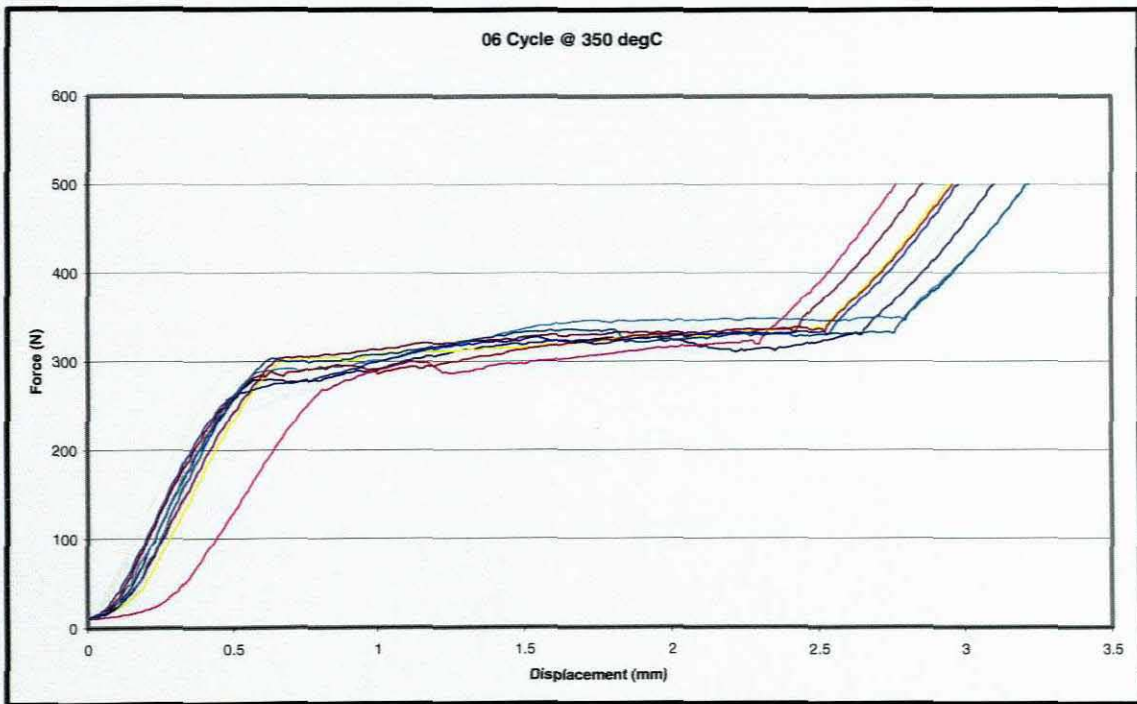
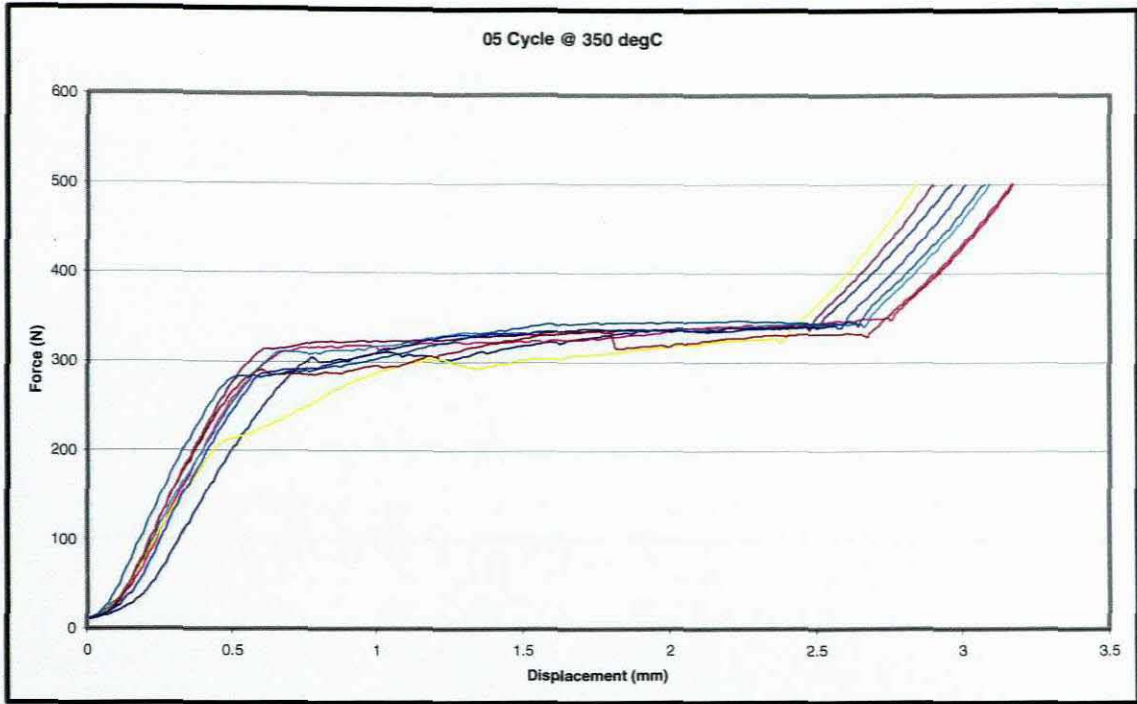


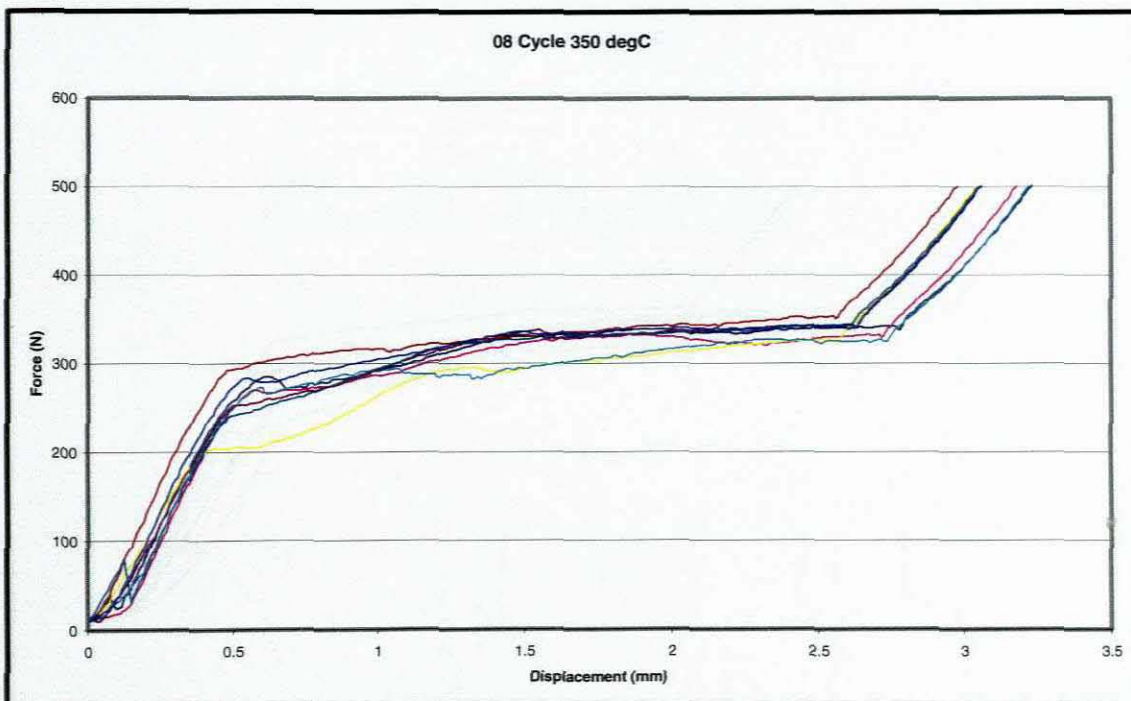
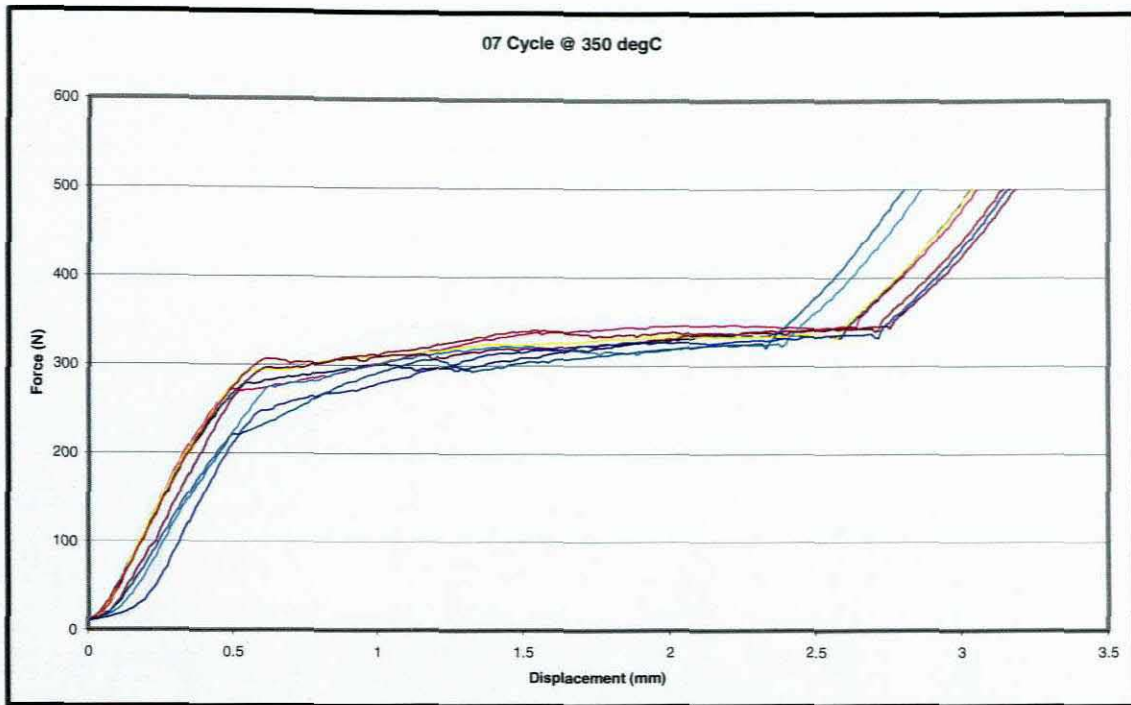


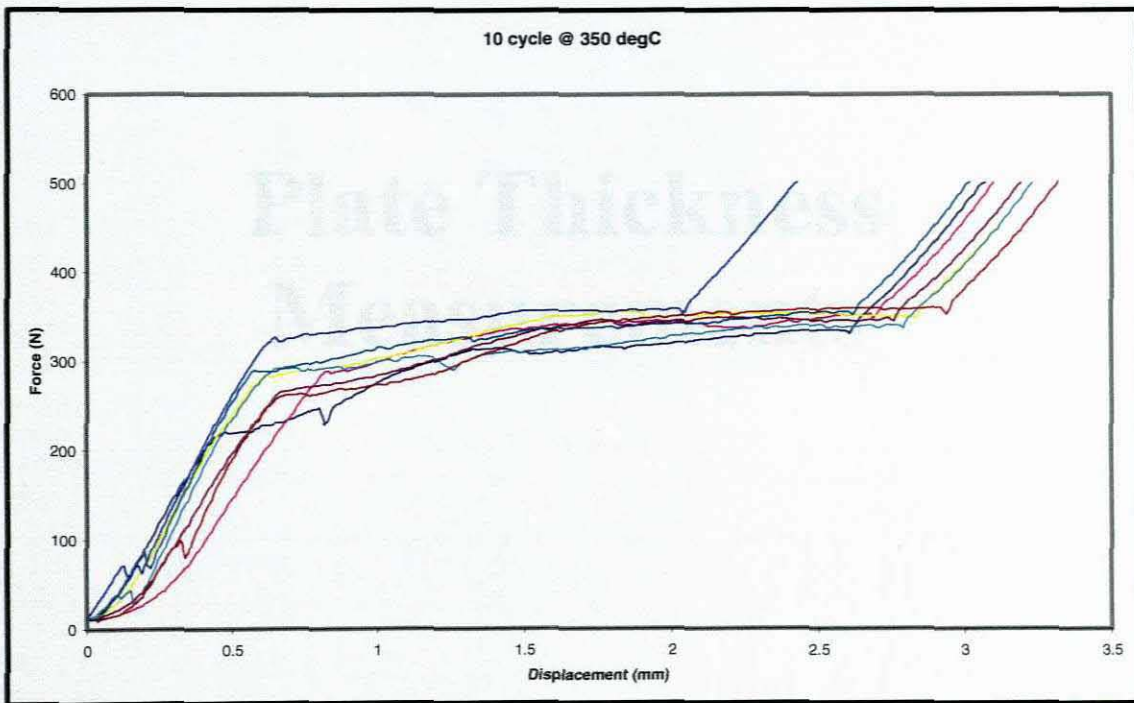
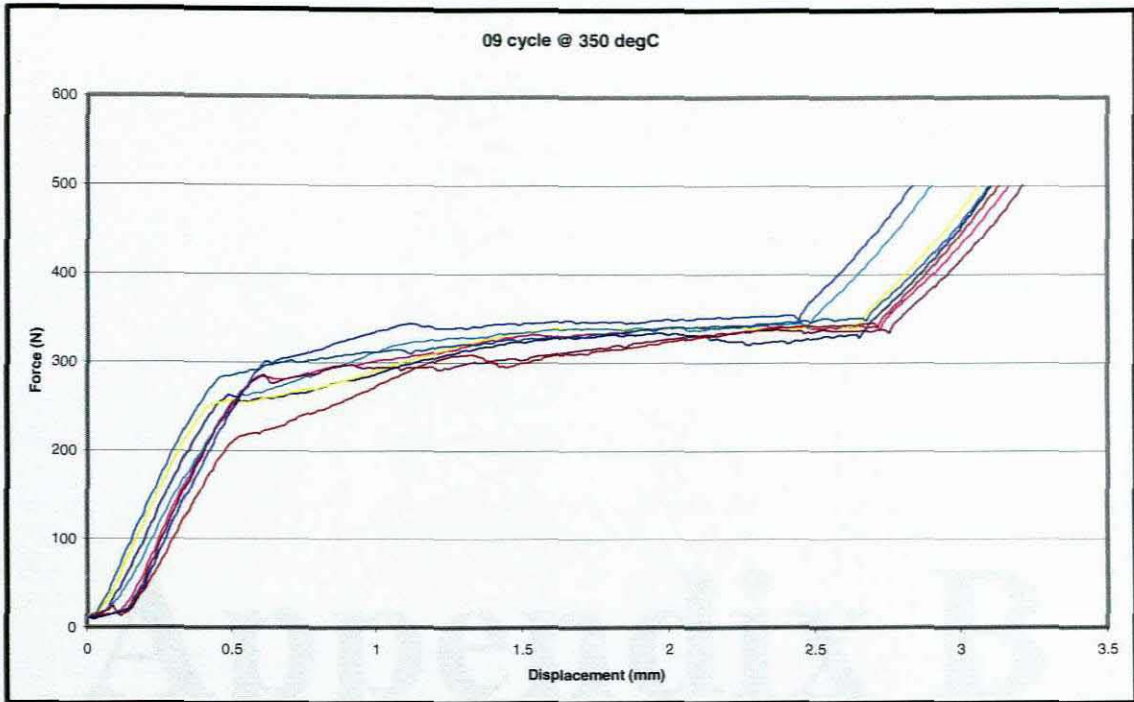
350°C Aging Temperature











Appendix B

Plate Thickness Measurements

Plate Thickness along all axis

| | Plate 1 4.04mm | | | | Plate 2 4.05mm | | | |
|----------------|----------------|-------|--------|--------|----------------|--------|--------|--------|
| | Length | | Width | | Length | | Width | |
| | X1 | X2 | Y1 | Y2 | X1 | X2 | Y1 | Y2 |
| x1 | 4.06 | 4.05 | 4.02 | 4.01 | 4.03 | 4.04 | 4.07 | 4.08 |
| x2 | 4.06 | 4.06 | 4.03 | 4.03 | 4.00 | 4.04 | 4.08 | 4.07 |
| x3 | 4.02 | 4.04 | 4.12 | 4.11 | 4.03 | 4.05 | 4.11 | 4.1 |
| x4 | 4.01 | 4.03 | 4.09 | 4.09 | 4.02 | 4.01 | 4.09 | 4.09 |
| x5 | 4.02 | 4.02 | 4.06 | 4.06 | 4.04 | 4.02 | 4.11 | 4.11 |
| x6 | 4.00 | 4.01 | 4.10 | 4.10 | 4.02 | 4.02 | 4.10 | 4.10 |
| x7 | 4.00 | 4.00 | 4.12 | 4.12 | 4.05 | 4.03 | 4.04 | 4.06 |
| x8 | 4.01 | 4.01 | 4.09 | 4.08 | 4.02 | 4.02 | 4.07 | 4.09 |
| x9 | 3.99 | 3.99 | 4.06 | 4.06 | 4.02 | 4.02 | 4.07 | 4.07 |
| x10 | 3.99 | 4.00 | 4.11 | 4.09 | 4.02 | 4.02 | 4.09 | 4.09 |
| x11 | 4.00 | 4.00 | 4.04 | 4.04 | 4.05 | 4.02 | 4.06 | 4.07 |
| x12 | 4.00 | 4.00 | 4.02 | 4.03 | 4.02 | 4.02 | 4.09 | 4.09 |
| x13 | 3.97 | 3.98 | 4.09 | 4.09 | 4.00 | 4.02 | 4.09 | 4.08 |
| x14 | 3.98 | 3.99 | 4.11 | 4.11 | 4.00 | 4.01 | 4.10 | 4.11 |
| x15 | 3.97 | 4.01 | 4.07 | 4.06 | 4.02 | 4.04 | 4.08 | 4.06 |
| x16 | 3.98 | 3.98 | 4.075 | 4.072 | 4.02 | 4.02 | 4.083 | 4.085 |
| x17 | 3.99 | 4.03 | 4.09 | 4.08 | 3.97 | 3.99 | 4.09 | 4.09 |
| x18 | 4.00 | 4.00 | 4.09 | 4.09 | 4.02 | 3.98 | 4.09 | 4.09 |
| x19 | 4.00 | 4.01 | 0.0354 | 0.0336 | 4.02 | 4.01 | 0.0191 | 0.0164 |
| x20 | 4.03 | 4.04 | | | 4.04 | 3.99 | | |
| x21 | 4.04 | 4.04 | | | 4.02 | 4.00 | | |
| x22 | 4.02 | 4.03 | | | 4.02 | 4.00 | | |
| x23 | 4.03 | 4.03 | | | 4.02 | 4.01 | | |
| x24 | 4.05 | 4.05 | | | 4.05 | 4.04 | | |
| x25 | 4.06 | 4.06 | | | 4.05 | 4.04 | | |
| x26 | 4.07 | 4.06 | | | 4.06 | 4.05 | | |
| Mean | 4.01 | 4.02 | | | 4.024 | 4.020 | | |
| Median | 4.005 | 4.015 | | | 4.02 | 4.02 | | |
| Mode | 4.00 | 4.00 | | | 4.02 | 4.02 | | |
| Std dev | 0.0291 | 0.025 | | | 0.0194 | 0.0184 | | |

Plate 3 6.7mm

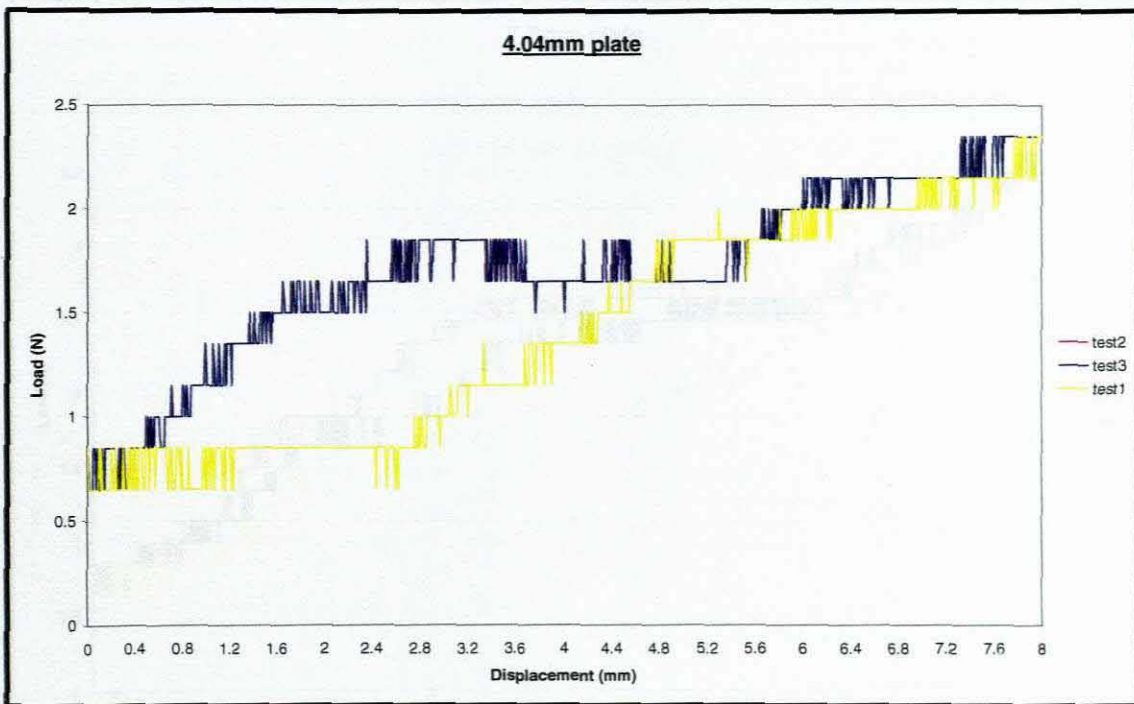
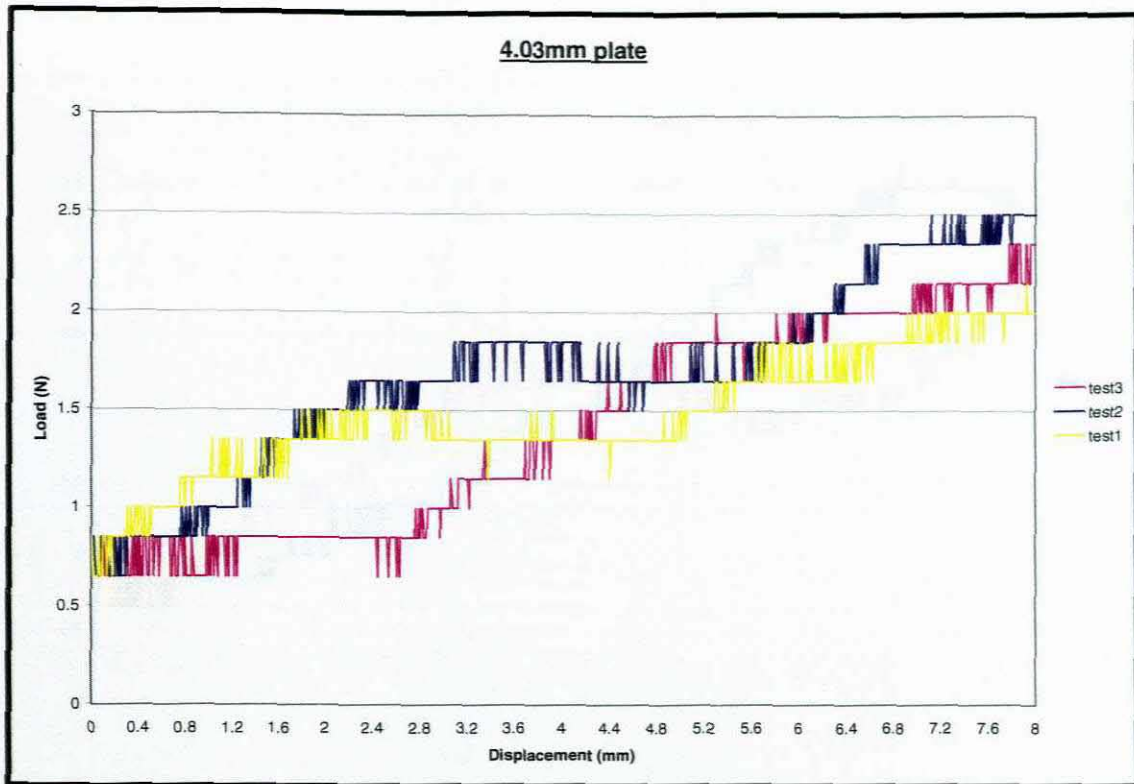
| | Length | | Width | |
|----------------|--------|-------|--------|--------|
| | X1 | X2 | Y1 | Y2 |
| x1 | 6.30 | 6.68 | 7.01 | 6.44 |
| x2 | 6.35 | 6.69 | 6.97 | 6.42 |
| x3 | 6.37 | 6.67 | 6.90 | 6.32 |
| x4 | 6.37 | 6.81 | 7.10 | 6.39 |
| x5 | 6.41 | 6.72 | 7.08 | 6.86 |
| x6 | 6.20 | 6.82 | 7.05 | 7.00 |
| x7 | 6.23 | 6.80 | 6.79 | 6.58 |
| x8 | 6.27 | 6.78 | 7.08 | 6.42 |
| x9 | 6.31 | 6.77 | 6.86 | 6.33 |
| x10 | 6.32 | 6.80 | 6.93 | 6.25 |
| x11 | 6.32 | 6.73 | 7.11 | 6.29 |
| x12 | 6.31 | 6.75 | 7.24 | 6.37 |
| x13 | 6.28 | 6.72 | 6.99 | 6.46 |
| x14 | 6.26 | 6.69 | 7.15 | 7.02 |
| x15 | 6.24 | 6.71 | 7.19 | 6.56 |
| x16 | 6.33 | 6.73 | 7.030 | 6.514 |
| x17 | 6.25 | 6.70 | 7.05 | 6.42 |
| x18 | 6.21 | 6.68 | 7.08 | 6.42 |
| x19 | 6.29 | 6.70 | 0.1253 | 0.2496 |
| x20 | 6.32 | 6.59 | | |
| x21 | 6.37 | 6.71 | | |
| x22 | 6.48 | 6.66 | | |
| x23 | 6.54 | 6.70 | | |
| x24 | 6.56 | 6.46 | | |
| x25 | 6.76 | 6.52 | | |
| x26 | 6.88 | 6.57 | | |
| Mean | 6.37 | 6.70 | | |
| Median | 6.320 | 6.705 | | |
| Mode | 6.37 | 6.70 | | |
| Std dev | 0.1618 | 0.086 | | |

Plate 4 7.7mm

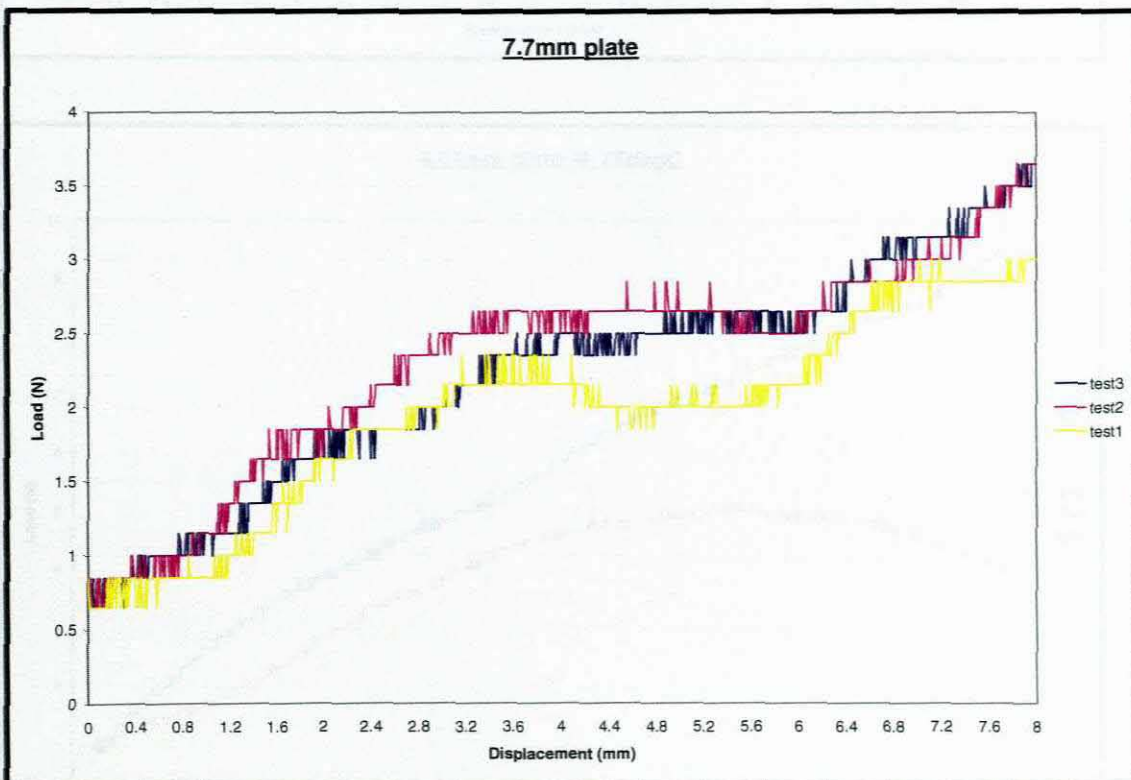
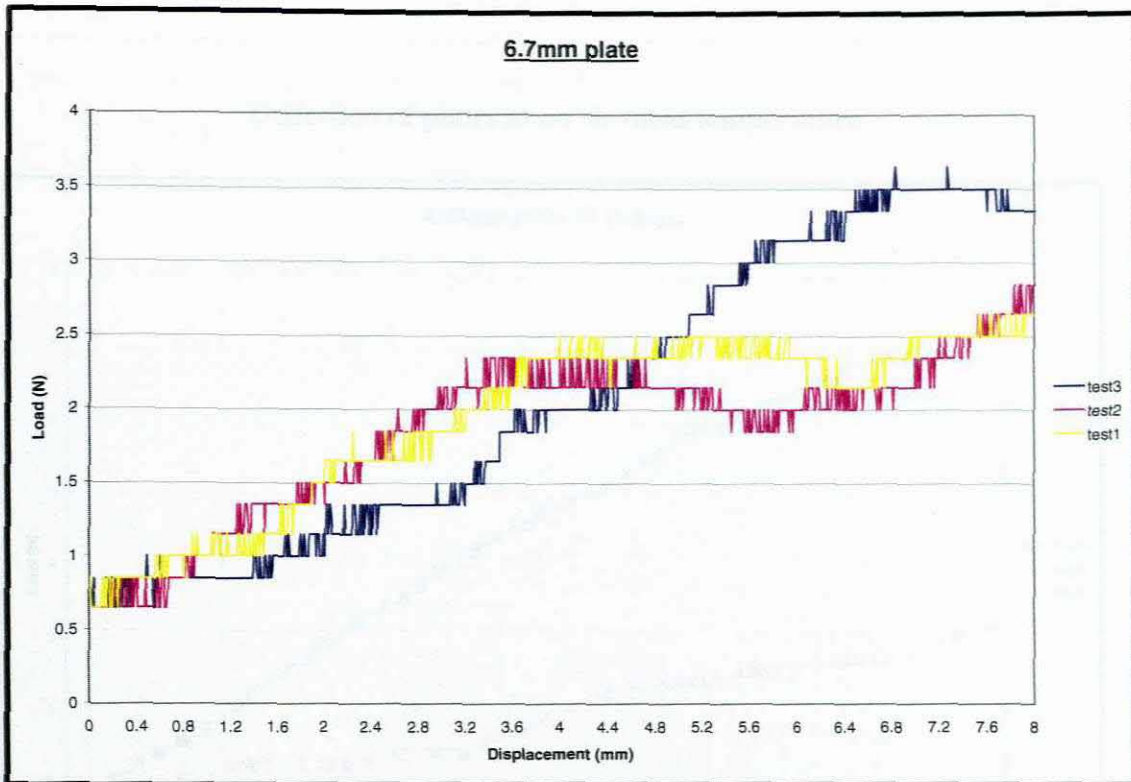
| | Length | | Width | |
|--|--------|--------|--------|--------|
| | X1 | X2 | Y1 | Y2 |
| | 7.89 | 7.76 | 8.01 | 7.91 |
| | 7.79 | 7.73 | 7.84 | 7.89 |
| | 7.65 | 7.68 | 7.92 | 7.88 |
| | 7.76 | 7.69 | 7.81 | 7.78 |
| | 7.72 | 7.73 | 7.86 | 7.71 |
| | 7.61 | 7.53 | 7.93 | 7.63 |
| | 7.72 | 7.78 | 7.68 | 7.84 |
| | 7.85 | 7.63 | 7.89 | 7.69 |
| | 7.77 | 7.59 | 7.71 | 7.91 |
| | 7.40 | 7.84 | 7.95 | 7.79 |
| | 7.59 | 7.67 | 7.71 | 7.73 |
| | 7.69 | 7.72 | 7.87 | 7.61 |
| | 7.64 | 7.48 | 7.84 | 7.82 |
| | 7.59 | 7.59 | 7.96 | 7.79 |
| | 7.48 | 7.80 | 7.89 | 7.88 |
| | 7.58 | 7.68 | 7.858 | 7.791 |
| | 7.65 | 7.52 | 7.87 | 7.79 |
| | 7.73 | 7.76 | 7.84 | 7.91 |
| | 7.66 | 7.66 | 0.0970 | 0.0987 |
| | 7.69 | 7.71 | | |
| | 7.72 | 7.64 | | |
| | 7.81 | 7.69 | | |
| | 7.83 | 7.70 | | |
| | 7.71 | 7.68 | | |
| | 7.00 | 7.65 | | |
| | 7.80 | 7.66 | | |
| | 7.667 | 7.676 | | |
| | 7.70 | 7.68 | | |
| | 7.72 | 7.68 | | |
| | 0.1758 | 0.0850 | | |

Appendix C

**Load – Deflection
behaviour for SMAHC
plates**

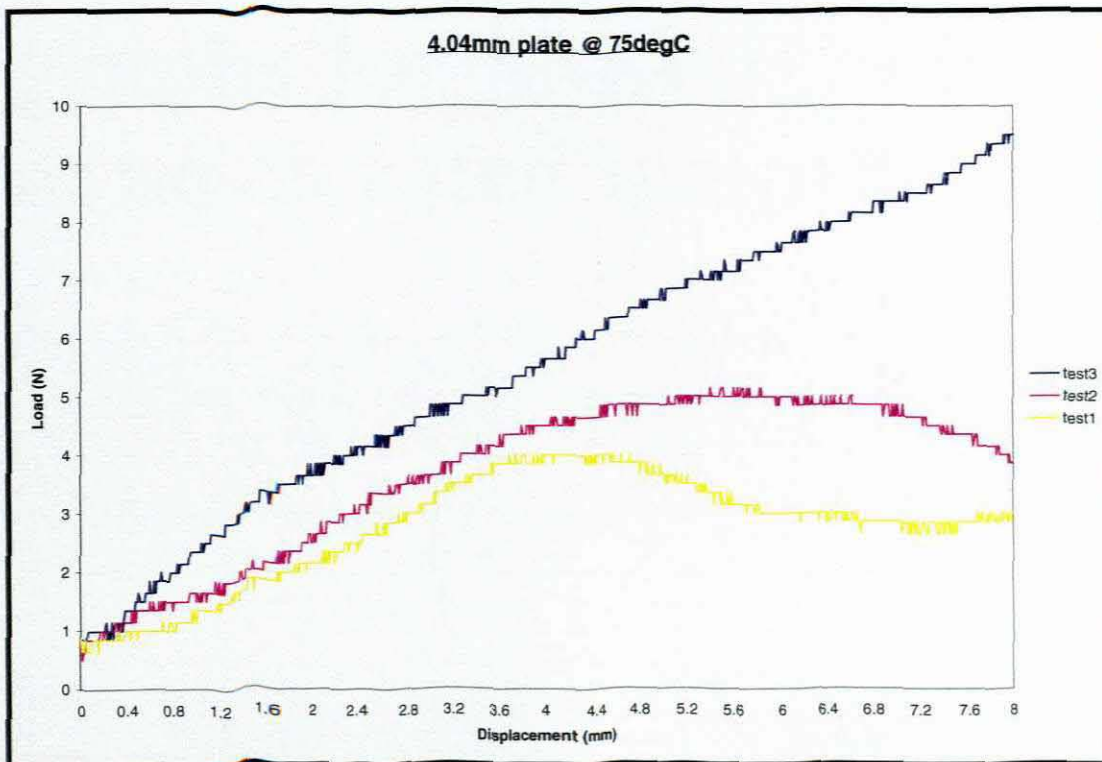
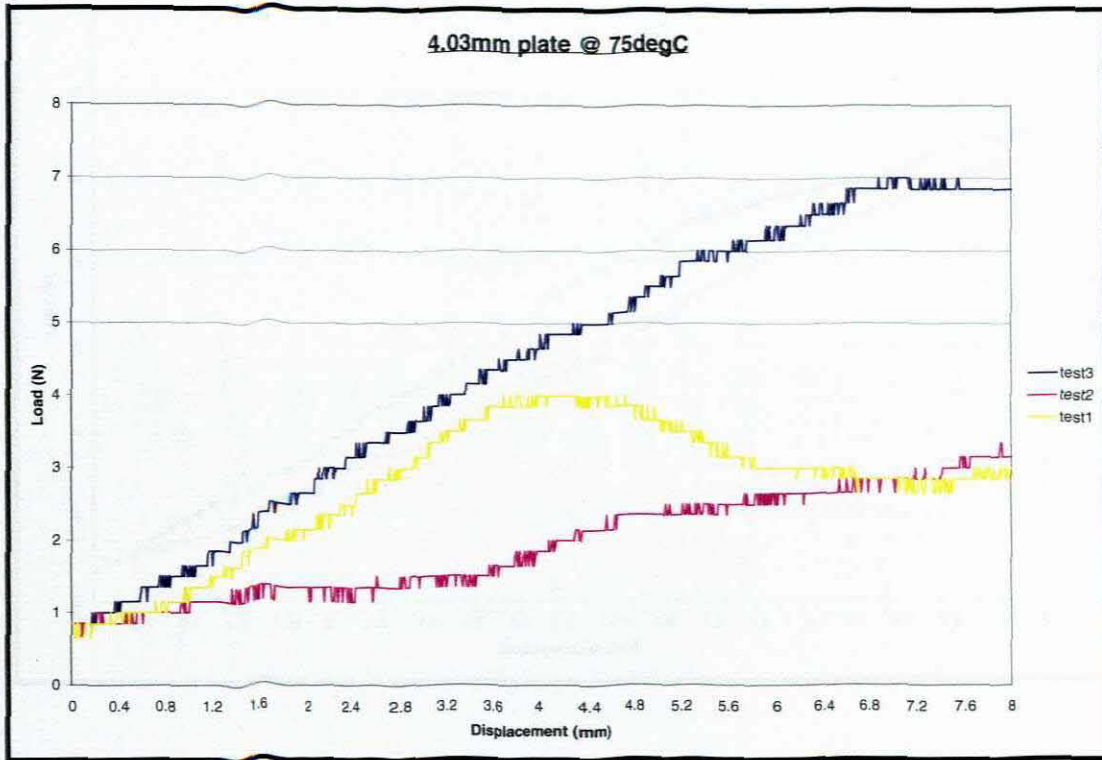


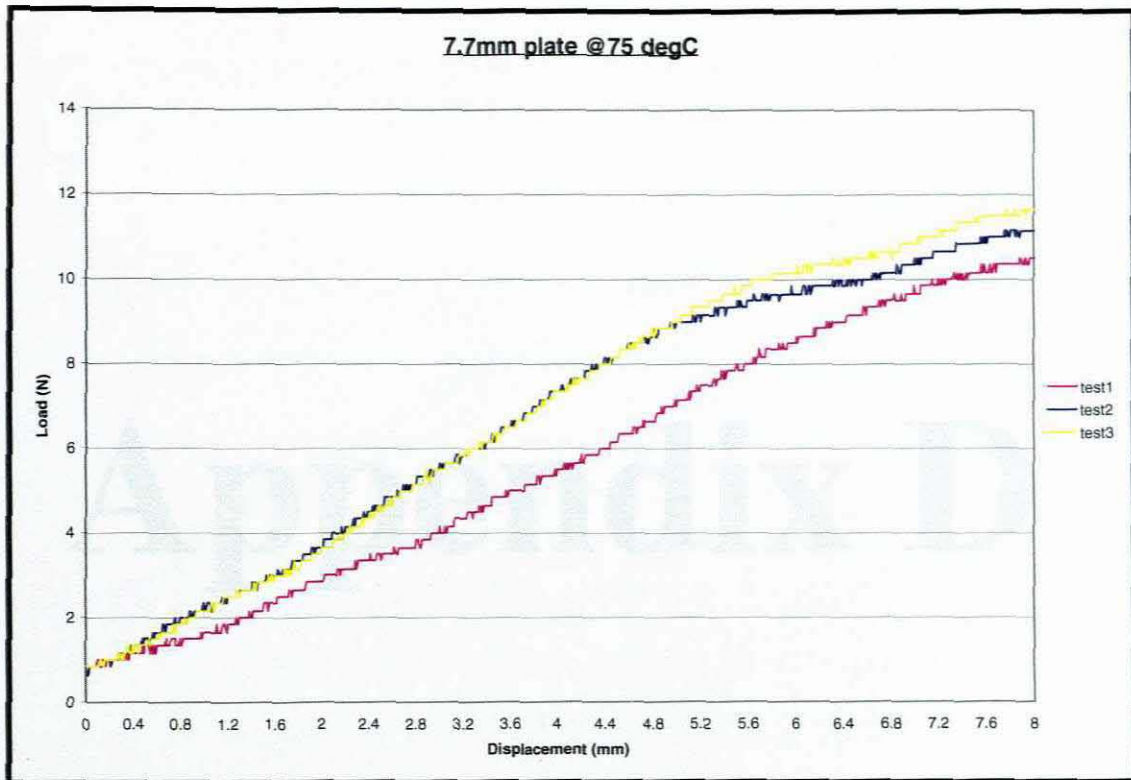
Behaviour of plates at stress and temperature



Deflection of plates at an elevated temperature

Deflection of plates at an elevated temperature

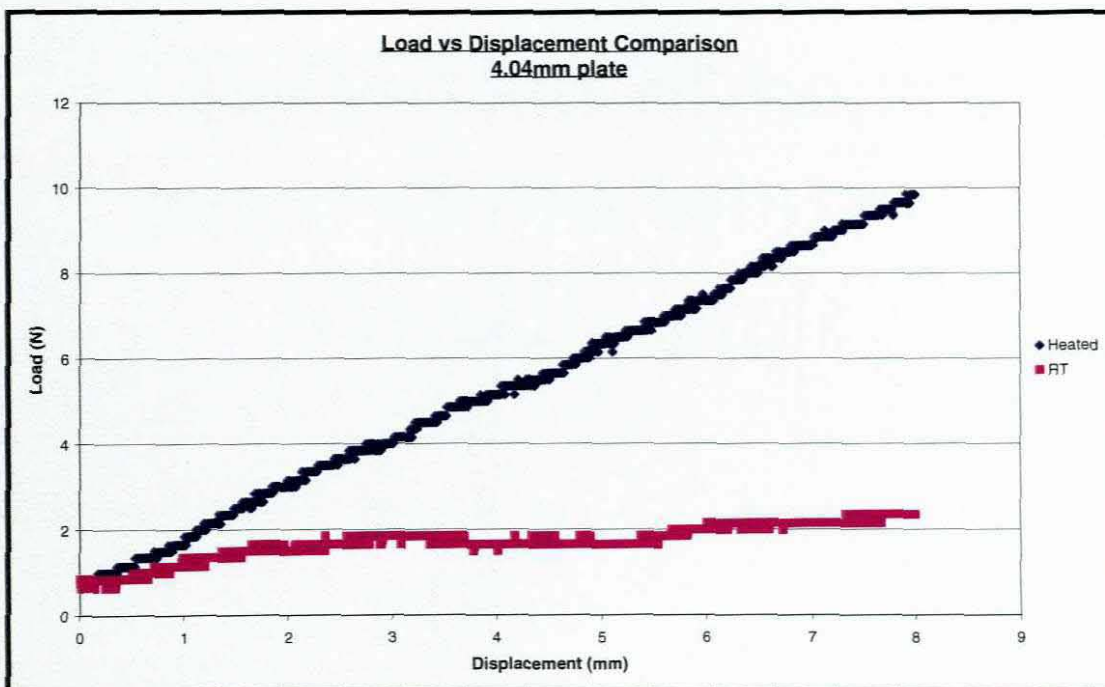
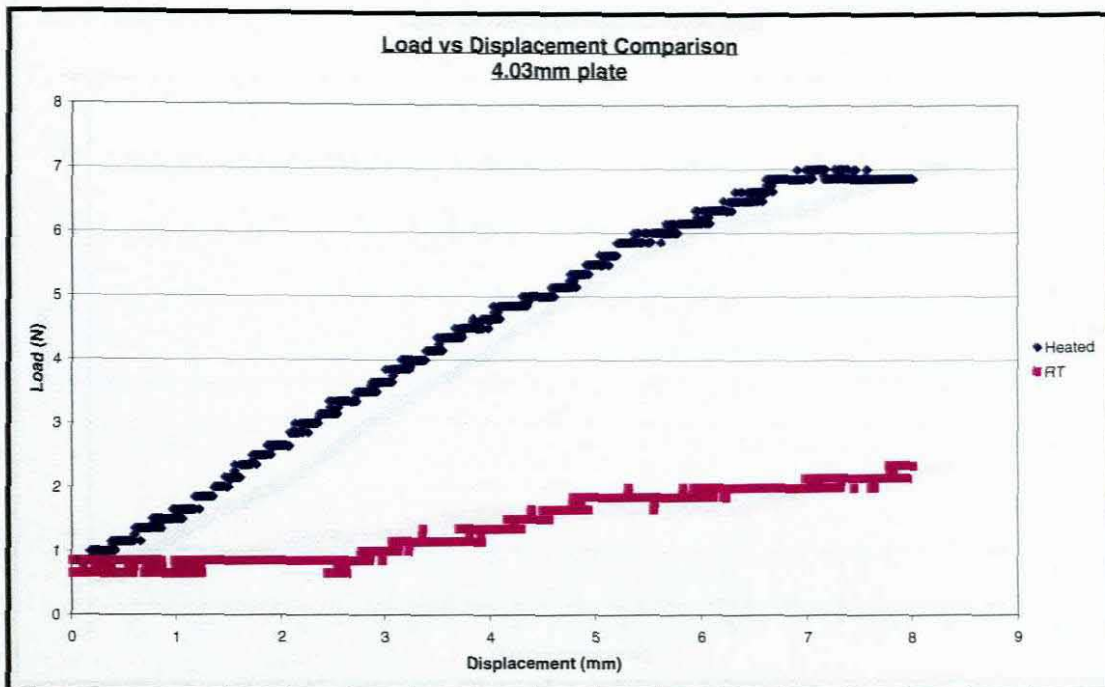


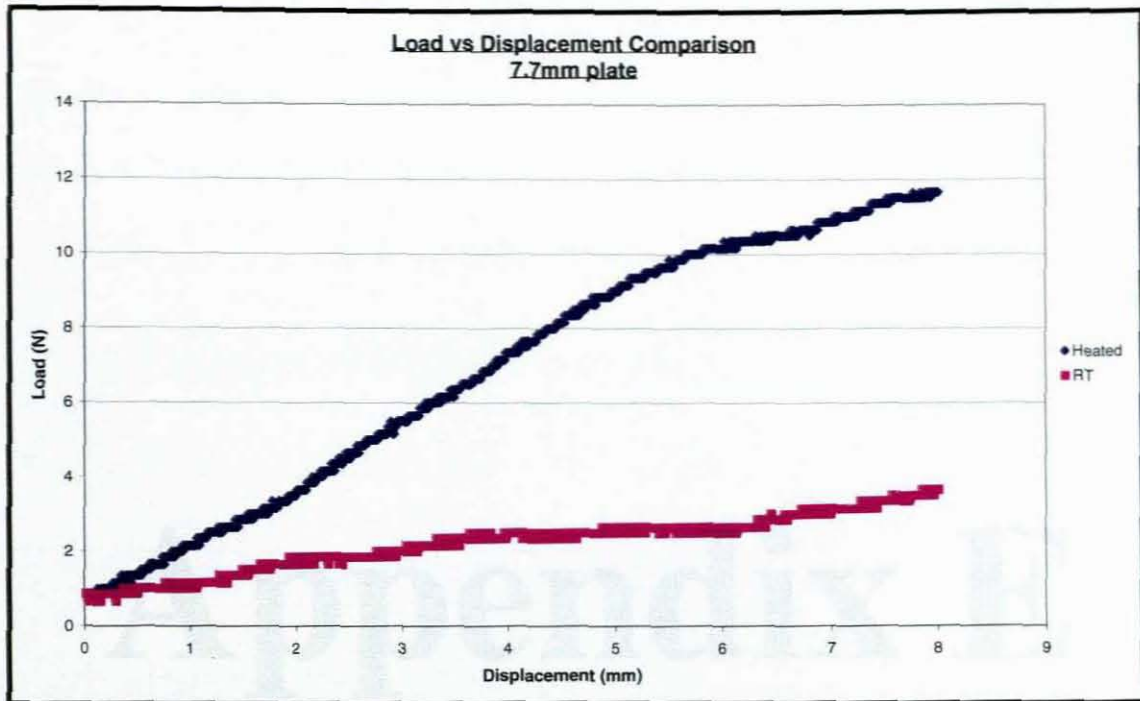


Selected Load - Deflection graphs for SMAHC plates at an elevated temperature

Appendix D

**Selected Load – Deflection
graphs for SMAHC plates
at an elevated temperature**





Deflection-of-beams
calculations applied to
SMAHC plates.

Appendix E

**Deflection-of-beams
calculations applied to
SMAHC plates.**

Beam calculations

Schematic of beam problem

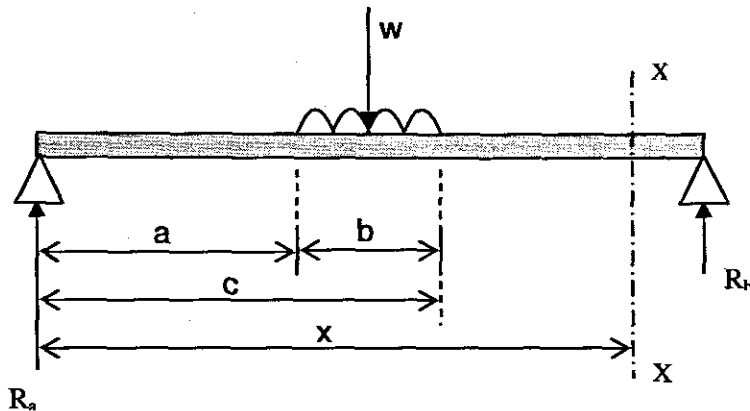


Figure E1: Beam loading experiment

Known:

Beam span, $l = 0.26m$

$b = 0.025m$

$\therefore a = 0.1175m$ and $c = 0.1425m$

For plate 1: Point load = 2.28 N, therefore $w = \frac{2.28}{0.025} = 91.2N/m$

and $y = 0.008 m$

Taking moments or using the summation of all vertical forces = 0, one obtain $R_a = 1.14 N$

$$BM_x = EI \frac{d^2y}{dx^2} = R_a x - \frac{w(x-a)^2}{2} + \frac{w(x-c)^2}{2}$$

$$EI \frac{dy}{dx} = \frac{R_a x^2}{2} - \frac{w(x-a)^3}{6} + \frac{w(x-c)^3}{6} + C$$

Using boundary conditions @ $x = l \Rightarrow \frac{dy}{dx} = 0$

$$0 = \frac{R_a l^2}{2} - \frac{w(l-a)^3}{6} + \frac{w(l-c)^3}{6} + C$$

$$0 = \frac{1.14(0.26)^2}{2} - \frac{91.2(0.26-0.1175)^3}{6} + \frac{91.2(0.26-0.1425)^3}{6} + C$$

$$0 = 0.0385 - 0.04398 + 0.02466 + C$$

$$C = -0.0192$$

Substituting into slope equation, we get:

$$EI \frac{dy}{dx} = \frac{R_a x^2}{2} - \frac{w(x-a)^3}{6} + \frac{w(x-c)^3}{6} - 0.0192$$

$$EIy = \frac{R_a x^3}{6} - \frac{w(x-a)^4}{24} + \frac{w(x-c)^4}{24} - 0.0192x + B$$

Using boundary conditions @ $x = l \Rightarrow y = 0$

$$0 = \frac{1.14(0.26)^3}{6} - \frac{91.2(0.26-0.1175)^4}{24} + \frac{91.2(0.26-0.1425)^4}{24} - 0.0192(0.26) + B$$

$$0 = 0.00334 - 0.00157 + 0.000724 - 0.004992 + B$$

$$B = 0.0025$$

Therefore the deflection equation for the above loading condition is:

$$EIy = \frac{R_a x^3}{6} - \frac{w(x-a)^4}{24} + \frac{w(x-c)^4}{24} - 0.0192x + 0.0025$$

For maximum deflection y_{\max} @ $x = \frac{l}{2}$

$$EIy = \frac{1.14(0.13)^3}{6} - \frac{91.2(0.13-0.1175)^4}{24} + \frac{91.2(0.13-0.1425)^4}{24} - 0.0192(0.13) + 0.0025$$

$$EIy = 0.000417 - 0.000000092 - 0.0025 + 0.0025$$

$$EIy = 0.000417$$

... (1)

Giving a flexural stiffness of $EI = \frac{0.000417}{0.008} = 0.052 \text{ Nm}^2$

For plate 2: Point load = 2.35 N, therefore $w = \frac{2.35}{0.025} = 94 \text{ N/m}$
and $y = 0.008 \text{ m}$

Taking moments or using the summation of all vertical forces = 0, one obtain $R_a = 1.18 \text{ N}$

Using boundary conditions @ $x = l \Rightarrow \frac{dy}{dx} = 0$

$$0 = \frac{R_a l^2}{2} - \frac{w(l-a)^3}{6} + \frac{w(l-c)^3}{6} + C$$

$$0 = \frac{1.18 \cdot (0.26)^2}{2} - \frac{94(0.26 - 0.1175)^3}{6} + \frac{94(0.26 - 0.1425)^3}{6} + C$$

$$0 = 0.0399 - 0.0453 + 0.0254 + C$$

$$C = -0.02$$

Substituting into slope equation, we get:

$$EI \frac{dy}{dx} = \frac{R_a x^2}{2} - \frac{w(x-a)^3}{6} + \frac{w(x-c)^3}{6} - 0.02$$

$$EIy = \frac{R_a x^3}{6} - \frac{w(x-a)^4}{24} + \frac{w(x-c)^4}{24} - 0.02x + B$$

Using boundary conditions @ $x = l \Rightarrow y = 0$

$$0 = \frac{1.18(0.26)^3}{6} - \frac{94(0.26 - 0.1175)^4}{24} + \frac{94(0.26 - 0.1425)^4}{24} - 0.02(0.26) + B$$

$$0 = 0.00346 - 0.00162 + 0.000747 - 0.0052 + B$$

$$B = 0.0026$$

$$EIy = \frac{R_a x^3}{6} - \frac{w(x-a)^4}{24} + \frac{w(x-c)^4}{24} - 0.02x + 0.0026$$

For maximum deflection y_{\max} @ $x = \frac{l}{2}$

$$EIy = \frac{1.18(0.13)^3}{6} - \frac{94(0.13-0.1175)^4}{24} + \frac{94(0.13-0.1425)^4}{24} - 0.02(0.13) + 0.0026$$

$$EIy = 0.000432 - 0.000000095 - 0.0026 + 0.0026$$

$$EIy = 0.000432$$

... (2)

Giving a flexural stiffness of $EI = \frac{0.000432}{0.008} = 0.054 \text{ Nm}^2$

For plate 3: Point load = 2.95 N, therefore $w = \frac{2.95}{0.025} = 118 \text{ N/m}$

And $y = 0.008 \text{ m}$

Taking moments or using the summation of all vertical forces = 0, one obtain $R_a = 1.48 \text{ N}$

Using boundary conditions @ $x = l \Rightarrow \frac{dy}{dx} = 0$

$$0 = \frac{R_a l^2}{2} - \frac{w(l-a)^3}{6} + \frac{w(l-c)^3}{6} + C$$

$$0 = \frac{1.48(0.26)^2}{2} - \frac{118(0.26-0.1175)^3}{6} + \frac{118(0.26-0.1425)^3}{6} + C$$

$$0 = 0.05 - 0.0569 + 0.0319 + C$$

$$C = -0.025$$

Substituting into slope equation, we get:

$$EI \frac{dy}{dx} = \frac{R_a x^2}{2} - \frac{w(x-a)^3}{6} + \frac{w(x-c)^3}{6} - 0.025$$

$$EIy = \frac{R_a x^3}{6} - \frac{w(x-a)^4}{24} + \frac{w(x-c)^4}{24} - 0.025x + B$$

Using boundary conditions @ $x = l \Rightarrow y = 0$

$$0 = \frac{1.48(0.26)^3}{6} - \frac{118(0.26 - 0.1175)^4}{24} + \frac{118(0.26 - 0.1425)^4}{24} - 0.025(0.26) + B$$

$$0 = 0.00434 - 0.00203 + 0.00094 - 0.0065 + B$$

$$B = 0.00325$$

$$EIy = \frac{R_a x^3}{6} - \frac{w(x-a)^4}{24} + \frac{w(x-c)^4}{24} - 0.025x + 0.00325$$

For maximum deflection y_{\max} @ $x = \frac{l}{2}$

$$EIy = \frac{1.48(0.13)^3}{6} - \frac{118(0.13 - 0.1175)^4}{24} + \frac{118(0.13 - 0.1425)^4}{24} - 0.025(0.13) + 0.00325$$

$$EIy = 0.00054 - 0.00000012 - 0.00325 + 0.00325$$

$$EIy = 0.00054$$

... (3)

Giving a flexural stiffness of $EI = \frac{0.00054}{0.008} = 0.0675 \text{ Nm}^2$ →

For plate 4: Point load = 3.43 N, therefore $w = \frac{3.43}{0.025} = 137.2 \text{ N/m}$

And $y = 0.008 \text{ m}$

Taking moments or using the summation of all vertical forces = 0, one obtain $R_a = 1.72 \text{ N}$

Using boundary conditions @ $x = l \Rightarrow \frac{dy}{dx} = 0$

$$0 = \frac{R_a l^2}{2} - \frac{w(l-a)^3}{6} + \frac{w(l-c)^3}{6} + C$$

$$0 = \frac{1.72(0.26)^2}{2} - \frac{137.2(0.26 - 0.1175)^3}{6} + \frac{137.2(0.26 - 0.1425)^3}{6} + C$$

$$0 = 0.058 - 0.0662 + 0.0371 + C$$

$$C = -0.0289$$

Substituting into slope equation, we get:

$$EI \frac{dy}{dx} = \frac{R_a x^2}{2} - \frac{w(x-a)^3}{6} + \frac{w(x-c)^3}{6} - 0.0289$$

$$EIy = \frac{R_a x^3}{6} - \frac{w(x-a)^4}{24} + \frac{w(x-c)^4}{24} - 0.0289x + B$$

Using boundary conditions @ $x = l \Rightarrow y = 0$

$$0 = \frac{1.72(0.26)^3}{6} - \frac{137.2(0.26 - 0.1175)^4}{24} + \frac{137.2(0.26 - 0.1425)^4}{24} - 0.0289(0.26) + B$$

$$0 = 0.005 - 0.00236 + 0.0011 - 0.0075 + B$$

$$B = 0.00376$$

$$EIy = \frac{R_a x^3}{6} - \frac{w(x-a)^4}{24} + \frac{w(x-c)^4}{24} - 0.0289x + 0.00376$$

For maximum deflection y_{\max} @ $x = \frac{l}{2}$

$$EIy = \frac{1.72(0.13)^3}{6} - \frac{137.2(0.13 - 0.1175)^4}{24} + \frac{137.2(0.13 - 0.1425)^4}{24} - 0.0289(0.13) + 0.00376$$

$$EIy = 0.00063 - 0.00000014 - 0.00376 + 0.00376$$

$$EIy = 0.00063$$

... (4)

$$\text{Giving a flexural stiffness of } EI = \frac{0.00063}{0.008} = 0.0788 \text{ Nm}^2$$

BEAM TESTS AT AN ELEVATED TEMPERATURE

Consider Fig. E1, with the same known quantities.

For plate 1: Point load = 4.33 N, therefore $w = \frac{4.33}{0.025} = 173.2 \text{ N/m}$
and $y = 0.008 \text{ m}$

Taking moments or using the summation of all vertical forces = 0, one obtain $R_a = 2.17 \text{ N}$

From the preceding calculations it was noted that the two terms containing the integration constants C and B cancel.

$$EIy = \frac{R_a x^3}{6} - \frac{w(x-a)^4}{24} + \frac{w(x-c)^4}{24} - \cancel{Cx} + \cancel{B}$$

In Macauly's method the negative Macauly - terms are neglected reducing the above to a general maximum deflection equation:

$$EIy = \frac{R_a x^3}{6} - \frac{w(x-a)^4}{24} \quad (5)$$

$$EIy = \frac{2.17(0.13)^3}{6} - \frac{173.2(0.13-0.1175)^4}{24}$$

$$EIy = 0.000795 - 0.000000176$$

$$EIy = 0.00079$$

$$\text{Giving a flexural stiffness of } EI = \frac{0.00079}{0.008} = 0.099 \text{ Nm}^2 \rightarrow$$

For plate 2: Point load = 5.45 N, therefore $w = \frac{5.45}{0.025} = 218 \text{ N/m}$
and $y = 0.008 \text{ m}$

Taking moments or using the summation of all vertical forces = 0, one obtain $R_a = 2.73 \text{ N}$

Substituting R_a and w into equation 5 we obtain:

$$EIy = \frac{2.73(0.13)^3}{6} - \frac{218(0.13-0.1175)^4}{24}$$

$$EIy = 0.0009996 - 0.000000222$$

$$EIy = 0.0009994$$

Giving a flexural stiffness of $EI = \frac{0.0009994}{0.008} = 0.125 \text{ Nm}^2$ \rightarrow

For plate 3: Point load = 9.78 N, therefore $w = \frac{9.78}{0.025} = 391.2 \text{ N/m}$
and $y = 0.008 \text{ m}$

Taking moments or using the summation of all vertical forces = 0, one obtain $R_a = 4.89 \text{ N}$

Substituting R_a and w into equation 5 we obtain:

$$EIy = \frac{4.89(0.13)^3}{6} - \frac{391.2(0.13 - 0.1175)^4}{24}$$

$$EIy = 0.00179 - 0.000000398$$

$$EIy = 0.00179$$

Giving a flexural stiffness of $EI = \frac{0.00179}{0.008} = 0.224 \text{ Nm}^2$ \rightarrow

For plate 4: Point load = 11.1 N, therefore $w = \frac{11.10}{0.025} = 444 \text{ N/m}$
and $y = 0.008 \text{ m}$

Taking moments or using the summation of all vertical forces = 0, one obtain $R_a = 5.55 \text{ N}$

Substituting R_a and w into equation 5 we obtain:

$$EIy = \frac{5.55(0.13)^3}{6} - \frac{444(0.13 - 0.1175)^4}{24}$$

$$EIy = 0.00203 - 0.000000452$$

$$EIy = 0.00203$$

Giving a flexural stiffness of $EI = \frac{0.00203}{0.008} = 0.254 \text{ Nm}^2 \rightarrow$

BEAM TESTS USING THE SAME LOAD UNDER CONTROLLED TEMPERATURE

Temperature 1 = room temperature ($\approx 22^\circ\text{C}$)

For plate 1: Point load = 4.66 N, therefore $w = \frac{4.66}{0.02} = 233 \text{ N/m}$
and $y = 0.022 \text{ m}$

Taking moments or using the summation of all vertical forces = 0, one obtain $R_a = 2.33 \text{ N}$

Substituting R_a and w into equation 5 we obtain:

$$EIy = \frac{2.33(0.13)^3}{6} - \frac{233(0.13 - 0.1175)^4}{24}$$

$$EIy = 0.00085 - 0.000000237$$

$$EIy = 0.00085$$

Giving a flexural stiffness of $EI = \frac{0.00085}{0.022} = 0.039 \text{ Nm}^2 \rightarrow$

For plate 2: Point load = 4.66 N, therefore $w = \frac{4.66}{0.02} = 233 \text{ N/m}$
and $y = 0.0213 \text{ m}$

Taking moments or using the summation of all vertical forces = 0, one obtain $R_a = 2.33 \text{ N}$

Substituting R_a and w into equation 5 we obtain:

$$EIy = \frac{2.33(0.13)^3}{6} - \frac{233(0.13 - 0.1175)^4}{24}$$

$$EIy = 0.00085 - 0.000000237$$

$$EIy = 0.00085$$

Giving a flexural stiffness of $EI = \frac{0.00085}{0.02127} = 0.04 \text{ Nm}^2 \rightarrow$

For plate 3: Point load = 4.66 N, therefore $w = \frac{4.66}{0.02} = 233 \text{ N/m}$
and $y = 0.0174 \text{ m}$

Taking moments or using the summation of all vertical forces = 0, one obtain $R_a = 2.33 \text{ N}$

Substituting R_a and w into equation 5 we obtain:

$$EIy = \frac{2.33(0.13)^3}{6} - \frac{233(0.13 - 0.1175)^4}{24}$$

$$EIy = 0.00085 - 0.000000237$$

$$EIy = 0.00085$$

Giving a flexural stiffness of $EI = \frac{0.00085}{0.01743} = 0.049 \text{ Nm}^2 \rightarrow$

For plate 4: Point load = 4.66 N, therefore $w = \frac{4.66}{0.02} = 233 \text{ N/m}$
and $y = 0.0144 \text{ m}$

Taking moments or using the summation of all vertical forces = 0, one obtain $R_a = 2.33 \text{ N}$

Substituting R_a and w into equation 5 we obtain:

$$EIy = \frac{2.33(0.13)^3}{6} - \frac{233(0.13 - 0.1175)^4}{24}$$

$$EIy = 0.00085 - 0.000000237$$

$$EIy = 0.00085$$

Giving a flexural stiffness of $EI = \frac{0.00085}{0.01443} = 0.059 \text{ Nm}^2 \rightarrow$

Temperature 2 = 73°C

For plate 1: Point load = 4.66 N, therefore $w = \frac{4.66}{0.02} = 233 \text{ N/m}$
and $y = 0.0047 \text{ m}$

Taking moments or using the summation of all vertical forces = 0, one obtain $R_a = 2.33 \text{ N}$

Substituting R_a and w into equation 5 we obtain:

$$EIy = \frac{2.33(0.13)^3}{6} - \frac{233(0.13 - 0.1175)^4}{24}$$

$$EIy = 0.00085 - 0.000000237$$

$$EIy = 0.00085$$

Giving a flexural stiffness of $EI = \frac{0.00085}{0.00473} = 0.18 \text{ Nm}^2 \rightarrow$

For plate 2: Point load = 4.66 N, therefore $w = \frac{4.66}{0.02} = 233 \text{ N/m}$
and $y = 0.0046 \text{ m}$

Taking moments or using the summation of all vertical forces = 0, one obtain $R_a = 2.33 \text{ N}$

Substituting R_a and w into equation 5 we obtain:

$$EIy = \frac{2.33(0.13)^3}{6} - \frac{233(0.13 - 0.1175)^4}{24}$$

$$EIy = 0.00085 - 0.000000237$$

$$EIy = 0.00085$$

Giving a flexural stiffness of $EI = \frac{0.00085}{0.00457} = 0.186 \text{ Nm}^2 \rightarrow$

For plate 3: Point load = 4.66 N, therefore $w = \frac{4.66}{0.02} = 233 \text{ N/m}$
and $y = 0.0023 \text{ m}$

Taking moments or using the summation of all vertical forces = 0, one obtain $R_a = 2.33 \text{ N}$

Substituting R_a and w into equation 5 we obtain:

$$EIy = \frac{2.33(0.13)^3}{6} - \frac{233(0.13 - 0.1175)^4}{24}$$

$$EIy = 0.00085 - 0.000000237$$

$$EIy = 0.00085$$

Giving a flexural stiffness of $EI = \frac{0.00085}{0.00233} = 0.365 \text{ Nm}^2 \rightarrow$

For plate 4: Point load = 4.66 N, therefore $w = \frac{4.66}{0.02} = 233 \text{ N/m}$
and $y = 0.0021 \text{ m}$

Taking moments or using the summation of all vertical forces = 0, one obtain $R_a = 2.33 \text{ N}$

Substituting R_a and w into equation 5 we obtain:

$$EIy = \frac{2.33(0.13)^3}{6} - \frac{233(0.13 - 0.1175)^4}{24}$$

$$EIy = 0.00085 - 0.000000237$$

$$EIy = 0.00085$$

Giving a flexural stiffness of $EI = \frac{0.00085}{0.0021} = 0.405 \text{ Nm}^2 \rightarrow$